Molecular and Cellular Phenotypes of AUTS2 Deficiency in the Developing Mouse Cortex and Hippocampus

Anthony Scott Castanza

A dissertation
submitted in partial fulfillment of the
requirements for the degree of

Doctor of Philosophy

University of Washington
2018

Reading Committee:
Robert F. Hevner, Chair
Christopher D. Keene
Jan-Marino Ramirez

Program Authorized to Offer Degree:
Pathology

University of Washington

Abstract

Molecular and Cellular Phenotypes of AUTS2 Deficiency in the Developing Mouse Cortex and Hippocampus

Anthony Scott Castanza

Chair of the Supervisory Committee:
Robert F. Hevner, Professor
Pathology

Abstract

Variants in the gene Autism Susceptibility Candidate 2 (AUTS2) are a rare cause of intellectual disability, developmental delay and autistic features in patients. However, the mechanism by which loss of AUTS2 causes specific neurological symptoms, the underlying neuroanatomical abnormalities, and the syndrome's pathological progression are not well established. The core molecular function of this intellectual disability syndrome gene also remains uncertain. Previous studies have proposed two independent mechanisms of AUTS2 function. One found that Auts2 modifies the Polycomb repressive complex 1 (PRC1) to activate transcription of target neurodevelopmental genes by recruiting the histone

acetyltransferase EP300. A second study found that cytoplasmic AUTS2 regulates cytoskeletal assembly through PREX1 to promote neurite outgrowth and migration. To further investigate Auts2 functions, we screened for AUTS2 interactors in the cerebral cortex and profiled changes of transcript expression in the developing cortex of Auts2 conditional mutant mice. AUTS2 immunoprecipitation experiments identified interactions with proteins involved in pre-mRNA processing including the multifunctional RNA-processing regulator NONO. RNA-immunoprecipitation experiments identified enrichment of specific transcripts associated with AUTS2 including mRNAs which encode the previously identified effectors of Auts2 function EP300 and PREX1. Additional preliminary experiments identified a network of transcripts encoding a Notch signaling related protein-protein interaction network which were co-bound by AUTS2 and NONO. We propose that AUTS2 interacts with an RNA-binding complex that directly targets transcripts encoding Auts2 effectors. This mechanism provides a unifying model that accounts for previously disparate hypotheses of AUTS2 functions.

Prior work developed mouse models of Auts2 deficiency, however, these models did not fully account for additional, functional, isoforms expressed from the c-terminus of the locus. Our work developed a mouse model which is expected to ablate all c-terminal containing AUTS2 isoforms under the control of CRE-recombinase (Auts2 cKO). RNA-sequencing of frontal cortex and hippocampus from P0.5 Auts2 cKO mice identified dysregulation of RNAs which encode proteins previously identified to be effectors of AUTS2 and which were targeted by the AUTS2 complex. We additionally identified dysregulated pathways encoding developmental process including cytoskeletal organization, cell migration, adhesion, core

transcriptional and metabolic processes. These pathways provide a molecular link between AUTS2 and NONO deficiency and overlap with pathways dysregulated in a large study of human neurological disorder transcriptomes.

Histological examination of the AUTS2 deficient brain identified severe abnormalities in early post-natal hippocampal development. Dentate gyrus volume was reduced and early colonization of the adult neurogenic niche by TBR2+ intermediate neuronal progenitors was dramatically impaired. These hippocampi also exhibited near total absence of hilar mossy neurons, a population which regulates hippocampal interconnectivity and excitability. EEG analysis of recordings from these animals identified significant abnormalities consistent with disinhibition identified in both autism and epilepsy.

The work presented in this dissertation significantly expands on our understanding of the neurobiology regulated by AUTS2. We also identify functional and molecular connections with ASD and epilepsy pathology. These experiments identify mechanisms by which the pathogenesis of the AUTS2 syndrome can be further investigated.

TABLE OF CONTENTS

LIST OF FIGURES

Chapter 2

Chapter 3

Chapter 4

LIST OF TABLES

Chapter 2

Chapter 3

Chapter 4

Chapter 1: INTRODUCTION

1.1: Perspective on autism focused research

The broad spectrum of deviations from neurotypicality classified under the umbrella term of autism spectrum disorder (ASD) consists of a wide variety of atypical neurocognitive presentations with several key diagnostic commonalities. These diagnostic criteria consist mainly of deficits in measures of social communication and social interaction, identification of restricted interests or activities, and repetitive patterns of behavior. In ASD diagnosis, these features are also scored by symptom severity (American Psychiatric Association, 2013). This is joined by the many "autism-like" syndromes which present with some, but not all of the typical autism phenotypes. The severity and impact on social, behavioral, and cognitive abilities of patients with these syndromes are extraordinarily variable. On the more severe end of this diverse spectrum, autism phenotypes are frequently coupled with intellectual disability (ID) (Mazurek et al., 2018). These phenotypes are broadly thought to be the result of highly variable alterations in brain developmental processes influenced by both genetic and environmental factors (Muhle et al., 2018). At the extreme end, autism-associated pathologies can severely and permanently impact the ability of affected individuals to lead functional, socially integrated, lives as the symptoms persist into adulthood. Management of ASD symptoms is predominantly the realm of behavioral therapy and additional educational support, treatment options which are highly involved and often reliant on underfunded support programs. Attempts at the pharmacological treatment of ASD have been remarkably unsuccessful despite substantial advancements in treating other

psychiatric disorders such as schizophrenia and depression. Despite the lack of success at treating core autism symptoms, pharmacological interventions have shown some promise managing common comorbidities such as aggression, self-injury, and associated sleep disorders (Kaplan and McCracken, 2012). The failure to identify promising therapeutic targets in ASD likely stems somewhat from the fact that despite significant advances in the field of diagnosis of genetic disease generally, only around 20-25% of ASD cases have an identified genetic cause (Miles, 2011). Continued technological advances have reduced the cost for next-generation sequencing of patient samples substantially, which has led to the increasingly widespread clinical adoption of exome sequencing. These advancements have resulted in the identification of nearly 1000 genes associated with autism and autism-like syndromes, more than 80% of which consist of rare single gene mutations (SAFARI Gene Database, Retrieved March 2018). While identification of these 1,000 genes represents a significant advancement in understanding the underlying biology of ASD, and related syndromes, over three-quarters of ASD cases do not present with any currently identifiable underlying genetic cause. However, as projects like ENCODE have demonstrated, our understanding of how gene expression programs are regulated, and the functional relevance of non-coding elements is still in its infancy. As the regulatory landscape of the genome continues to be untangled, further study may reveal causal variants in regulatory regions, non-protein coding RNAs, or other genomic features for more of these cases in time. Indeed, preliminary work in this area has identified an enrichment for variants which affect putative regulatory regions in a study of ASD patients (Turner et al., 2016). The significance of non-coding variants substantially contributing to the development of ASD symptoms is

underscored by the recent identification that de-novo mutations in Human Accelerated Regions (HARs) are enriched in individuals affected with ASD (Doan et al., 2016). HARs frequently function as transcriptional enhancers which are active in brain development (Capra et al., 2013).

HAR target genes are significantly enriched for phenotypes of abnormal nervous system development, abnormal neuronal morphology, and perinatal lethality as well as biological processes involved in neuron differentiation. Mutations in 12 HARs, the majority of which were annotated as enhancers, including one within the *AUTS2* locus, have been implicated in autism spectrum disorders and associated phenotypes (Doan et al., 2016; Oksenberg et al., 2013). These patients, which did not exhibit gene coding sequence mutations, predominantly exhibited ASD with accompanying intellectual disability. The identification of these HAR mutations which are associated with ASD suggests that mutations which affect gene expression may contribute to 1some percentage of the 75-80% of cases where exome sequencing has failed to identify causal variants. Mutations which modify these regulatory regions may influence the expression of genes more subtly, by minor perturbations in levels of critical genes or by affecting tightly regulated spatiotemporal expression patterns. Further identification of affected regulatory regions may capture more of the genomic landscape of ASD biology by identifying, for example, essential genes which do not tolerate more severe loss-of-function deletions, or where regulation of specific isoform expression is a critical aspect of functionality. The difficulty of identifying these potentially pathogenic changes is compounded by the effect of variants which may not cause overt disease in isolation, but which may make an individual vulnerable to additional insults such as

environmental factors, of which many are known to influence the risk of ASD (Karimi et al., 2017).

However, even for those cases where a likely underlying genetic cause has been identified, the specific effects on neurodevelopmental pathways are often poorly understood and complicated by multiple factors. Many of these patients do not present with morphological brain abnormalities, and as the majority of brain development is complete by the time autism symptoms are typically diagnosable in early childhood it is not possible to identify transient alterations in neurological development. Furthermore, access to patient neuronal tissue is extremely limited which prevents the study transcriptomic alterations in native tissue and protocols to generate iPS derived mature human neurons are still in their infancy. These facts have made it exceptionally difficult to design targeted treatments even when the pathology has been identified. This reinforces the need to study the basic processes of neurodevelopment using animal models where the complete unfolding of brain development can be analyzed in a whole organismal context, complemented by human cellular models to assess human-specific processes as these techniques improve. Discovery of these shared biological features which when altered lead to disease gives us the best hope of delivering meaningful improvements in the quality of life for ASD patients. The remarkable variance in ASD and ID pathogenesis is also a stark reminder of the complexity of the human brain and how easily small perturbations in neurodevelopment can cascade into a lifetime of disability.

1.2: Identification of AUTS2 as a clinically relevant gene for pathogenesis of autism, intellectual disability and other neurological phenotypes

AUTS2 was originally identified as a gene of clinical significance for the development of autistic features in a genomic study of a pair of monozygotic twins (Sultana et al., 2002). These twins had previously been diagnosed with autism and mental retardation (de la Barra et al., 1986). The study by Sultana et al., identified that a translocation breakpoint involving 7q11.2 and 20p11.2 disrupted expression of a previously unidentified gene spanning 1.2Mb on 7q11. This locus which encoded a 1259 amino acid protein which was deemed AUTS2 (Autism Susceptibility Candidate 2). Additional studies identified variants in *AUTS2* as the cause of severe intellectual disability and autistic features in multiple patients. MRIs were performed on eight of these patients which appeared largely normal and without structural brain malformations (Beunders et al., 2016). However, further clinical analysis of AUTS2 patients has identified pathological features which define the "AUTS2 Syndrome". All patients studied exhibited some degree of developmental delay or learning difficulty with language delay and accompanying intellectual disability (Beunders et al., 2013, 2015, 2016; Kalscheuer et al., 2007; Sengun et al., 2016). Auts2 syndrome patients exhibit repetitive and obsessive behaviors reminiscent of Autism and a hypersensitivity to textures and sounds. The adult patients also exhibited a characteristic aversion to eye contact. However behavioral phenotypes which were not entirely consistent with classical autism features were also observed in these patient cohorts. These patients did not appear to exhibit the social aversion which is characteristic of Autism. Several patients were described as "hyper-social", lacking characteristic inhibition to social contact. Many of these patients also exhibited

atypical physical characteristics in addition to their cognitive and behavioral phenotypes. The majority of Auts2 patients exhibited hypertonia in their limbs which was preceded by hypotonia in infancy (Beunders et al., 2016). These patients also exhibited some facial dysmorphism. All reported cases also exhibited feeding difficulties of various severity with frequently reported instances of choking, however, the underlying cause of the feeding difficulties was not determined. So far, 143 individuals have been identified with variants in the AUTS2 locus (SAFARI Gene Database, Retrieved January 2018) with approximately 50 patients which have been described in the literature.

Variants in AUTS2 are distributed throughout the approximately 1.1 Mb locus, and appear to result in haploinsufficiency of the protein. 14 “protein coding” transcripts appear to be expressed from this locus from at least two independent promoters, a standard upstream promoter (ENSR00000213170) and one residing within the 3’ portion of the locus in intron 5 (ENSR00000213289). These multiple promoters appear likely to independently regulate the expression of both “full-length” and “c-terminal” isoforms of Auts2. Mutations which affect the c-terminus of the locus impacting the expression of the c-terminal isoforms have been reported to have more severe Auts2 syndrome scores than variants which affect only the full-length isoforms (Beunders et al., 2013). Morpholino-mediated knockdown of Auts2 expression in zebrafish induced microcephalic phenotypes, consistent with patient findings. Expression of mRNA encoding the human c-terminal variant appeared capable of rescuing this developmental phenotype in zebrafish (Beunders et al., 2013; Oksenberg et al., 2013). This suggests that the c-terminal isoforms of AUTS2 regulated by the internal promoter region encode a critical functional protein which is required for AUTS2 function.

In addition to the eponymous intellectual disability syndrome, polymorphisms in *AUTS2* have been associated with other neurological disorders. *AUTS2* has been linked to schizophrenia (Zhang et al., 2014), epilepsy (Mefford et al., 2010), consumption of alcohol (Kapoor et al., 2013; Schumann et al., 2011), suicide under the influence of alcohol (Chojnicka et al., 2013), response to antidepressants (Myung et al., 2015), and heroin dependence (Dang et al., 2014). The studies which found an association between AUTS2 and alcohol and heroin use identified linkage with the rs6943555 polymorphism located in the fourth intron of Auts2. This SNP sits between two ENCODE annotated enhancers ENSR00000213244 and the overlapping ENSR00000213255/ENSR00000326640. Different SNPs were associated with response to antidepressants, rs7785360, and rs12698828. These two SNPs in intron 2 flank a trio of ENCODE elements annotated as "promoter flanking regions" ENSR00000213214, ENSR00000213215, and ENSR00000213216. The specific regulatory implications of these SNPs are not known, however, their proximity to these annotated regulatory regions within the *AUTS2* locus suggests that they may be linked to altered transcriptional control of *AUTS2* expression. Characterization of AUTS2 several putative enhancer regions in a mouse study identified that these internal regulatory sequences drive expression in tissues (Oksenberg et al., 2013), including brain and muscle at various developmental periods which recapitulate some of the normal expression patterns of Auts2 during development. This suggests the possibility that AUTS2 is a highly dosage sensitive gene where even minor alterations in expression may prove to be pathogenic.

1.3: Regulation and expression patterns of AUTS2

The *AUTS2* locus contains several regions that were identified as the subject of human-specific accelerated evolution. These regions are suspected regulatory elements associated with human-specific neurological evolution. These include Human Accelerated Region (HAR) 31 in intron four (Pollard et al., 2006), and two human-accelerated conserved non-coding sequences (HACNS) in intron one and intron 6, HACNS369 and 174 respectively (Prabhakar et al., 2006). These sequences were included in a set of 40 candidate regulatory regions which were analyzed for their ability to regulate gene expression (Oksenberg et al., 2013). Sequences selected for this study were identified by sequence conservation, ChIP-seq studies and nucleotide variants in the Human-Neanderthal Sweep (Green et al., 2010) for analysis. Utilizing a combination of zebrafish and mouse models, several of these sequences were identified by Oksenberg et al. (2013), to be active enhancers capable of driving gene expression in the central nervous system (including forebrain, midbrain, and cerebellum), as well as somatic muscle and the eye (which is consistent with the observations of altered muscle tone and strabismus in AUTS2 syndrome patients).

This study confined their assessment of regulatory elements to the sequence spanning the first four introns of *AUTS2*. A portion of this region consisting of 293 consecutive SNPs was identified as the most significantly altered region in the comparison between the human and Neanderthal genome (Green et al., 2010). However, subsequent work has implicated the c-terminus of AUTS2, and the independent isoforms expressed from this portion of the locus as necessary for AUTS2's function (Beunders et al., 2013; Oksenberg et al., 2014).

Additional enhancer candidates exist outside the identified 5' sequences studied. These additional regulatory regions are particularly relevant for understanding expression regulation of the c-terminal isoform which is associated with more severe disease, however, these sequences remain an area for future exploration.

Previous work from the Hevner lab examined the developmental expression pattern of Auts2 in mouse brain and the regulatory cascade by which cortical expression of Auts2 is activated (Bedogni et al., 2010a, 2010b). These studies found that the neurodevelopmental T-Box Transcription Factor TBR1 directly binds Auts2 locus regulatory elements and that TBR1 mediated transcriptional activation is necessary for Auts2 expression during cortical development. Auts2 is highly expressed in developing cortical plate, expressing as early as E12 in the first preplate neurons. Some evidence was found that AUTS2 may also be expressed in a subset of PAX6 and TBR2 positive neuronal progenitors during early stages of development. Auts2 expression in the cortex became increasingly restricted throughout development. At birth Auts2 expression localized primarily to rostral cortex with the greatest expression in the superficial cortical layers, but with some expression maintained in TBR1+ layer 5 neurons. Expression continues to decline and become increasingly restricted to frontal cortex during the post-natal period. By P60, cortical plate expression of AUTS2 is all but absent which corresponds to the completion of cortical maturation.

This temporally and spatially restricted expression does not appear to be replicated in other neuronal populations which highly express Auts2, particularly in the hippocampus and cerebellum. Auts2 is highly expressed in cerebellar development, with expression in both

the deep cerebellar nuclei and precursors of cerebellar granule and Purkinje neurons. In the developing cerebellum, Auts2 expression did become increasingly restricted with age, however expression in the mature Purkinje neuronal population did not diminish even in the fully mature cerebellum. Similarly, Auts2 expression in the hippocampus did not diminish with age with both immature and mature granule neurons, as well as a population of hilar neurons expressing Auts2 in perpetuity. This expression pattern suggests that AUTS2 is involved in regulating development of the cortex transiently, however, possesses a long-term role in the maintenance or regulation of properties of hippocampal and cerebellar neurons that is continually necessary for their long-term function. This long-term preservation of AUTS2 expression suggests that these structures might be uniquely involved in the pathogenesis of the AUTS2 syndrome.

1.4: Previous models disrupting AUTS2 propose novel but molecularly inconsistent functions in neurodevelopment

Two previous attempts have been made to understand how alterations in AUTS2 affect nervous system development (Gao et al., 2014; Hori et al., 2014). Two studies developed mouse models which incompletely disrupt the expression of Auts2's multiple isoforms. These studies targeted exons included in the full-length isoform, and a predicted variant with a transcription start site in exon 8, respectively, but did not affect an isoform originating from a transcription start site in exon 9 (Beunders et al., 2015) which was observed to be upregulated in response to upstream Auts2 targeting (Hori et al., 2014). This

oversight renders previous knockout studies incomplete as they fail to target all AUTS2 isoforms. These models leave intact an isoform which has the largest number of human disease-associated variants in the protein, and which was able to rescue phenotypes observed when full length Auts2 was knocked down in the zebrafish brain (Beunders et al., 2013). The upregulation observed by Hori et al. (2014) also suggests the possibility of either a potential auto-regulatory effect of AUTS2 or the existence of a repressor sequence in this region. In order to rectify these oversights, our study has designed a construct which deletes an exon of AUTS2 that is included in all c-terminal containing isoforms and is expected to entirely ablate AUTS2 protein function. These previous studies largely did not attempt to identify pathological changes in the development of brain structures with a high level of Auts2 expression such as the hippocampus or the cerebellum, although one study did identify transient deficits in cortical neuron migration and callosally projecting axon development (Hori et al., 2014). Using our c-terminal deletion model we aim to identify neuronal populations which are affected by AUTS2 deletions which may be masked by the incomplete deletion, and compensatory upregulation observed in previous models.

The AUTS2 protein bears little homology to any characterized protein family, with the only significant homology being to another relatively uncharacterized protein FBRSL1 (Sultana et al., 2002) and both exhibit an extremely low level of homology to the secreted fibrogenic lymphokine Fibrosin (Prakash et al., 1995) – a homology which is unlikely to have functional relevance due to the substantial differences in both sequence, and localization of the proteins.. In order to determine the function of AUTS2, the two previously described studies performed some molecular analysis of AUTS2's protein-protein interactions. One study

identified a novel Polycomb complex which recruits AUTS2 (Gao et al., 2014). The authors claimed that this complex subsequently recruits EP300 to acetylate histone tails enabling transcriptional activation, a canonical function of EP300. This process appeared to be dependent upon recruitment of Casein kinase II to phosphorylate EP300. Mutations in EP300 and its highly homologous family member CREBBP are implicated in the pathogenesis of Rubinstein-Taybi Syndrome (Van Belzen et al., 2011), and mutations in CSNK2A1 which encodes a subunit of Casein Kinase are a cause of Okur-Chung neurodevelopmental syndrome (Okur et al., 2016). However, while these experiments supported AUTS2's role as a transcriptional coactivator, they were largely performed by forced expression of Auts2 in non-neuronal cell lines and neither the transcription factors targeted by this complex nor the in-vivo molecular consequences of AUTS2's genetic regulation were investigated. A second study identified a potential role for AUTS2-dependent regulation of cytoskeletal assembly to promote outgrowth of lamellipodia and regulate neuronal migration (Hori et al., 2014). The effects observed in this study were dependent on AUTS2 activation of RAC1 activity through regulation of the Rho guanine nucleotide exchange factor PREX1 and required AUTS2 to localize to the cytoplasm. These two proposed mechanisms of AUTS2 function are extremely different from one another. They did not identify any shared molecular adapters and the functions required localizing to different cellular compartments, yet they both appeared to be dependent, at least partially, on the same n-terminal domain, which is not contained within the c-terminal, nuclear localizing, isoform of the protein. This leaves several unanswered questions about AUTS2's molecular function: what is the true interactome of the AUTS2 protein, what is the function

of the c-terminal isoform, what is the developmental expression pattern of the isoforms, and is there a single mechanism which can explain both molecular actions?

1.5: Functional relevance of EP300 and CSNK2A1 to neurodevelopmental syndromes

A previous study identified an interaction between AUTS2 and the histone acetylase EP300. These proteins are both linked to developmental neurocognitive disorders in patients. Loss of function variants in EP300 resulting in haploinsufficiency have been identified as a cause of Rubenstein-Taybi syndrome (RTS) (Foley et al., 2009; López et al., 2018; Roelfsema et al., 2005; Zimmermann et al., 2007). Approximately 8% of RTS patients carry EP300 mutations with the majority carrying mutations in the highly homologous CREB Binding Protein (CBP). RTS patients carrying EP300 mutations exhibit a number of phenotypic features which resemble the AUTS2 syndrome. These included autistic features, intellectual disability, microcephaly, infant feeding difficulty, psychomotor and language delay, and facial dysmorphisms (López et al., 2018). As in AUTS2 syndrome a minority of RTS patients present with a seizure disorder (Schorry et al., 2008)

Additional mutations have been identified in EP300 and CREBBP which exhibit distinctions from RTS, however, these too exhibit similar phenotypic overlap with the AUTS2 syndrome including developmental delay, autistic behaviors, microcephaly, and feeding difficulty (Menke et al., 2018).

Mouse models of RTS have been designed which affect both CBP, which accounts for the majority of RTS patients, as well as EP300. A mouse model of CBP mediated RTS exhibited

reduced neonatal vocalization (Wang et al., 2010) which was a phenotype also observed in the incomplete Auts2 mutant mice generated by Gao et al. An EP300 loss of function mouse model exhibited deficits in long-term memory formation as well as hippocampus-dependent contextual fear memory (Oliveira et al., 2011). Heterozygous Auts2 deletion mice have also been shown to exhibit deficits in fear responses related to associative memory formation (Hori et al., 2015).

Additionally, AUTS2 was identified to interact with the catalytic subunits of Casein Kinase CSNK2A1 and CSNK2A2. Mutations in CSNK2A1 have been linked to the rare Okur-Chung neurodevelopmental syndrome (OCNS) (Okur et al., 2016). OCNS, like RTS patients, exhibit intellectual disability, developmental delay, and behavioral problems, accompanied by hypotonia, dysmorphic features, speech problems and microcephaly. Patient MRIs revealed pachygyria (incomplete lissencephaly) in 3/5 patients, a feature indicative of neuronal migration defects (Pang et al., 2008) such as that caused by mutations in the gene RELN (Chang et al., 2007), another ASD linked neurodevelopmental gene.

1.6: RAC1 signaling in neurodevelopment

Some isoforms of AUTS2 may localize to the cytoplasm of neurons, however, the developmental stage of cytoplasmic AUTS2 localization, if it occurs in-vivo, is unclear. However, cytoplasmic AUTS2 was shown to interact with the Rho guanine nucleotide exchange factor PREX1 to regulate activation of RAC1 signaling in cultured cells, including cultured hippocampal neurons (Hori et al., 2014). The significance of PREX1 dependent RAC1 signaling regulation in neurodevelopment is less clear than that for the nuclear AUTS2

interaction partner EP300. However, AUTS2 mediated activation of RAC1 signaling appeared to be involved in process outgrowth in cultured neurons, and potentially axon outgrowth in the cortex. This effect appeared to be dependent on PREX1, however, PREX1 mutations are not associated with any known human neurodevelopmental syndromes, and the effect of RAC1 mutations on human neurodevelopment is also unclear. Specific deletions of PREX1 in mouse models did not identify any significant neurological abnormalities, although a compound deletion of PREX1 and PREX2 exhibited significant abnormalities in the development of Purkinje neuron processes (Donald et al., 2008).

There is some evidence, however, that RAC1 signaling processes may, in fact, be involved in the regulation of neuronal migration. Localized activation of RAC1 signaling has been shown to occur directly in response to RELN signaling (Leemhuis and Bock, 2011). RELN mutant mice exhibit substantial abnormalities in neuronal development including a characteristic “inside-out” presentation of cortical lamination, as well as substantial abnormalities in hippocampal development including truncated infrapyramidal blade development and granule neuron disorganization (Ha et al., 2017). This implies that proper activation of RAC1, mediated by AUTS2 dependent PREX1 signaling, may be necessary for RELN regulated migration of neurons and neuronal progenitors. RAC1 activation mediated by AUTS2-PREX1 signaling may play a minor role in the cellular response to RELN, and AUTS2 mutations may result in reduced response to RELN signaling in normally AUTS2 expressing cells. If this were the case, an overlap in neuroanatomical abnormalities that depend on RELN between AUTS2 mutants and RELN mutants may be expected. Notably,

mutations in RELN are also a known cause of Autism syndrome pathology in patients (Fatemi, 2002).

1.7: Summary

Autism and autism-like intellectual disability syndromes present with a diverse array of symptoms, neurodevelopmental alterations, and co-morbidities. The genes involved in these syndromes are frequently involved in the pathogenesis of other neurodevelopmental disorders such as schizophrenia and epilepsy. AUTS2 is one such gene with links to the pathogenesis of an intellectual disability syndrome, developmental delay, behavioral disorders, schizophrenia, and epilepsy. The AUTS2 syndrome also represents a potential intersection point of the rare Rubenstein-Taybi, and Okur-Chung neurodevelopmental syndromes through its interaction partners - EP300 in the case of Rubenstein-Taybi and Casein Kinase in Okur-Chung. Previous analysis of AUTS2's molecular functions which identified functions dependent on these proteins provides a potential framework for beginning to understand how AUTS2 may regulate neurodevelopment and contribute to the pathogenesis of these disorders, through altering transcriptional programs in new neurons and regulating how they migrate and integrate into networks. These syndromes and the AUTS2 syndrome have a number of pathological features in common, including their intellectual disability, developmental delay, speech pathology and microcephaly phenotypes, and appear to be linked by a common molecular pathway. The implications of this "molecular family" of neurodevelopmental syndromes are unclear, however, the identification of clusters of molecularly linked syndromes may inform future research into

potential avenues of treatment. Variances in the presentation of these syndromes may be due to differential expression of AUTS2 and its interactors in non-brain tissues, as well as variable developmental expression patterns. As these molecular pathways become better understood, identification of additional interacting and co-regulating proteins through protein-protein interaction networks and elucidation of signaling cascades may enable the identification of other members of this potential syndromic family. Previously, much of this work has taken place in cultured cells and non-neuronal cell lines with ectopically expressed proteins, and a substantial gap exists in determining how AUTS2 executes its action, what other interactions partners may exist, and which isoforms of AUTS2 are functionally relevant in developing brain tissue. Furthermore, the proposed molecular actions of AUTS2 in previous research are inconsistent with a distinct molecular mechanism and require AUTS2 to perform a wildly divergent molecular activity from the same protein domain depending on how the protein localizes. Our work aims to elucidate the molecular action of AUTS2 in its native context through the study of brain regions which express it during normal development and to assess the impact of the loss of AUTS2 in structures which express it perpetually.

We identify an additional AUTS2 containing protein complex which appears to be involved in regulation of mRNA splicing activity through an interaction with the RNA-Binding protein NONO. NONO, like other proteins which have been found to interact with AUTS2, appears associated with a distinct neurodevelopmental syndrome, however, its phenotypes appear in opposition to AUTS2 (Mircsof et al., 2015; Scott et al., 2017). This complex appears to target mRNAs encoding the effectors identified in previous studies which are

downregulated in Auts2 cKO animals. We perform additional pathway analysis to determine how AUTS2 and NONO regulate affected molecular pathways in these disease models. We also identify distinct morphological defects in the hippocampal development of Auts2 cKO animals which resemble, in some respects, the REELER mouse neural progenitor phenotype with the additional phenotype of a near total loss of hilar mossy neurons. We additionally identify abnormalities of respiratory rhythm generation in both whole CNS and forebrain-specific models of AUTS2 deletion. Finally, we identify electrophysiological abnormalities in the AUTS2 deficient mice with implications for understanding the comorbidity of autism spectrum disorder and epilepsy.

Chapter 2: An AUTS2-Containing RNA-Binding Complex Regulates Transcript Expression in Developing Cerebral Cortex

2.1: INTRODUCTION

In humans, *Autism Susceptibility Candidate 2* (*AUTS2)* variants and disruptions are a rare but well-established cause of intellectual disability (ID), developmental delay, autistic features, and other neurological and somatic disorders, which together define the *AUTS2* syndrome (Beunders et al., 2016; McRae et al., 2017; Sultana et al., 2002). However, the underlying mechanisms by which *AUTS2* disruptions cause specific neurological deficits are not understood. This is, in part, because the *AUTS2* gene has no close homologues and no recognized domain structures that would suggest specific functions. Furthermore, the gene is very large and complex, with 19 exons (in humans and mice), and two main protein isoforms: a full-length isoform of ~139 kDa, and a C-terminal isoform of ~79 kDa produced from a transcriptional start site in exon 9 (Beunders et al., 2013; Hori et al., 2014). The C-terminal isoform, corresponding to "variant 2" of Hori et al. (2014), is thought to be functional, as indicated by genotype-phenotype correlations in humans, and rescue assays in zebrafish (Beunders et al., 2013). An additional possible isoform originating one exon upstream of variant 2 —"variant 1" of Hori et al. (2014)—has also been predicted.

Previously, we reported that *Auts2* in mice is highly expressed in developing cerebral cortex, especially frontal cortex, and in other brain areas (such as cerebellum) that are important in the pathogenesis of autism and/or ID (Bedogni et al., 2010a). We also found that AUTS2

protein, detected by immunofluorescence with an antibody that recognizes both isoforms, was localized predominantly or exclusively in cell nuclei, and was present in specific subsets of neurons and neuronal precursors, but not in glial cells. These findings suggested that AUTS2 is important for nuclear functions (such as transcription) during the development of some neurons, including glutamatergic projection neurons in the cerebral cortex.

More recently, the functions of AUTS2 were investigated using *Auts2* conditional mutant mice (Gao et al., 2014; Hori et al., 2014). The mutant mice exhibited distinct behavioral and morphological abnormalities, such as craniofacial malformations and loss of normal vocalizations, consistent with some human *AUTS2* syndrome phenotypes. However, these models, in which exon 7 (Gao et al., 2014) or exon 8 (Hori et al., 2014) were deleted, disrupted expression of only the long isoform of AUTS2, and left expression of the C-terminal isoform intact, or even elevated (Hori et al., 2014). Moreover, the functions attributed to AUTS2 were completely different between studies: one reported that AUTS2 interacts with Polycomb repressive complex 1 (PRC1) to regulate transcription (Gao et al., 2014), while the other reported that AUTS2 functions in cytoplasm to regulate cytoskeletal organization and neurite outgrowth (Hori et al., 2014). While AUTS2 could potentially have multiple independent molecular functions, these discrepancies emphasize the necessity of further studies to elucidate AUTS2 functions.

Towards this goal, we generated a new mouse model in which *Auts2* exon 15 is conditionally deleted to generate a frameshift and premature stop codon, thus reducing the expression of both AUTS2 isoforms and achieving conditional knockout (cKO). In addition, we performed

an updated bioinformatic analysis of the AUTS2 protein sequence and identified novel partner proteins that interact with AUTS2. Since these studies suggested that AUTS2 might be involved in RNA binding and processing, we tested this possibility using AUTS2 antibodies for RNA immunoprecipitation and sequencing (RIP-seq). Also, we profiled mRNA expression by RNA purification and sequencing (RNA-Seq) in frontal cortex from *Auts2* cKO and control neonatal mice and compared changes in the transcriptome with mRNA bound by AUTS2 complex (RIP-seq), and with genomic regions bound by AUTS2, as determined by AUTS2 chromatin immunoprecipitation and sequencing (ChIP-seq) from a previous study (Gao et al., 2014).

Our results suggest that AUTS2 participates in a complex that bridges transcription initiation with the processing of nascent mRNAs. In this complex, AUTS2 interacts with NONO/p54^{NRB}, and other proteins that have been implicated in RNA processing. Importantly, we found that transcripts dysregulated in *Auts2* cKO frontal cortex overlapped much more robustly with mRNA bound by AUTS2 complex (RIP-seq) than with genes bound by AUTS2 complex (ChIP-seq), supporting the conclusion that AUTS2 functions primarily as a regulator of RNA processing. Finally, remarkable correlations in the phenotypes of human *AUTS2* and *NONO* syndromes also reinforce this conclusion. In sum, the present study identifies a novel function of AUTS2 in RNA processing, which may complement or underlie previously reported functions of AUTS2 in transcriptional regulation and cytoskeletal organization.

2.2: RESULTS

2.2.1: Bioinformatic analysis reveals domains that implicate AUTS2 in RNA processing

Experimental data on AUTS2 structure are not available and are unlikely to be generated with current techniques due to the extremely disordered nature predicted from the peptide sequence. In order to form hypotheses as to AUTS2's function, bioinformatic approaches, utilizing comparisons of sequence motifs to other proteins have been utilized. The most recent previous bioinformatic analysis of AUTS2 was reported more than 15 years ago (Sultana et al., 2002). Since then the amount of public information on protein sequences, across the evolutionary tree has increased nearly 700-fold (from 163,235 sequence entries in UniProt 3.0 in 2004 to 111,425,245 sequence entries in March 2018). This explosion of bioinformatic resources has enabled significant improvements in bioinformatic protein function prediction. In the present study, we conducted a new bioinformatic analysis of AUTS2, which takes advantage of the significant recent expansion of protein structure databases and understanding of protein structure-function relationships to train machine-learning algorithms.

Standard sequence analysis indicated that both AUTS2 isoforms (full-length and C-terminal) contain nuclear localization sequences identified by cNLS Mapper (Kosugi et al., 2009), as well as proline- and/or histidine-rich sequences, and are highly basic (predicted pI >9.25), as typical of nuclear proteins (Schwartz et al., 2001). In addition, several putative domains were newly identified in AUTS2 using different tools.

The NCBI Conserved Domain tool identified a PAT1 (Protein associated with Topoisomerase II/Processing body mRNA decay factor) superfamily domain (amino acids 297-490), previously annotated in part as containing proline-rich and Dwarfin homology regions (Sultana et al., 2002). This domain, present only in the full-length AUTS2 isoform, is implicated in translation repression, mRNA uncapping, and targeted degradation of specific mRNAs (Pilkington and Parker, 2008). Interestingly, the putative PAT1 domain of AUTS2 partially overlaps regions previously associated with the lamellipodia-inducing activity (Hori et al., 2014) and transcriptional activating activity (Gao et al., 2014). These domains reside primarily in the N-terminus of the AUTS2 protein.

Utilizing the ProDom database of protein domain predictions (Bru et al., 2005) we identified four more putative domains in AUTS2, one in the N-terminal region and three in the C-terminal region **(Figure 1A)**. One of the ProDom-predicted C-terminal domains (PD360677) is homologous across the AUTS2/Fibrosin-like superfamily and is dubbed the "AUTS domain" (pfam15336). These analyses suggest that the developmentally enriched, C-terminal isoform has core functions conferred by the AUTS2 domain, as well as PDC8X5A6 and PD718162 domains. Full-length AUTS2 contains, in addition to these core domains, PAT1 and PD718837 domains **(Figure 1B)**.

To determine if the putative domains of AUTS2 are associated with specific molecular functions, the peptide sequence of each domain was submitted to UniGOPred (Rifaioglu et al., 2018). The domains identified by ProDom scored significantly for multiple functions, including predicted DNA and RNA binding activity **(Table 1)**.

In order to assess which domains are likely to be biologically relevant for the developmental functions of AUTS2, we assessed the N and C terminal expression of AUTS2 proteins by performing immunohistochemistry on adjacent sections. In-house designed antibodies for the AUTS2 N-terminus and AUTS2 C-terminus. These experiments determined that the N-terminal isoform is not expressed at detectable levels in the neonatal cortex **(Figure 1C)** however the C-Terminal isoform is strongly expressed in the neonatal cortical plate **(Figure 1D)**. Notably, both isoforms were detected in the neonatal cerebellum (Figure 1(C2), and (D2) respectively). Based on this expression pattern, we conclude that the N-terminal resident domains identified in the previous assessments of AUTS2 molecular function are not likely to be substantially involved in the developmental function of AUTS2 in the cortical plate and that it is rather the C-terminal domains that confer AUTS2's molecular action.

A prior study of the RNA-Bound Proteome identified FBRSL1 (fibrosin-like 1), one of the few proteins with significant homology to AUTS2 and which shares sequence motifs such as a Poly-HQHT repeat, as a candidate RNA-binding protein (Baltz et al., 2012). AUTS2 has previously been shown to associate with chromatin (Gao et al., 2014; Oksenberg et al., 2014), however, the potential for AUTS2 to bind RNA has not been assessed. Many RNA-binding proteins transiently associate with nucleosomes in transcriptionally active chromatin, and that nucleosome architecture is intricately involved in splicing regulation (Allemand et al., 2016; Kfir et al., 2015). Based on these considerations, we hypothesized that AUTS2 may exhibit co- or post-transcriptional regulation of mRNA processing through RNA binding interactions.

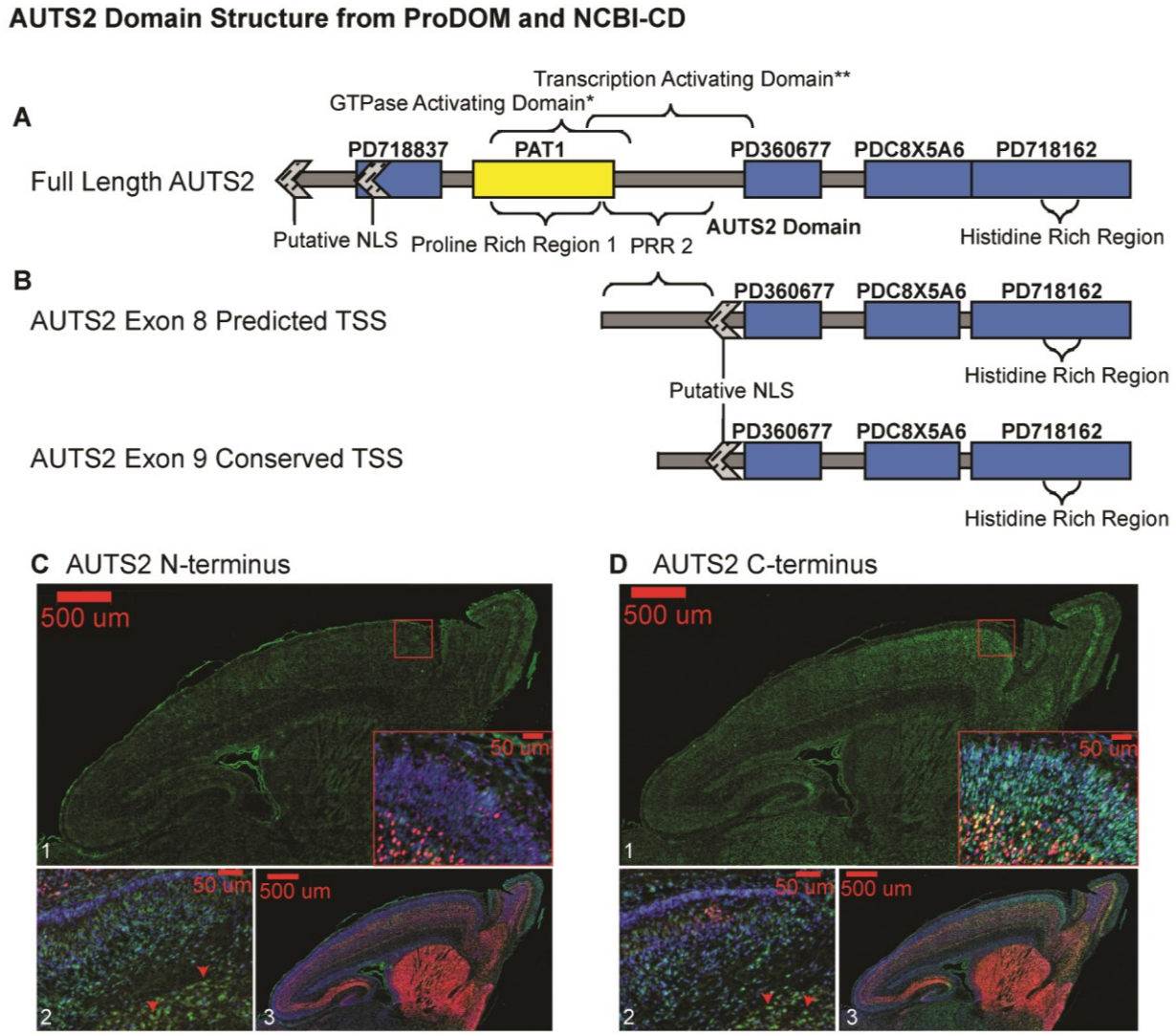

Figure 1: Putative domain structure of murine AUTS2 generated from NCBI-CD and ProDom searches of UNIPROT reference A0A087WPF7 and expression of the N vs. C terminal sequence

(A) Two N-terminal specific conserved domains identified in full-length AUTS2, including a PAT1 domain. *=Rho GTPase regulatory region (Hori et al., 2014). **=Transcriptional Activation associated region (Gao et al., 2014). **(B)** Additional domains identified in full length and C-terminal isoforms originating from Exon 8 and Exon 9 of the *Auts2* locus. PD360677 corresponds to the canonical AUTS2 superfamily domain (pfam15336). **(C)** Immunofluorescent staining of an antibody generated against N-terminal AUTS2 amino acids 1-17 (1) in the P0.5 cortex (inset – magnified frontal cortex) (2) in P0.5 exposure matched cerebellum. (3) co-localized with CTIP2 a marker of L5/L6 cortical neurons. **(D)** Immunofluorescent staining of an antibody generated against C-terminal AUTS2 amino acids 1245-1261 (1) in the P0.5 cortex (inset – magnified frontal cortex) (2) in P0.5 exposure matched cerebellum. (3) co-localized with CTIP2 a marker of L5/L6 cortical neurons

Table 1: UniGoPred analysis of AUTS2 domain sequences.
GO term prediction scores (probability) >0.90

Domain	GO Term	Definition	Prediction Score
PD718837	GO:0008092	cytoskeletal protein binding	0.98
	GO:0003723	RNA binding	0.95
	GO:0044822	poly(A) RNA binding	0.93
	GO:0003676	nucleic acid binding	0.92
PAT1	GO:0005102	receptor binding	0.99
	GO:0003676	nucleic acid binding	0.99
	GO:0003677	DNA binding	0.98
	GO:1901363	heterocyclic compound binding	0.96
	GO:0030246	carbohydrate binding	0.93
	GO:0043565	sequence-specific DNA binding	0.93
PD360677	GO:0044822	poly(A) RNA binding	0.96
	GO:0003723	RNA binding	0.96
PDC8X5A6	NO Terms Over .90 Cutoff	N/A	N/A
	GO:0005515	protein binding	0.84
PD718162	GO:0001085	RNA polymerase II transcription factor binding	0.96
	GO:0005102	receptor binding	0.93
	GO:0003723	RNA binding	0.92
	GO:1901363	heterocyclic compound binding	0.9

2.2.2: AUTS2 interacts with multifunctional RNA-processing proteins

The bioinformatic analysis of AUTS2 suggested a potential ability to associate with mRNAs. However, AUTS2 is not known to contain any canonical RNA (or DNA) recognition motifs. We hypothesized that AUTS2 might function as part of an RNA-binding protein complex.

To identify proteins that interact with AUTS2 and may facilitate interactions with RNA, we utilized antibodies against AUTS2 for immunoprecipitation of native complexes from neonatal cortical nuclear lysate. We then performed mass spectrometry of the immunoprecipitated complex to identify the proteins bound to AUTS2. The complex isolated by this procedure included, in addition to several histones, NONO (Non-POU Domain Containing Octamer Binding Protein; also known as $P54^{NRB}$), a member of the *Drosophila Behavior/Human Splicing* (DBHS) protein family; DDX5 and DDX17 RNA helicases; HNRNPA2B1, an RNA-binding protein that associates with pre-mRNAs; and multiple splicing factors **(Table S1)**.

Analysis of these data using the STRING database of protein-protein interactions (Szklarczyk et al., 2015) identified a known protein interaction network. This network consisted primarily of two classes of proteins: RNA-processing components and nucleosome-associated protein-DNA complex assembly proteins. **(Figure 2A, Supplementary).** STRING's internal GO: Molecular Function analysis indicated that the most significant enrichment of proteins was associated with RNA-processing, RNA Binding, and Poly(A) RNA binding, and the KEGG Spliceosome pathway **(Table S2)**. This finding is consistent with our bioinformatic predictions of AUTS2 domain function, which identified

candidate RNA-interacting domains, and domains involved in association to RNA-Polymerase II-dependent active transcription (**Table 1**).

The most highly enriched non-histone protein in the complex was NONO (**Table S1**). Like other DBHS family proteins, NONO is involved in multiple levels of RNA metabolism (Knott et al., 2016): transcriptional activity, pre-mRNA processing, mRNA localization, and translation. To confirm the AUTS2 interaction with NONO, we performed reciprocal co-IP western blots on proteins extracted from P0.5 cortex (**Figure 2 B, C**).

To further validate the potential for an interaction of AUTS2 and NONO in the developing brain *in vivo*, we compared their distribution by double-label immunofluorescence at several developmental ages. We found that NONO is co-expressed with AUTS2 in the nuclei of neurons in the cortical plate (**Figure 2 D-G**). Indeed, virtually all AUTS2 positive cells appeared to express NONO. An assessment of the expression patterns of several other candidate AUTS2 interacting proteins using the GenePaint atlas (Visel, 2004) indicated that these proteins also exhibit the spatiotemporal expression patterns necessary for interaction with AUTS2 in neurons (**Figure S1**).

Together, these data implicated AUTS2 in a protein interaction network which couples nucleosome reorganization at transcriptionally active chromatin to co- and post-transcriptional processing of nascent mRNA. Moreover, these data substantiate the bioinformatic analysis implicating AUTS2 in RNA processing.

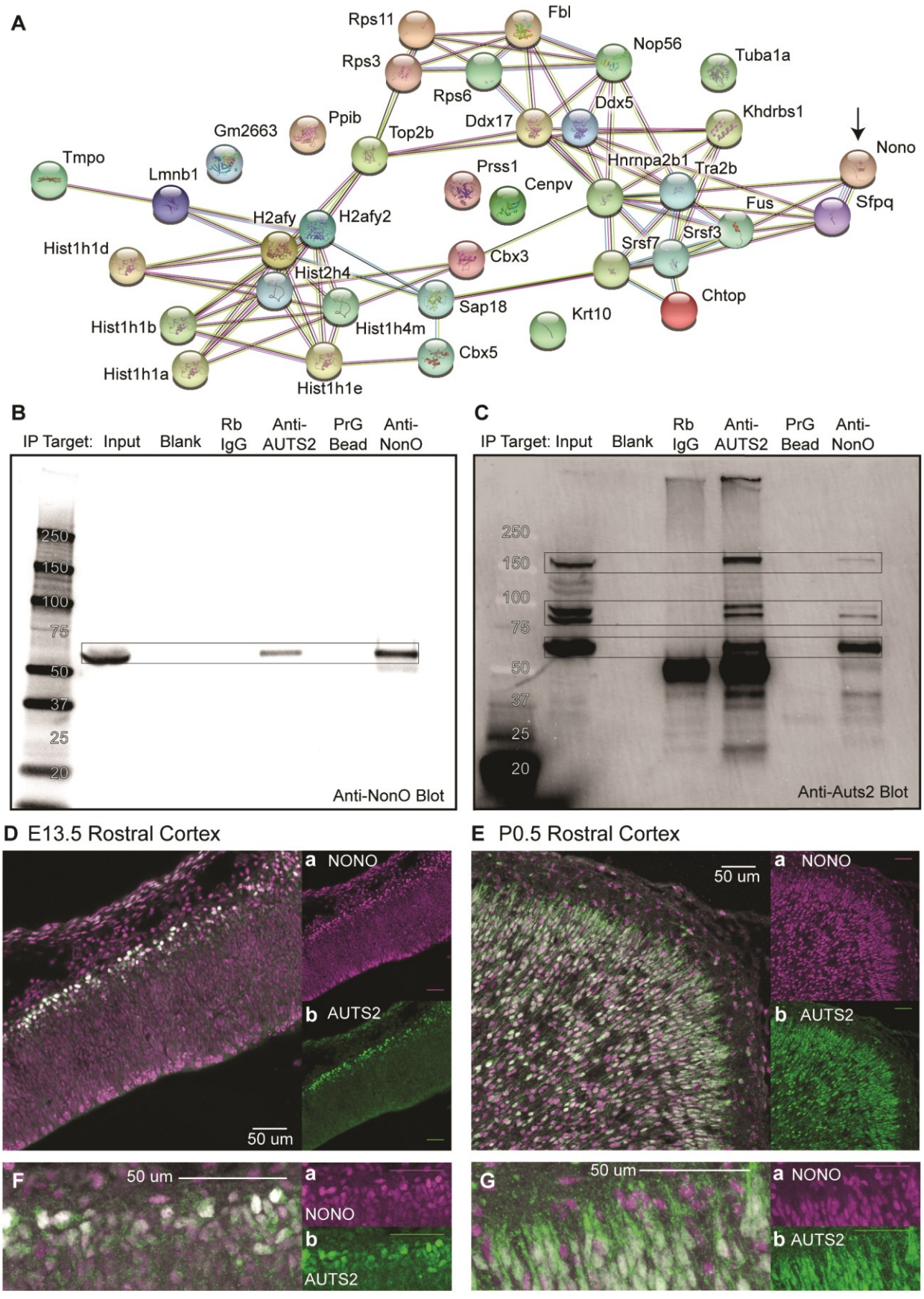
A
Rps11
Fbl
Nop56
Rps3
Tuba1a
Rps6
Ddx5
Khdrbs1
Ppib
Ddx17
Gm2663
Top2b
Nono
Tmpo
Hnrnpa2b1
Tra2b
Prss1
Cenpv
Lmnb1
Fus
Sfpq
H2afy
H2afy2
Srsf3
Srsf7
Hist1h1d
Cbx3
Hist2h4
Chtop
Sap18
Krt10
Hist1h1b
Hist1h4m
Cbx5
Hist1h1a
Hist1h1e
B
IP Target: Input Blank Rb IgG Anti-AUTS2 PrG Bead Anti-NonO
250
150
100
75
50
37
25
20
Anti-NonO Blot
C
IP Target: Input Blank Rb IgG Anti-AUTS2 PrG Bead Anti-NonO
250
150
100
75
50
37
25
20
Anti-Auts2 Blot
D E13.5 Rostral Cortex
a NONO
b AUTS2
50 um
E P0.5 Rostral Cortex
50 um
a NONO
b AUTS2
F
50 um
a
NONO
b
AUTS2
G
50 um
a NONO
b AUTS2

Figure 2: Identification of AUTS2 complex partners and validation of the AUTS2-NONO interaction

(A) STRING-DB Network summary view of the top 25% Spectra/Length of AUTS2 interaction partners isolated from neuronal lysate. Network PPI Enrichment P=1.0e-16

(B) IP-Western of AUTS2 and NONO IPs probed for NONO.

(C) IP-Western of AUTS2 and NONO IPs probed for AUTS2.

(D-F) Confocal images of 12 uM C56BL6/J cortical plate sections stained for AUTS2 (Green) and NONO (Magenta) at E13.5 **(D)**, and P0.5 (**E)**, 63X Oil immersion images **(F, G)**.

2.2.3: The AUTS2 complex binds specific RNA transcripts in developing cerebral cortex

To test the hypothesis that an AUTS2 complex binds RNA in developing cortical neurons, we used AUTS2 antibodies for RIP-Seq of neonatal cortex lysate. We identified 1208 transcripts that were significantly enriched over both IgG and input control samples ($q<0.05$) in these samples **(Figure 3A, Table S3)**. This result confirmed that the AUTS2 complex binds specific RNAs in developing cortex.

To identify molecular functions and biological processes regulated by AUTS2 complex-bound mRNAs, we performed GO analysis of these transcripts using geneSCF (Subhash and Kanduri, 2016). This analysis identified 27 Molecular Function terms, corresponding to 6 Biological Processes, that were significantly enriched (Benjamini and Hochberg FDR <0.05) in the AUTS2 complex bound mRNAs **(Figure 3 B, C).** The top 3 Biological Processes were mRNA processing, regulation of GTPase activity, and covalent chromatin modification. These Biological Processes were associated with Molecular Functions of, among others, helicase activity, chromatin binding, Rac/Rho GTPase regulation, and actin/microtubule binding **(Table S4)**.

Also notably, transcripts encoding both EP300, the effector of AUTS2-mediated transcriptional activation activity identified in one previous study (Gao et al., 2014), and PREX1, the effector of AUTS2 function identified in another previous study (Hori et al., 2014), were significantly enriched in the AUTS2-mRNA complex. The Biological Processes and Molecular Functions mediated by AUTS2 complex-bound mRNAs are overall consistent with previous reports that AUTS2 activates transcription (Gao et al., 2014) and regulates of

Rho/Rac-dependent cytoskeletal reorganization (Hori et al., 2014). These observations suggest an alternative explanation of how AUTS2 regulates transcription and cytoskeletal organization, by controlling the processing of mRNAs encoding transcriptional and cytoskeletal regulatory proteins.

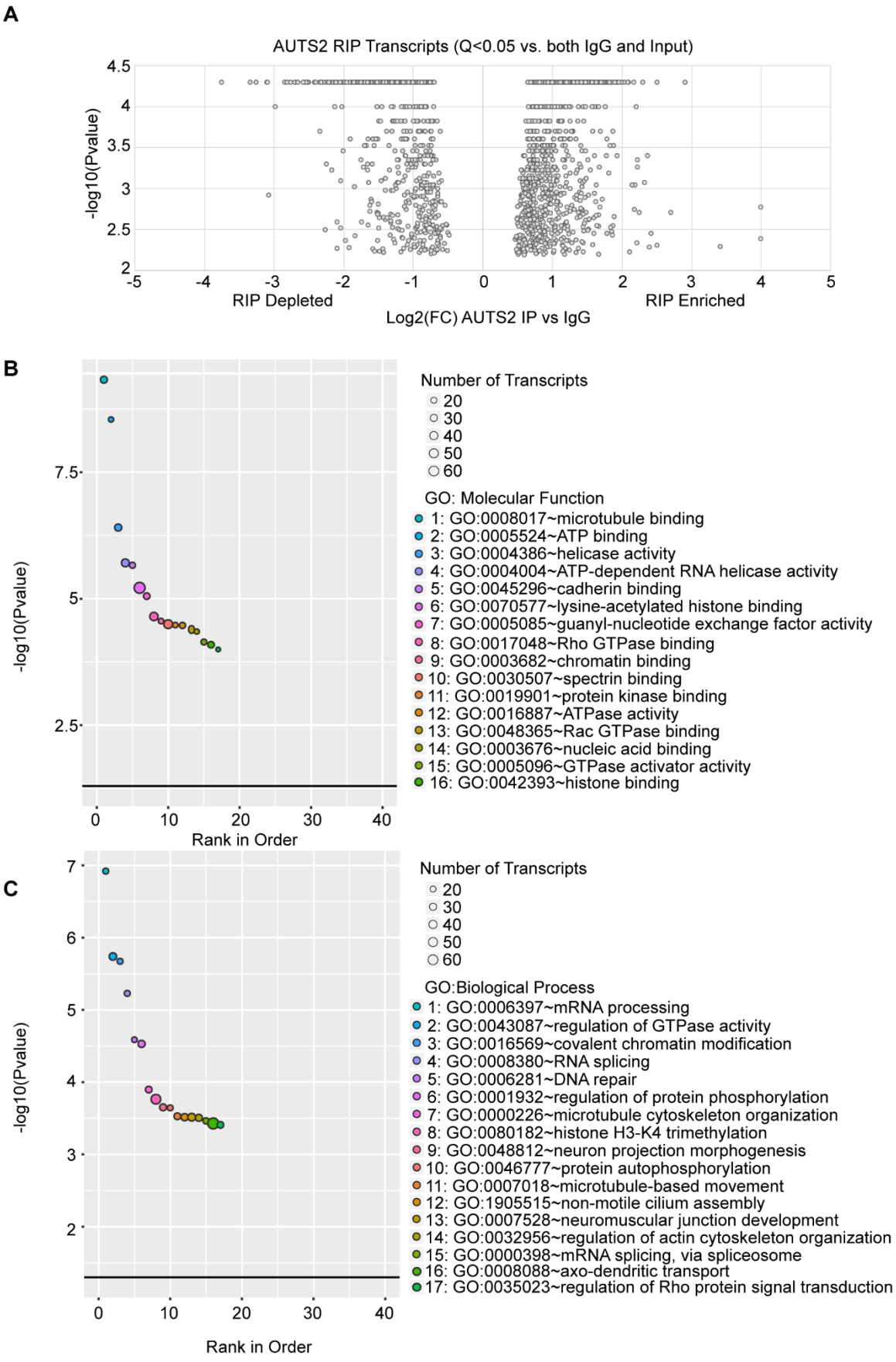
A
AUTS2 RIP Transcripts (Q<0.05 vs. both IgG and Input)
-log10(Pvalue)
RIP Depleted
RIP Enriched
Log2(FC) AUTS2 IP vs IgG
B
-log10(Pvalue)
Rank in Order
Number of Transcripts
20
30
40
50
60
GO: Molecular Function
1: GO:0008017~microtubule binding
2: GO:0005524~ATP binding
3: GO:0004386~helicase activity
4: GO:0004004~ATP-dependent RNA helicase activity
5: GO:0045296~cadherin binding
6: GO:0070577~lysine-acetylated histone binding
7: GO:0005085~guanyl-nucleotide exchange factor activity
8: GO:0017048~Rho GTPase binding
9: GO:0003682~chromatin binding
10: GO:0030507~spectrin binding
11: GO:0019901~protein kinase binding
12: GO:0016887~ATPase activity
13: GO:0048365~Rac GTPase binding
14: GO:0003676~nucleic acid binding
15: GO:0005096~GTPase activator activity
16: GO:0042393~histone binding
C
-log10(Pvalue)
Rank in Order
Number of Transcripts
20
30
40
50
60
GO:Biological Process
1: GO:0006397~mRNA processing
2: GO:0043087~regulation of GTPase activity
3: GO:0016569~covalent chromatin modification
4: GO:0008380~RNA splicing
5: GO:0006281~DNA repair
6: GO:0001932~regulation of protein phosphorylation
7: GO:0000226~microtubule cytoskeleton organization
8: GO:0080182~histone H3-K4 trimethylation
9: GO:0048812~neuron projection morphogenesis
10: GO:0046777~protein autophosphorylation
11: GO:0007018~microtubule-based movement
12: GO:1905515~non-motile cilium assembly
13: GO:0007528~neuromuscular junction development
14: GO:0032956~regulation of actin cytoskeleton organization
15: GO:0000398~mRNA splicing, via spliceosome
16: GO:0008088~axo-dendritic transport
17: GO:0035023~regulation of Rho protein signal transduction

Figure 3: Enrichment analysis of the AUTS2 complex targeted transcriptome

(A) Volcano plot of all transcripts with significant (Cuffdiff Q<0.05) differential enrichment between AUTS2 RIP and both IgG RIP control, and 10% Input control. Values plotted are for enrichment over IgG sample.

(B) geneSCF calculated GO: Molecular function terms enriched (Benjamini and Hochberg (FDR) <0.005) in the AUTS2 Complex RIP-Target Transcripts.

(C) GO: Biological Process terms enriched (Benjamini and Hochberg (FDR) <0.1) in the AUTS2 RIP-Target Transcripts

2.2.4: *Auts2* inactivation alters transcript expression in developing cerebral cortex

In order to conditionally inactivate full-length as well as C-terminal AUTS2 isoforms, we produced a novel *Auts2* conditional knockout (cKO) allele, with LoxP sites flanking exon 15 **(Figure 4A(1)).** Deletion of exon 15 induces a frameshift in the *Auts2* transcript when exon 14 is spliced to exon 16. A frameshift is also induced in the event of exon 14 splice junction with exon 17 (a rare event detected in our RNA-seq data). Analysis of RNA-Seq reads mapped to the *Auts2* locus determined that exon 15 exhibits no detectable instances of alternative splicing in control mouse brain and is thus included in all native *Auts2* transcripts **(Figure 4A(2))**.

Since *Auts2* inactivation in the whole central nervous system caused spontaneous neonatal death (data not shown), for the present study we used *Emx1*-Cre mice to drive recombination (Gorski et al., 2002). In these mice, recombination is restricted to glutamatergic neurons of the dorsal telencephalon, including Cajal-Retzius, subplate, hippocampal, and cortical plate pyramidal neurons. In *Auts2* cKO mice, expression of *Auts2* mRNA was confirmed to be reduced in forebrain by qPCR (not shown), and by RNA-seq; and AUTS2 protein was undetectable by immunohistochemistry **(Figure 4B).** While *Auts2* cKO (*Emx1*-Cre) mice were born in a mendelian ratio, survival was reduced in the immediate postnatal period. Pups that survived the neonatal period reached maturity and bred successfully.

The brains of *Auts2* cKO mice exhibited no gross morphological abnormalities. Cortical layers and somatosensory barrels also appeared normal (Supplementary Figure S1),

indicating that AUTS2 does not play a critical role in cortical lamination or patterning. Rather, AUTS2 may play a more subtle role in neuronal maturation, such as in regulation of neurite growth or synaptic plasticity.

To investigate how neuronal molecular programs are altered in *Auts2* cKO cortex, we dissected rostral (frontal) cortex from quartets of P0.5 control (no Cre) and *Auts2* cKO mice to perform RNA-seq. Comparison of the transcriptomes identified 58 differentially expressed transcripts with FDR q<0.05, including two *Auts2* mRNA sequences **(Table S2)**, and 383 transcripts with p<0.01.

The list of 383 differentially expressed transcripts with p<0.01 was submitted for gene ontology (GO) analysis. Biological processes associated with these transcripts included positive and negative modulation of DNA-templated transcription, Notch signaling, cell differentiation, regulation of neurogenesis, sterol biosynthesis, axon guidance, cell adhesion, and locomotor behavior **(Figure 4C)**. These pathways represent critical biological processes in the development and integration of newborn neurons into cortical networks and furthermore overlap with previously reported biological functions of AUTS2 in transcriptional activation (Gao et al., 2014) and neurite outgrowth (Hori et al., 2014).

To confirm results from RNA-seq, we used *in situ* hybridization (ISH) to study the expression of *Penk*, which was significantly upregulated in *Auts2* cKO cortex according to RNA-seq ($log_2FC=1.43$; p=5E-05, q=0.032) By ISH in P0.5 mice, we found that *Penk* was dramatically upregulated in a subset of cortical layer 1 cells in *Auts2* cKO mice, presumably corresponding to Cajal-Retzius neurons (**Figure 5**). While *Penk* was not detectable in control P0.5

neocortex, Cajal-Retzius cells in *Auts2* cKO neocortex expressed elevated levels of *Penk* **(Figure 5A).** This aberrant expression of *Penk* was maintained postnatally though at least P7.5 **(Figure 5B)**. These results not only validated the results of RNA-seq but also suggested a potential mechanism by which AUTS2 might regulate neurite outgrowth. Previously, exposure to Met-enkephalin (*Penk* gene product) has been shown to inhibit neurite elongation in cerebellar granule neuron cultures (Hauser et al., 2000). Neurons in the developing cortical plate appear to express the delta opioid receptors (*Oprd1*) responsible for mediating responses to Met-enkephalin (Allen Brain Atlas Developing Mouse Brain).

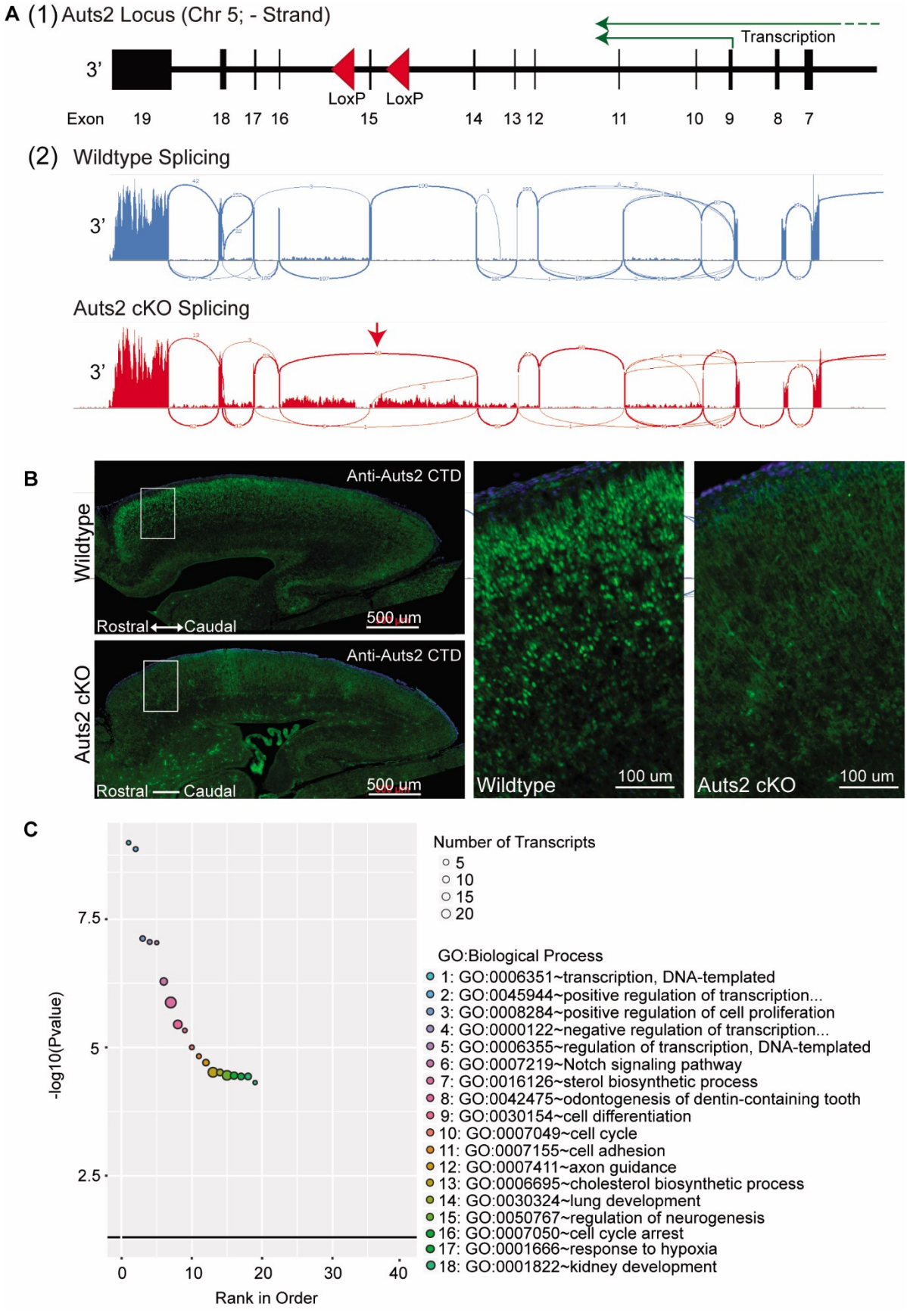
A (1) Auts2 Locus (Chr 5; - Strand)
Transcription
3'
LoxP
LoxP
Exon 19 18 17 16 15 14 13 12 11 10 9 8 7
(2) Wildtype Splicing
3'
Auts2 cKO Splicing
3'
B
Anti-Auts2 CTD
Wildtype
Rostral ⟷ Caudal
500 um
Anti-Auts2 CTD
Auts2 cKO
Rostral — Caudal
500 um
Wildtype
100 um
Auts2 cKO
100 um
C
Number of Transcripts
5
10
15
20
GO:Biological Process
1: GO:0006351~transcription, DNA-templated
2: GO:0045944~positive regulation of transcription...
3: GO:0008284~positive regulation of cell proliferation
4: GO:0000122~negative regulation of transcription...
5: GO:0006355~regulation of transcription, DNA-templated
6: GO:0007219~Notch signaling pathway
7: GO:0016126~sterol biosynthetic process
8: GO:0042475~odontogenesis of dentin-containing tooth
9: GO:0030154~cell differentiation
10: GO:0007049~cell cycle
11: GO:0007155~cell adhesion
12: GO:0007411~axon guidance
13: GO:0006695~cholesterol biosynthetic process
14: GO:0030324~lung development
15: GO:0050767~regulation of neurogenesis
16: GO:0007050~cell cycle arrest
17: GO:0001666~response to hypoxia
18: GO:0001822~kidney development
-log10(Pvalue)
7.5
5
2.5
0
10
20
30
40
Rank in Order

Figure 4: Construction and analysis of the Auts2 c-terminal cKO mouse model

(A) (1) Diagram of the terminal 13 exons of the *Auts2* locus. LoxP sites (Red Arrowheads) flanking Exon 15. Exons 1-6 not shown. **(2)** Sashimi splicing plots of Wildtype (top) and Auts2 cKO (bottom) loci. Exon 14-16 splice created by exon 15 deletion indicated by red arrowhead.

(B) AUTS2 fluorescent immunohistochemistry performed on sagittal sections of P0.5 Wildtype and cKO cortex using an in-house Rabbit polyclonal antibody to the AUTS2 c-terminus.

(C) GO: Biological Process terms enriched in differentially expressed transcripts ($P<0.01$) from RNA-sequencing data of frontal cortex of *Auts2* cKO vs Wildtype P0.5 neonates using geneSCF.

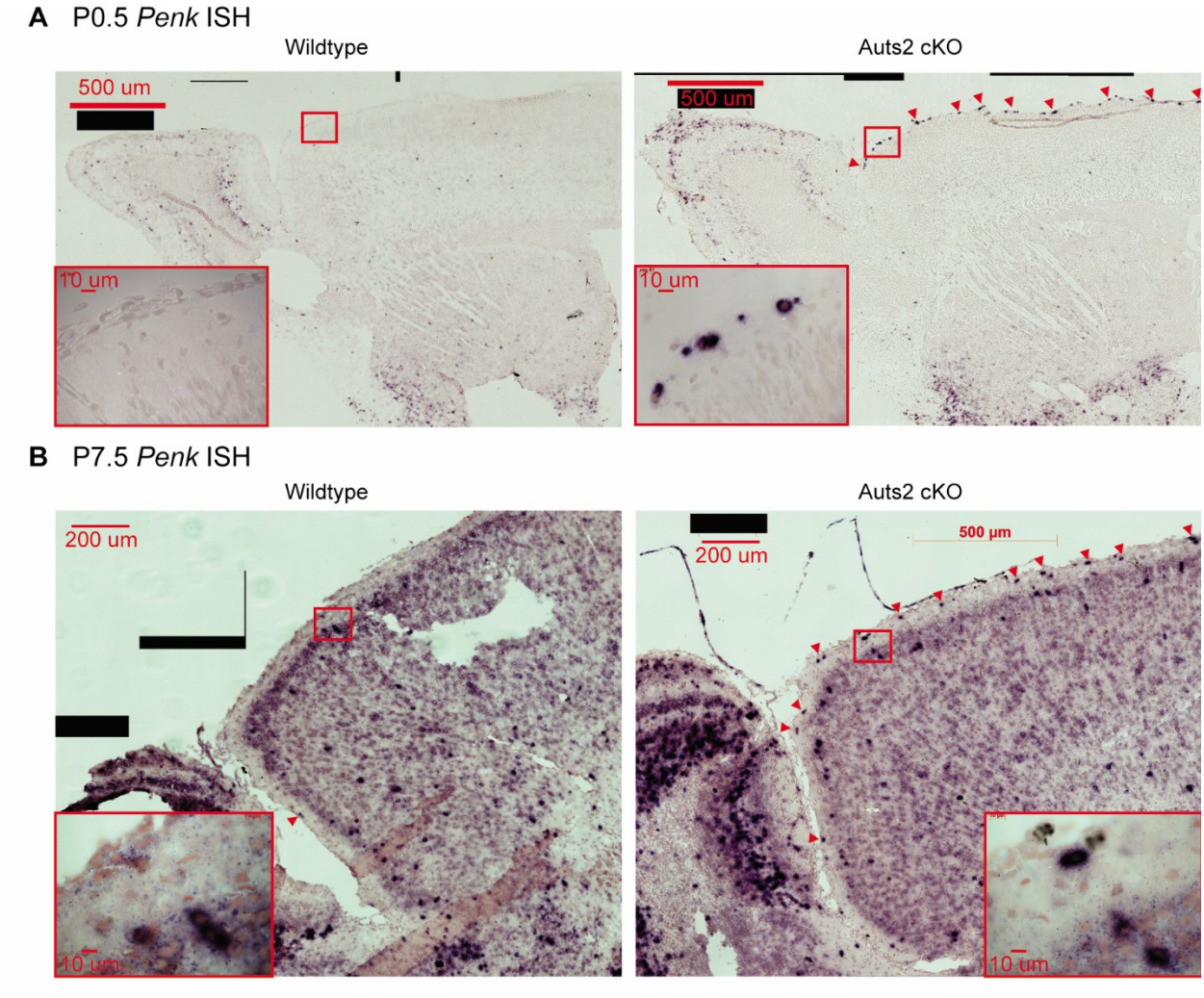

Figure 5: In-situ hybridization of *Penk* on sagittal sections of Auts2 conditional knockout and wildtype mouse cortex

(A) P0.5 wildtype (left) and *Auts2* knockout (right).

(B) P7.5 Wildtype (left) and *Auts2* knockout (right). *Penk* is ectopically expressed in horizontally oriented Layer 1 neurons (arrowheads) in the knockout but not wildtype cortex.

Inset: 63X magnification of affected neurons.

2.2.5: Transcripts bound by the AUTS2 complex are differentially regulated in Auts2 cKO

To determine if RNAs bound by the AUTS2 complex are differentially regulated by AUTS2, we concatenated the list of RIP-seq enriched transcripts with the list of differentially expressed transcripts in *Auts2* cKO frontal cortex. Of the 58 differentially expressed transcripts with FDR q<0.05, 11 (18.97%) were significantly enriched in the RIP-Seq dataset **(Table 2)**; and of the 383 differentially expressed transcripts with p<0.01, 56 (14.62%) were significantly enriched in the RIP-Seq dataset **(Figure 6A, Table S1)**. In comparison, only 3.21% of the total transcriptome was enriched in AUTS2 complex-bound RNA, representing potential RIP-seq background.

Among the 56 transcripts that were both bound by AUTS2 complex (RIP-seq, q<0.05) and differentially expressed in *Auts2* cKO cortex (RNA-seq, p<0.01), 42 (75%) were downregulated in *Auts2* cKO cortex. Significantly, the downregulated direct target transcripts included mRNAs encoding proteins involved in phenotypes that have previously been linked to AUTS2 function. These included *Ep300* (log_2FC=-0.283; p=0.00595) and *Crtc3* (*CREB Regulated Transcription Coactivator 3*) (log_2FC=-0.336; p=0.0035), which may contribute to the transcriptional activation previously associated with AUTS2 (Gao et al., 2014); as well as *Prex1* (log_2FC=-0.48; p=5E-05) and *Rasgrf2* (log_2FC=-0.333; p=0.0059), which may contribute to RAC/RAS-mediated regulation of cytoskeletal organization and neurite outgrowth (Hori et al., 2014). In addition, we found that *Cdc42ep2* mRNA, encoding another regulator of RAC/RAS signaling and filopodia outgrowth (Farrugia and Calvo, 2016), was upregulated in *Auts2* cKO cortex, although not directly bound by the AUTS2 complex.

To determine if AUTS2-bound and -regulated transcripts represent a functional biological network, the list of 56 transcripts (RIP-seq q<0.05, RNA-seq p<0.01) was submitted to STRING-DB (Szklarczyk et al., 2015) for interactome analysis. STRING identified an enriched protein-protein interaction network (p=0.00965) indicating that the proteins encoded by these transcripts interact significantly more than expected for a random list. The identified network appears to be involved in regulation of Notch signaling, including transcripts which encode *Jag2* and *Notch2*, which was also a pathway identified in our GO analysis of these transcripts **(Figure 6B)**.

To investigate whether differentially expressed genes in *Auts2* cKO cortex might be regulated transcriptionally by AUTS2 binding to chromatin, we assessed whether AUTS2 ChIP-seq signals were significantly associated with differentially expressed transcripts in *Auts2* cKO frontal cortex. We assessed transcripts within 5kb of previously identified AUTS2 ChIP-seq peaks (Gao et al., 2014), and found that the differentially expressed transcripts in *Auts2* cKO cortex were not significantly enriched (p <0.05) above the ChIP background level. **(Table S3)** Using STRING-DB, we also noted that, unlike transcripts bound by AUTS2 complex (RIP-seq), genes bound by AUTS2 (ChIP-seq) did not identify an enriched protein network. This was despite a similar number of targets, indicating genes bound by AUTS2 do not collectively form a biologically relevant network **(Figure 6C)**.

Together, our data indicate that, while AUTS2 may associate with chromatin, as supported by our identification of histones and other chromatin-associated proteins in the AUTS2

complex (Co-IP), it is the binding of AUTS2 complex to RNA (and presumably, related RNA processing activities) that most significantly regulates transcript expression and biological functions in the developing cerebral cortex.

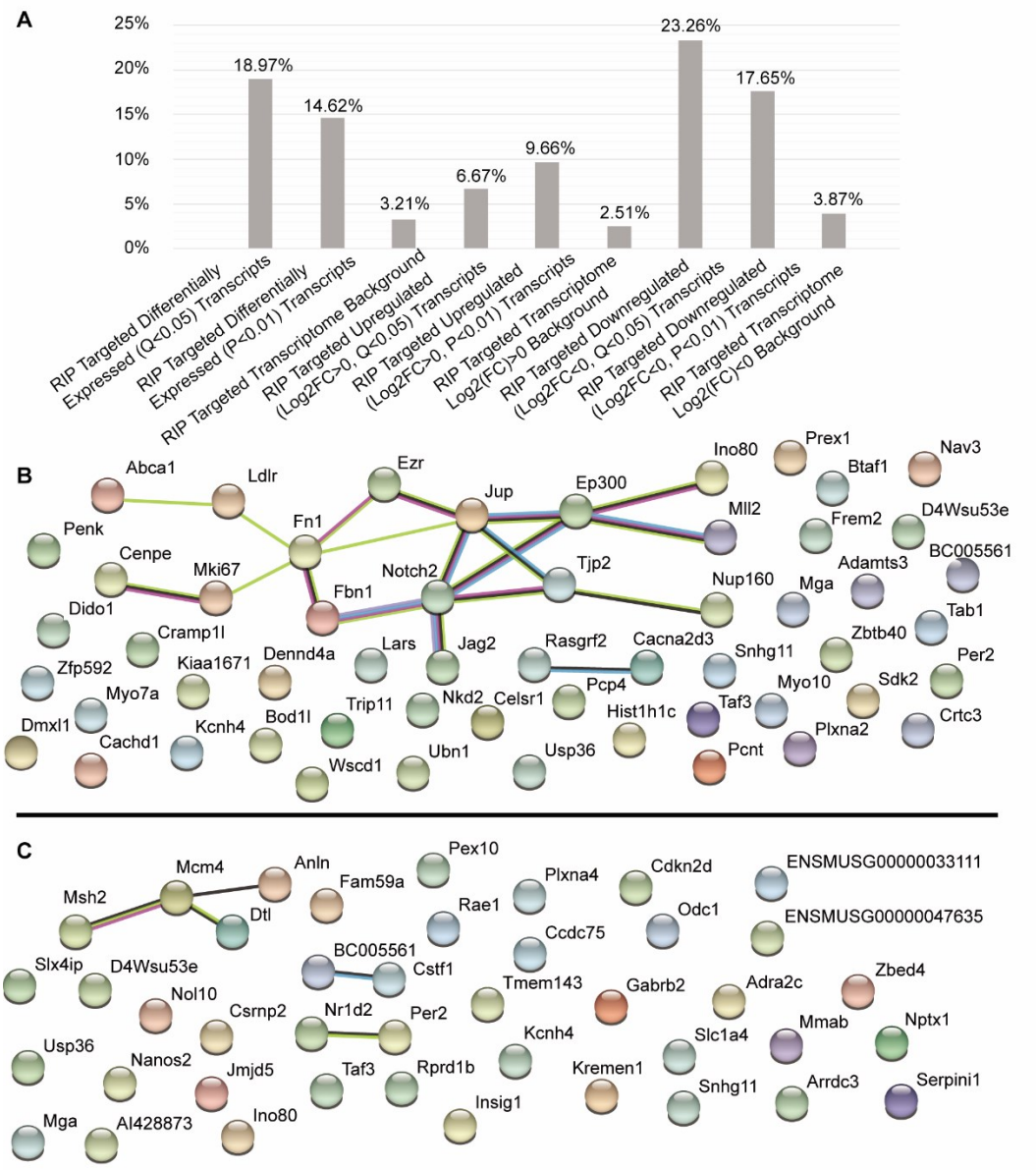

Figure 6: Analysis of differentially expressed transcripts targeted by the AUTS2-RNA complex

(A) Analysis of RIP enriched (FDR Q<0.05) transcripts within each total differentially expressed transcript category (Q<0.05, P<0.01, Background), and split by upregulated or downregulated. **(B)** STRING-DB network summary view of AUTS2-RIP targeted (Q<0.05) transcripts which are differentially expressed (P<0.01). Network PPI enrichment P=0.00965

(C) STRING-DB network summary view of differentially expressed (P<0.01) AUTS2-ChIP targeted transcripts (peak within ±5kb of transcript TSS). Network PPI enrichment P=0.153 (n.s.).

Table 2: Differentially expressed transcripts (Q<0.05) with AUTS2 RIP enrichment and AUTS2 ChIP peak marking annotated

				Auts2 cKO vs. WT		
Transcript ID	**Gene Symbol**	**RIP Enriched (Q<0.05)**	**ChIP Peak (±5kB)**	**log2(FC)**	**P value**	**Q value (FDR)**
ENSMUST00000161374.7	Auts2			-1.69	5E-05	0.032
ENSMUST00000140770.1	Plekhd1			-1.55	5E-05	0.032
ENSMUST00000199177.1	Gm43625			-1.46	5E-05	0.032
ENSMUST00000035115.4	Vipr1			-1.22	5E-05	0.032
ENSMUST00000033751.7	Vegfd			-1.11	5E-05	0.032
ENSMUST00000040914.2	Hist1h1c	+		-1.06	5E-05	0.032
ENSMUST00000199119.1	B230303O12Rik			-1.03	5E-05	0.032
ENSMUST00000048860.8	Mreg			-0.97	5E-05	0.032
ENSMUST00000161226.8	Auts2			-0.93	5E-05	0.032
ENSMUST00000022287.5	Fst			-0.91	5E-05	0.032
ENSMUST00000020662.14	Kremen1		+	-0.90	5E-05	0.032
ENSMUST00000061628.6	Pcdh20			-0.89	5E-05	0.032
ENSMUST00000024660.8	Smoc2			-0.87	5E-05	0.032
ENSMUST00000008032.13	Crlf1			-0.85	5E-05	0.032
ENSMUST00000045196.3	Kcns1			-0.80	5E-05	0.032
ENSMUST00000053239.2	Sstr3			-0.78	5E-05	0.032
ENSMUST00000205228.2	Cyp26b1			-0.72	5E-05	0.032
ENSMUST00000061274.7	Gpr156			-0.71	5E-05	0.032
ENSMUST00000032738.6	Chrna7			-0.70	5E-05	0.032
ENSMUST00000050544.7	Has2			-0.68	5E-05	0.032
ENSMUST00000069620.9	Per2	+	+	-0.65	5E-05	0.032
ENSMUST00000027422.6	Slc16a14			-0.65	5E-05	0.032
ENSMUST00000055168.4	Kcna1			-0.65	5E-05	0.032
ENSMUST00000023015.13	Wnt7b			-0.64	5E-05	0.032
ENSMUST00000179308.2	Edaradd			-0.63	5E-05	0.032
ENSMUST00000172278.7	Chrm2			-0.62	5E-05	0.032
ENSMUST00000022051.13	Nkd2	+		-0.62	5E-05	0.032
ENSMUST00000017544.8	Stac2			-0.61	5E-05	0.032
ENSMUST00000165117.7	Cdk6			-0.57	5E-05	0.032
ENSMUST00000045756.13	S100a10			-0.56	5E-05	0.032
ENSMUST00000061103.13	Ccbe1			-0.53	5E-05	0.032
ENSMUST00000142742.8	Nos1			-0.52	5E-05	0.032
ENSMUST00000027952.11	Plxna2	+		-0.51	5E-05	0.032
ENSMUST00000028633.12	Fbn1	+		-0.49	5E-05	0.032
ENSMUST00000030010.3	Abca1	+		-0.49	5E-05	0.032
ENSMUST00000036719.11	Prex1	+		-0.48	5E-05	0.032
ENSMUST00000108511.7	Wscd1	+		-0.48	5E-05	0.032
ENSMUST00000020227.10	Cry1			-0.46	5E-05	0.032
ENSMUST00000041627.13	Sdk2	+		-0.46	5E-05	0.032
ENSMUST00000029084.8	Ntsr1			-0.45	5E-05	0.032
ENSMUST00000161949.7	Pag1			-0.45	5E-05	0.032
ENSMUST00000079812.7	Notch2	+		-0.44	5E-05	0.032
ENSMUST00000051065.5	Gprin3			-0.43	5E-05	0.032
ENSMUST00000031766.11	Asns			0.43	5E-05	0.032
ENSMUST00000087600.9	Gda			0.48	5E-05	0.032
ENSMUST00000168574.8	Pid1			0.48	5E-05	0.032

ENSMUST00000023138.7	Shisa9			0.49	5E-05	0.032
ENSMUST00000109428.8	Tox2			0.60	5E-05	0.032
ENSMUST00000055458.4	Cdc42ep2			0.61	5E-05	0.032
ENSMUST00000109157.1	Tshz2			0.73	5E-05	0.032
ENSMUST00000038775.5	Ndn			0.80	5E-05	0.032
ENSMUST00000172356.7	Thsd7a			0.80	5E-05	0.032
ENSMUST00000004480.3	Sst			0.82	5E-05	0.032
ENSMUST00000020040.4	Nts			0.97	5E-05	0.032
ENSMUST00000109159.2	Tshz2			1.07	5E-05	0.032
ENSMUST00000070375.7	Penk	+		1.43	5E-05	0.032
ENSMUST00000127786.2	Xist			1.59	5E-05	0.032
ENSMUST00000117673.1	Gm9157			INF	5E-05	0.032

2.3: DISCUSSION

2.3.1: Auts2 is implicated in RNA metabolism as part of an RNA-binding complex

AUTS2 plays a significant role in human neurodevelopment, as mutations in this gene adversely affect cognition and cause an array of neurological disorders including autism, ID, epilepsy, and attention deficit-hyperactivity disorder (Beunders et al., 2016). Conservation of peptide sequence (full-length, 93% identity to human; C-terminal isoform: 87%) and expression in mice allow us to informatively model disruptions of this gene, which has very little homology to any known class of protein, or domain structures. In the present study, we have identified novel putative domains and mechanisms, whereby AUTS2 regulates RNA processing through interactions with both DNA and RNA binding proteins. We hypothesize that through these interactions, AUTS2 may play a role in regulating RNA splicing, stability, and other aspects of transcript expression.

In the present study, several lines of evidence indicated that AUTS2 has a role in the processing of RNA species that are important in brain development. First, unbiased sequence analysis indicated that AUTS2 protein contains putative domains that may be linked to RNA metabolism (**Figure 1**). The core "AUTS2 domain" and three other putative domains are present in the C-terminal isoform of AUTS2, while two additional domains, including the putative PAT1 domain, are present in full-length AUTS2. Presumably, the extra domains in full-length AUTS2 provide added functionality that is not essential to core functions of C-terminal AUTS2.

Second, co-IP revealed that AUTS2 interacts with NONO and other RNA-regulating proteins (**Figure 2, Table 1**), and is indeed co-expressed with NONO in developing cortical neurons (**Figure 2**). These results suggested that AUTS2 interacts with NONO in a large complex which contains other DNA and RNA binding components in the developing cortex. One of these components, HNRNPA2B1, has recently been shown to be involved in m^6A RNA methylation (Alarcón et al., 2015), an as yet poorly understood process with implications for RNA regulation in corticogenesis, specifically in vertebrates (Yoon et al., 2017). This process appears necessary for regulating the production of late-born neurons from NSCs and NSC renewal through a mechanism which involves targeting of transcripts encoding histone modifying enzymes (Wang et al., 2018). HNRNPA2B1 has also been found to interact preferentially with Casein Kinase 2A (Pancetti et al., 1999), an enriched component of the putative AUTS2 transcriptional regulatory complex identified in a previous study (Gao et al., 2014). Additional members of the AUTS2 containing protein-protein interaction complex, Fibrillarin and Nop56 are also associated with canonical rRNA and snoRNA O-methylation activity in plants (Rakitina et al., 2011). We also identified interactions with DEAD-box RNA helicases DDX5 and DDX17, which were previously found to interact with CREB Binding Protein (CREBBP), EP300, and RNA Pol II to regulate nascent mRNA processing co-transcriptionally, as well as to regulate specific developmental alternative splicing events (Dardenne et al., 2014; Fuller-Pace, 2013). EP300 was previously identified as an interacting partner of AUTS2 in the putative transcriptional activation complex (noncanonical PRC1) identified in a previous study (Gao et al., 2014).

Third, RIP-seq demonstrated that the AUTS2 complex binds specific mRNA species, including *Penk, Ep300,* and *Prex1*, that regulate multiple critical biological processes in brain development. These data suggest that a single RNA-centric mechanism may underlie both of the previously proposed functions of AUTS2 in transcriptional activation (Gao et al., 2014) and cytoskeletal reorganization (Hori et al., 2014).

Fourth, inactivation of Auts2 in developing cortex resulted in changes in the expression of specific mRNAs, many of which were also bound by AUTS2 complex **(Figure 6)**. Among these were transcripts involved in the Notch-Jagged signaling pathway. Previous work studying the oscillatory regulation of somitogenesis identified that Auts2 was regulated in concert with other Notch signaling pathway genes (Dequéant et al., 2006; William et al., 2007). Additionally, previous research has shown that Rac1 signaling and Notch2 signaling are co-regulated in models of ischemic cortical injury (Meng et al., 2015). Treatment of a cortical ischemia-reperfusion injury model with the RAC1 siRNA and a RAC-GTPase inhibitor NSC23766 which inhibit RAC1 signaling both induced downregulation of Notch2. This effect was dependent on NF-kB activation. Auts2, but not Notch2, Jag2, Prex1, or Rac1 was previously identified as a direct transcriptional target of NFkB in a study of the human kidney (O'Brown et al., 2015). These data support a role for AUTS2 as the mediating factor in synchronization between RAC1 and Notch signaling pathways downstream of NFkB through its RNA-binding interactions. Interestingly, an evolutionary duplication of Notch2, Notch2nl, appears to be necessary for promoting clonal expansion of neural progenitors specifically in the human brain, which results in an increased output of cortical neurons (Suzuki et al., 2017). Auts2 expression is not widely detected in mouse neural progenitors,

however, this has not been studied in human tissue. Auts2 may act on this pathway either directly though interactions with the Notch2 mRNA in a limited progenitor population, or indirectly though interactions with the transcript encoding the Notch2 ligand Jag2 expressed in neurons. Finally, on the strength of correlations between RNA binding and regulation by Auts2, as well as neurodevelopmental processes regulated by AUTS2 target mRNAs, RNA processing appears to be a primary function of Auts2.

2.3.2: Phenotypic overlap in human *AUTS2* and *NONO* syndromes

The proposed interaction between Auts2 and NONO gains added support and interest from the highly related consequences of human *AUTS2* and *NONO* mutations. Intellectual disability, developmental delay (language and motor), feeding difficulties, strabismus, altered muscular tone (hyper- or hypotonia), kyphosis or scoliosis, facial dysmorphisms, finger malformations (such as clinodactyly), cryptorchidism, and cardiac anomalies (including atrial septal defect) are among the many shared phenotypes in *AUTS2* (Beunders et al., 2016) and *NONO* syndromes (Mircsof et al., 2015; Reinstein et al., 2016; Scott et al., 2017). Interestingly, some clinical parameters are inversely affected by *AUTS2* and *NONO* mutations: microcephaly in *AUTS2*, macrocephaly in *NONO* syndrome; round or square face in *AUTS2*, long face in *NONO* syndrome; outgoing demeanor in *AUTS2*, shy demeanor in *NONO* syndrome. These data suggest that AUTS2 and NONO regulate the same developmental pathways, but with potentially antagonistic effects. The interaction of AUTS2 with NONO may, for example, modulate the activity or mRNA targeting of the RNA-processing complex.

2.3.3: Relation of RNA processing to other proposed functions of Auts2

The *Drosophila behavior/human splicing (DBHS)* protein family, of which NONO is a member, localize not only to euchromatin but also to a subnuclear RNA processing compartment known as the paraspeckle (Fox et al., 2002). DBHS proteins are involved in many levels of RNA metabolism, including positive and negative regulation of transcription initiation, recruitment of splicing factors to nascent mRNAs, splicing, mRNA transport and translation initiation (Knott et al., 2016). Our identification of Auts2 as a NonO interacting protein may help elucidate the complicated integration of DBHS proteins and their complexes in molecular regulation at all levels of RNA processing. Our current understanding of the shared regulatory effects of AUTS2 and NONO would be complemented by RNA-sequencing analysis of *Nono* mutant mouse frontal cortex and RIP-sequencing of NONO targeted RNAs at a comparable age to identify co-binding of RNA targets and shared dysregulated pathways. The study conducted by Mircsof et al., also showed mechanistic evidence of NONO regulating the abundance of synaptically targeted mRNAs and in independent work, Hori et al., showed potential localization of Auts2 to neurites. An extra-nuclear interaction between AUTS2 and NONO to regulate processing mRNAs encoding Rho/Rac effectors in the neurite, as well as the nucleus, could further confirm a unified mechanism for Auts2's nuclear and non-nuclear function.

The possibility that AUTS2 regulates RNA metabolism is further supported by previously reported evidence of an interaction between AUTS2 and RBM14 (Gao et al., 2014). RBM14 (RNA Binding Motif Protein 14; also known as Paraspeckle Protein 2) localizes to the same nuclear compartment as NONO and functions as a nuclear splicing regulator through its

two highly conserved RNA recognition motifs (Hennig et al., 2015). RBM14 also acts as an activator of transcription through interactions with both EP300 and CREBBP histone acetyltransferase (HAT) complexes via a thyroid hormone receptor binding protein (THRBP) interacting domain, or, as a repressor through an isoform lacking this third domain (Iwasaki et al., 2001). Thus, it is possible that AUTS2 may be targeted to chromatin through shared interactions with partners of EP300/CREBBP complexes, which are also involved in post-transcriptional RNA regulation, rather than through an interaction with Polycomb complex members such as RING1B, as previously suggested. In fact, only ~35% of AUTS2 marked loci were co-occupied by RING1B, and the authors of that study posit that AUTS2 recruitment to chromatin may be mediated through Polycomb independent mechanisms.

Notably, the same methodology that was used to propose an interaction between AUTS2 and the noncanonical PRC1 subunit PCGF5, also identified a putative interaction between the distant AUTS2 paralog fibrosin (FBRS) and PCGF5 (Gao et al., 2014; Hauri et al., 2016). Indeed, on co-IP, PCGF5 showed a greater affinity for fibrosin than for AUTS2. However, the interaction between fibrosin and Pcgf5 seems implausible because fibrosin is a secreted fibrogenic lymphokine and not a nuclear protein, suggesting an off-target interaction in the system used. Likewise, the possibility that PCGF5 does not interact with AUTS2 in developing neurons *in vivo* should be considered.

Hori et al. (2014), reported an interaction between AUTS2 and PREX1 at the protein-protein level in the cytoplasm, however, this was performed in non-neuronal cell lines ectopically expressing tagged AUTS2. The degree to which AUTS2 localizes to the cytoplasm in neurons

in-vivo is still unclear. A functional interaction between AUTS2 protein and *Prex1* mRNA as well as AUTS2 and EP300/CRTC3 mRNAs are consistent with a single mechanism for AUTS2 regulation of both EP300 dependent transcriptional coactivation as described by Gao et al., and RAC1 dependent cytoskeletal reorganization described by Hori et al. Should this occur in the cytoplasm, it may form an activity-dependent feedback loop incorporating both physical interactions with PREX1 as well as interactions with *Prex1* mRNA. The possibility of a role in the regulation of synaptically localized RNA trafficking though AUTS2 interactions with NONO presents an intriguing area of future research into the mechanisms by which neurons undergo their final stages of maturation, process organization, and functional integration.

2.3.4: Excess opioid receptor signaling may contribute to *AUTS2* syndrome

Persistent alterations in the expression of preproenkephalin (*Penk*) observed in the present study suggest a role for AUTS2 in the establishment of proper transcriptional programming of Cajal-Retzius (CR) cells, and for CR cells in the pathogenesis of *AUTS2* syndrome. Processed enkephalin peptides have been shown to suppress neurogenesis and neuritogenesis dependent on the type of opioid receptors expressed at the relevant neuronal stage (Hauser et al., 2000) the effects of which were mitigated by application of Naloxone. Anomalous overexpression and secretion of enkephalins by CR cells into developing cortex may drive some of the neuronal morphological defects observed in *Auts2* deficient mice, such as transiently impaired neural migration reported by Hori et al, (2014). These

observations suggest that excessive enkephalin signaling could potentially be a target for treatment of *AUTS2* syndrome, for example, by application of Naloxone or Naltrexone. As these drugs are extremely well tolerated with few adverse effects, investigation of Naloxone or Naltrexone as possible therapeutic avenues for mitigating some of the effects of *AUTS2* syndrome in animal models may be worth further study. Clinical studies of Naltrexone for treatment of aggression and self-injury in a cohort of ASD patients provided some evidence that these may be useful therapeutic interventions (Desjardins et al., 2009; Parikh et al., 2008). However, the number of patients studied was small and the effect highly variable indicating that the efficacy of the intervention in this signaling pathway may be highly dependent on the underlying molecular pathology.

In sum, we have identified a novel AUTS2 complex that is implicated in RNA processing and regulation of critical neurodevelopmental genes. Based on these data, we propose that AUTS2 may act as a novel multifunctional RNA regulator coupling chromatin remodeling, transcriptional activation, and recruitment of RNA splicing factors to promote prolonged transcript stability and delay upregulation of neuronal maturation pathways.

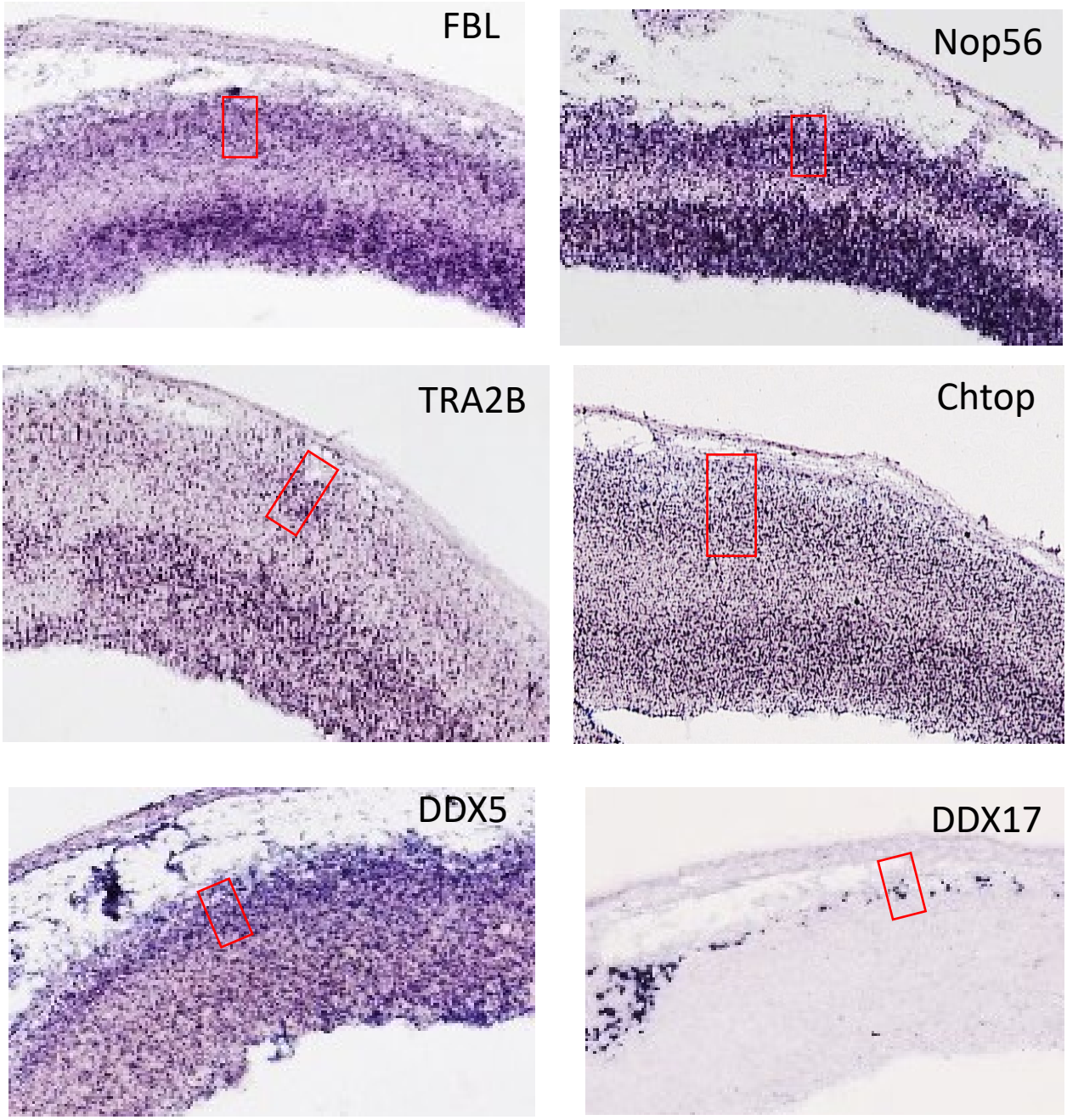

Figure S1, Related to Figure 1: Expression of selected putative AUTS2 interacting proteins in the E15.5 cortical plate

ISH images courtesy of the GenePaint 2 atlas. Selected AUTS2 interaction partners from the mass-spec dataset. Factors largely exhibit a bimodal expression distribution in upper cortical plate neurons the region in which AUTS2 is largely expressed (boxed), and VZ. DDX17 appears expressed in Cajal-Retzius Cells.

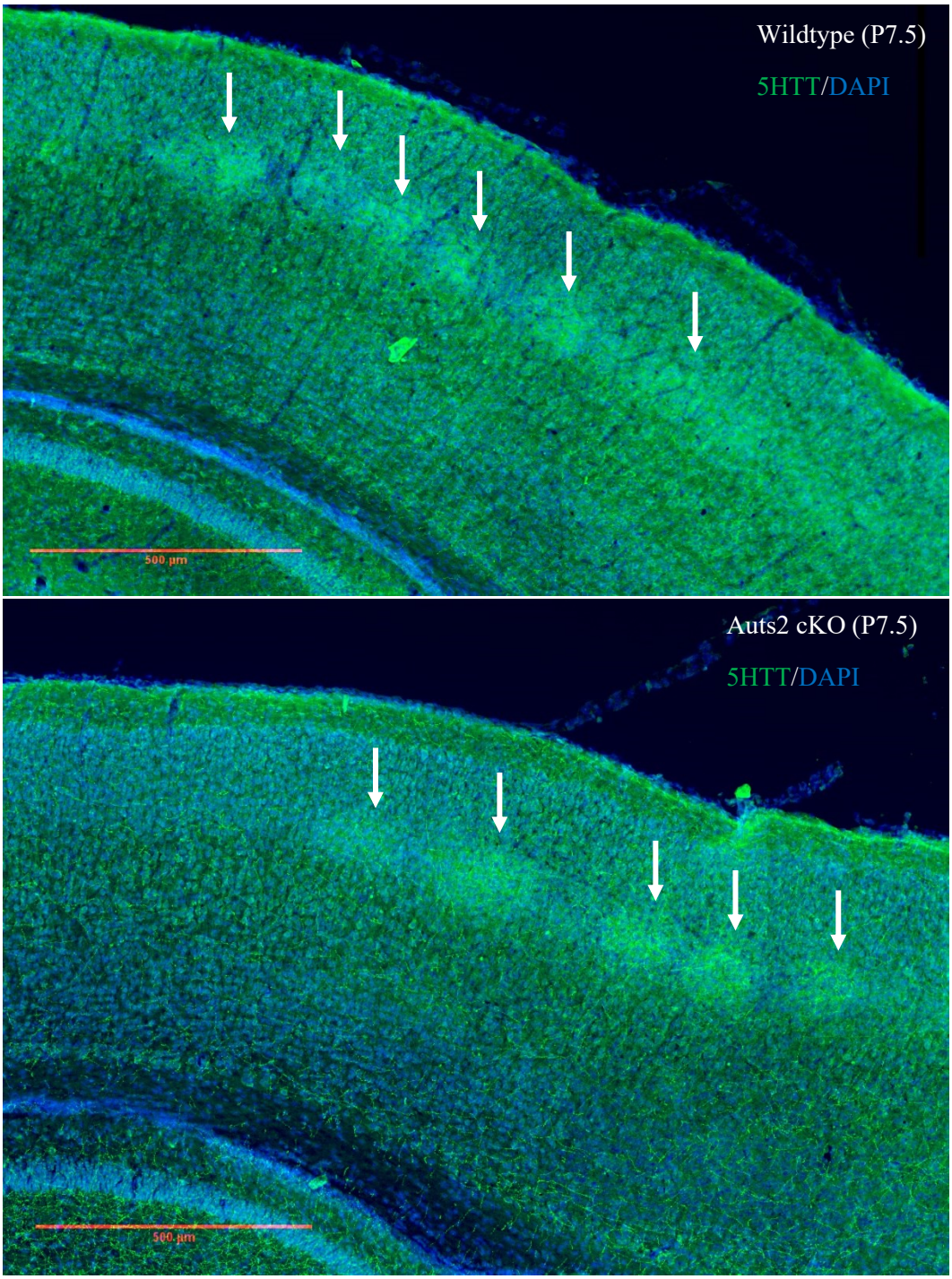

Figure S2, Related to Figure 4: Expression of 5HTT identifies cortical barrels in P7.5 Auts2 cKO and wildtype mice

20 um coronal section of P7.5 Wildtype (Top) and Auts2 cKO (Bottom) cortex stained for Serotonin Transported (5HTT) Green, and DAPI (Blue). Cortical Barrels indicated by arrows.

Table S1, Related to Figure 2: Consensus species identified by mass-spec detection from AUTS2 co-immunoprecipitation replicates

– See additional files –

Table S2: STRING-DB GO: molecular function and KEGG pathway enrichment of top 25% enriched proteins from AUTS2 co-IP mass-spec

STRING GO: Molecular Function				
#pathway ID	pathway description	observed gene count	false discovery rate	matching proteins in your network (labels)
GO.0044822	poly(A) RNA binding	19	5.85E-13	Chtop,Ddx17,Ddx5,Fbl,Fus,Hist1h1d,Hist1h1e,Hist2h4,Hnrnpa2b1,Khdrbs1,Nono,Nop56,Ppib,Rps3,Rps6,Sfpq,Srsf3,Srsf7,Tra2b
GO.0003676	nucleic acid binding	22	2.31E-08	Chtop,Ddx17,Ddx5,Fbl,Fus,H2afy,H2afy2,Hist1h1b,Hist1h1d,Hnrnpa2b1,Khdrbs1,Nono,Nop56,Ppib,Rps3,Rps6,Sfpq,Srsf3,Srsf7,Tmpo,Top2b,Tra2b
GO.0031490	chromatin DNA binding	5	2.08E-05	H2afy,H2afy2,Hist1h1a,Hist1h1d,Hist1h1e
GO.0043566	structure-specific DNA binding	6	0.000801	H2afy,H2afy2,Hist1h1a,Hist1h1d,Hist1h1e,Hnrnpa2b1
GO.0003682	chromatin binding	7	0.0044	Cbx5,H2afy,H2afy2,Hist1h1a,Hist1h1d,Hist1h1e,Top2b
GO.0003677	DNA binding	12	0.00442	Fus,H2afy,H2afy2,Hist1h1b,Hist1h1d,Hist2h4,Hnrnpa2b1,Nono,Rps3,Sfpq,Tmpo,Top2b
GO.1901363	heterocyclic compound binding	19	0.00577	Chtop,Ddx17,Ddx5,Fbl,Fus,H2afy,H2afy2,Hist1h1b,Hist1h1d,Hnrnpa2b1,Khdrbs1,Nop56,Ppib,Rps3,Rps6,Srsf3,Tmpo,Top2b,Tuba1a
GO.0097159	organic cyclic compound binding	19	0.00614	Chtop,Ddx17,Ddx5,Fbl,Fus,H2afy,H2afy2,Hist1h1b,Hist1h1d,Hnrnpa2b1,Khdrbs1,Nop56,Ppib,Rps3,Rps6,Srsf3,Tmpo,Top2b,Tuba1a
GO.0043274	phospholipase binding	2	0.0444	Lmnb1,Srsf3
STRING KEGG Enrichment				
#pathway ID	pathway description	observed gene count	false discovery rate	matching proteins in your network (labels)
3040	Spliceosome	4	0.0129	Ddx5,Srsf3,Srsf7,Tra2b

Table S3, Related to Figures 3, 4, 6: Whole transcriptome integration of Auts2 cKO vs. wildtype frontal cortex RNA-sequencing, Auts2 cortical RIP-seq, and Auts2 cortical ChIP-seq datasets

– See additional files –

Table S4, Related to Figure 3: GeneSCF GO: biological process enrichment of AUTS2 (Q<0.05) targeted transcripts in P0.5 cortex (Pathway FDR<0.1)

Genes	Process~Name	# Genes	Gene group	percentage	P-value	Benjamini and Hochberg (FDR)
Acin1; Adar; Akap8l; Aqr; Cactin; Ccar2; Cdc5l; Cdk12; Cpsf1; Ddx39b; Ddx41; Ddx5; Dhx8; Eftud2; Gpatch1; Hnrnpl; Hsf1; Ik; Kin; Luc7l3; Pcbp1; Pdcd11; Phrf1; Pnn; Prpf3; Prpf39; Prpf4b; Prpf8; Rbbp6; Rbm26; Rbm28; Rbm5; Sart1; Sart3; Scaf1; Sf3b1; Sf3b3; Sfpq; Skiv2l2; Slu7; Snrnp200; Son; Srpk1; Srrm1; Srrm2; Srsf7; Supt5; Supt6; Sympk; Tfip11; Thoc2; Thoc5; Wbp11; Wbp4; Wdr33; Xrn2; Zcchc8;	GO:0006397~mRNA processing	57	329	17.33	1.20E-07	0.000426137
Agrn; Als2; Dab2ip; Gapvd1; Iqgap1; Iqgap2; Mtor; Nf1; Ngef; Plxnb2; Plxnd1; Rab3gap1; Rab3gap2; Ralbp1; Rasa3; Rictor; Sbf1; Sipa1l1; Tbc1d10b; Tiam1; Vav2;	GO:0043087~regulation of GTPase activity	21	72	29.17	1.82E-06	0.002511874
Ash1l; Asxl1; Atrx; Bahd1; Baz2a; Brd3; Brd4; Brd8; Brd9; Chd1; Chd2; Chd5; Chd6; Chd7; Chd8; Daxx; Dnmt1; Ehmt1; H2afy2; Hcfc1; Hdac7; Hmgn5; Jak2; Jmjd1c; Kansl3; Kdm1b; Kdm5a; Kdm5b; Kmt2a; Kmt2c; Kmt2d; Mysm1; Ncor1; Nsd1; Phf2; Pkn1; Setd2; Setdb1; Smarca4; Smarcc2; Suds3; Tet2; Trrap; Tspyl2; Ubn1; Utp3; Zmynd11;	GO:0016569~covalent chromatin modification	47	275	17.09	2.12E-06	0.002511874
Acin1; Aqr; Cactin; Ccar2; Cdc5l; Cdk12; Ddx39b; Ddx41; Ddx5; Dhx8; Eftud2; Ik; Luc7l3; Mapkbp1; Pnn; Prpf3; Prpf39; Prpf4b; Prpf8; Rbm28; Rbm5; Sart1; Sart3; Scaf1; Sf3b1; Sf3b3; Sfpq; Skiv2l2; Slu7; Snrnp200; Son; Srpk1; Srrm1; Srrm2; Srsf7; Supt6; Tfip11; Thoc2; Thoc5; Wbp11; Wbp4; Zcchc8; Zfp638;	GO:0008380~RNA splicing	43	252	17.06	5.90E-06	0.005239125
Abl1; Ascc3; Atm; Atr; Atrx; Bod1l; Cdc5l; Cep164; Dclre1a; Ddb1; Dot1l; Ercc6; Herc2; Hsf1; Huwe1; Ino80; Kin; Lig1; Mdc1; Mtor; Mum1; Parp1; Paxip1; Pds5b; Prkdc; Psme4; Rad50; Rev1; Rev3l; Rif1; Setd2; Sfpq; Sfr1; Shprh; Slx4; Smc1a; Smc3; Smc5; Smg1; Supt16; Taok3; Topbp1; Trip12; Trrap; Ubr5; Usp7; Vcp; Xpc; Xrn2; Zfyve26;	GO:0006281~DNA repair	50	334	14.97	2.59E-05	0.017454173
Agrn; Ccdc88a; Ccdc88c; Celsr3; Dicer1; Dvl1; Flcn; Fn1; Itpkb; Lrp4; Mtor; Phip; Phlpp1; Plxnb2; Ppp1r9b; Ptk2; Rictor; Stat2;	GO:0001932~regulation of protein phosphorylation	18	68	26.47	2.95E-05	0.017454173
Apc2; Atxn7; Bbs1; Camsap1; Camsap3; Cdk5rap2; Dclk2; Dock7; Map1a; Map1s; Map7d1; Map7d2; Mark1; Nefh; Nefm; Ptk2; Ranbp10; Son; Tubgcp6;	GO:0000226~microtubule cytoskeleton organization	19	85	22.35	0.00012657	0.064207278
Arid4a; Ctr9; Hist1h1c; Hist1h1d; Hist1h1e; Kmt2a; Tet2; Zfp335;	GO:0080182~histone H3-K4 trimethylation	8	16	50.00	0.000171992	0.076342861
Als2; Ankrd27; Atxn2; Cdk5; Dab2ip; Dicer1; Dnm2; Epb41l3; Kif20b; Map1s; Mink1; Myo16; Plxnb1; Slit1; Srgap2; Zfp335;	GO:0048812~neuron projection morphogenesis	16	67	23.88	0.000222771	0.07902495
Abl1; Atm; Atr; Bcr; Brd4; Cad; Cdk12; Cdk5; Dapk1; Epha8; Hk1; Jak1; Jak2; Map3k11; Map3k9; Mink1; Mtor; Pdgfra; Pdgfrb; Peak1; Ptk2; Slk; Smg1; Stk10; Stk25; Taf1; Taok3; Trpm7; Ulk1; Wnk1;	GO:0046777~protein autophosphorylation	30	181	16.57	0.000226637	0.07902495
Cenpe; Dync1h1; Dync2h1; Kif13a; Kif13b; Kif1a; Kif20b; Kif21a; Kif21b; Kif26a; Kif26b; Kif27; Kif3a; Klc1; Stard9; Wdr60;	GO:0007018~microtubule-based movement	16	69	23.19	0.000296266	0.07902495
Ahi1; Bbs1; Bbs2; C2cd3; Cep131; Cep250; Dctn1; Dync2h1; Ift140; Ift172; Kif3a; Nphp3; Pcdh15;	GO:1905515~non-motile cilium assembly	13	48	27.08	0.000304969	0.07902495
Agrn; Als2; Cacnb3; Dvl1; Kalrn; Lamb2; Nedd4; Pdzrn3; Tnc; Unc13a; Unc13b;	GO:0007528~neuromuscular junction development	11	35	31.43	0.000305079	0.07902495
Abl1; Arhgap18; Ccdc88a; Celsr1; Dlc1; Hip1r; Lrp1; Mtor; Pdgfrb; Rictor; Rock1; Rock2; Taok2; Triobp;	GO:0032956~regulation of actin cytoskeleton organization	14	55	25.45	0.00031156	0.07902495
Aqr; Ddx39b; Ddx41; Dhx38; Dhx40; Dhx8; Prpf3; Prpf8; Pspc1; Raver1; Rnpc3; Sart1; Sart3; Sf3b1; Sf3b2; Sf3b3; Snrnp200; Snrnp70; Spen; Srrm1; Zrsr1;	GO:0000398~mRNA splicing, via spliceosome	21	109	19.27	0.000343451	0.081306272
App; Bsn; Htt; Klc1; Nefm; Spg11;	GO:0008088~axo-dendritic transport	6	9	66.67	0.000372497	0.081427632
Als2; Arhgef2; Bcr; Dlc1; Farp1; Kalrn; Mcf2l; Myo9b; Ngef; Ophn1; Prex1; Rasgrf1; Rasgrf2; Tiam1; Trio; Vav2;	GO:0035023~regulation of Rho protein signal transduction	16	71	22.54	0.000389825	0.081427632

Table S5, Related to Figure 3: GeneSCF GO: molecular function enrichment of AUTS2 targeted transcripts (Q<0.05) in P0.5 cortex (Pathway FDR<0.05)

Genes	Process~Name	# Genes	gene_group	percentage	P-value	Benjamini and Hochberg (FDR)
Arhgef2; Camsap1; Camsap3; Ccdc88a; Ccdc88c; Cdk5rap2; Cenpe; Cep350; Clip1; Clip2; Dctn1; Dnm1; Dnm2; Dst; Eml5; Ezr; Fsd1; Gli1; Golga2; Jakmip1; Jakmip3; Katnb1; Kif13a; Kif1a; Kif20b; Kif21a; Kif21b; Kif26a; Kif26b; Kif27; Kif3a; Kif5a; Macf1; Map1a; Map1s; Map4; Mast2; Mtcl1; Mtus2; Nav3; Nf1; Numa1; Ppp5c; Stard9; Tiam1; Tubgcp6; Vps41; Whamm;	GO:0008017~microtubule binding	48	207	23.19	4.70E-10	4.17E-07
Aacs; Aars; Aars2; Abca1; Abca2; Abca3; Abcc1; Abcc5; Abcf1; Abcf2; Abl1; Acaca; Acsbg1; Actr1b; Adcy5; Adcy6; Ascc3; Atm; Atp13a1; Atp1a1; Atp8b2; Atp9b; Atr; Atrx; Baz1b; Bcr; Cad; Camkv; Cdc42bpb; Cdk12; Cdk5; Cenpe; Chd2; Chd5; Chd6; Chd7; Chd8; Cit; Clcn7; Dapk1; Dclk2; Dclk3; Ddx10; Ddx21; Ddx24; Ddx27; Ddx39b; Ddx41; Ddx42; Ddx5; Ddx54; Dgkz; Dhx29; Dhx36; Dhx40; Dhx57; Dhx8; Dicer1; Dync1h1; Dync2h1; Epha8; Ephb6; Eprs; Ercc6; Fam20c; Hist1h1e; Hk1; Hsp90aa1; Hspa5; Hunk; Iars; Ighmbp2; Ikbkap; Ino80; Jak1; Jak2; Kalrn; Kif13a; Kif1a; Kif20b; Kif21a; Kif21b; Kif26a; Kif26b; Kif27; Kif3a; Ksr1; Lars; Lig1; Lonp1; Magi1; Magi3; Map3k1; Map3k11; Map3k4; Map3k9; Mapk11; Mark1; Mast1; Mast2; Mast3; Mcm3; Mink1; Mki67; Mtor; Myh9; Myo10; Myo16; Myo18a; Myo6; Myo7a; Myo9b; Nat10; Nav3; Nek9; Nrbp2; Nvl; Pdgfra; Pdgfrb; Peak1; Pfkl; Pfkp; Pi4ka; Pik3c2a; Pik3c3; Pkn1; Plk2; Ppp5c; Prag1; Prkdc; Prpf4b; Psmc3; Psmc4; Ptk2; Rad50; Rock1; Rock2; Sars; Scn8a; Scyl1; Shprh; Sik3; Skiv2l2; Slk; Smarca4; Smc1a; Smc3; Smc5; Smchd1; Smg1; Snrnp200; Speg; Srpk1; Stard9; Stk10; Stk25; Taf1; Taok2; Taok3; Top2a; Trap1; Trio; Trpm7; Ube2m; Ube2o; Ube4b; Ulk1; Vars; Vcp; Vwa8; Wnk1;	GO:0005524~ATP binding	171	1380	12.39	2.87E-09	1.27E-06
Ascc3; Atrx; Chd1; Chd2; Chd5; Chd6; Chd7; Chd8; Ddx10; Ddx21; Ddx24; Ddx27; Ddx39b; Ddx41; Ddx42; Ddx5; Ddx54; Dhx29; Dhx36; Dhx40; Dhx57; Dhx8; Dicer1; Ighmbp2; Ino80; Mcm3; Shprh; Skiv2l2; Smarca4; Snrnp200;	GO:0004386~helicase activity	30	124	24.19	3.92E-07	0.000116
Ddx10; Ddx21; Ddx23; Ddx24; Ddx27; Ddx39b; Ddx41; Ddx42; Ddx5; Ddx54; Dhx29; Dhx36; Dhx37; Dhx38; Dhx40; Dhx57; Dhx8; Skiv2l; Skiv2l2; Snrnp200;	GO:0004004~ATP-dependent RNA helicase activity	20	66	30.30	1.96E-06	0.000387
Afdn; Ahnak; Ank3; Arhgap18; Atxn2l; Cc2d1a; Cdh13; Chmp2b; Dab2ip; Dbn1; Dhx29; Dock9; Eps15l1; Ezr; Fasn; Flna; Flnb; Fmnl2; Gapvd1; Gcn1l1; Gigyf2; Golga2; Golga3; Hcfc1; Hspa5; Iqgap1; Jup; Larp1; Micall1; Mprip; Myh9; Myo6; Notch3; Pcbp1; Pfkp; Pi4ka; Plcb3; Ppfibp1; Ptprm; Scrib; Scyl1; Slk; Sptan1; Sptbn1; Sptbn2; Tjp2; Tln1; Usp8;	GO:0045296~cadherin binding	48	284	16.90	2.18E-06	0.000387
Baz2a; Brd3; Brd7; Brd9; Kmt2a; Phip; Psme4; Smarca4; Taf1; Zmynd8;	GO:0070577~lysine-acetylated histone binding	10	16	62.50	6.09E-06	0.0009
Als2; Ankrd27; Arfgef1; Arfgef2; Arfgef3; Arhgef2; Bcr; Cyth3; Dennd6b; Dis3; Dock3; Dock4; Dock7; Dock9; Farp1; Flcn; Gapvd1; Hps1; Kalrn; Kndc1; Mcf2l; Ngef; Prex1; Rapgef2; Rapgef6; Rasgrf1; Rasgrf2; Sbf1; Tiam1; Trio; Vav2;	GO:0005085~guanyl-nucleotide exchange factor activity	31	156	19.87	8.89E-06	0.001126
Arhgef2; Cdc42bpb; Cit; Daam2; Dock9; Flna; Fmnl2; Iqgap1; Iqgap2; Myo9b; Ppp6r1; Rock1; Rock2; Strip1;	GO:0017048~Rho GTPase binding	14	41	34.15	2.24E-05	0.002487
Akap8; Ankrd17; Ash1l; Atrx; Atxn7; Bahd1; Brd3; Brd4; Ccnt1; Chd1; Chd5; Chd8; Cic; Cramp1l; Dnmt1; Ep300; Ercc6; Gli1; Gli2; Hcfc1; Hdac7; Hmgn5; Hsf1; Jun; Kdm5a; Kmt2a; Ncapd2; Ncor1; Ncor2; Nipbl; Noc2l; Noc3l; Notch1; Nsd1; Nup153; Parp1; Pelp1; Phc1; Phf12; Pkn1; Pola1; Polr1a; Polr3a; Rere; Safb; Setdb1; Sf3b1; Sfpq; Sin3b; Ski; Smarca4; Smarcc2; Smc1a; Smc3; Supt5; Taf2; Tnrc18; Top2a; Trrap; Tshz1; Tshz3; Ubtf; Zmynd11; Zmynd8;	GO:0003682~chromatin binding	64	469	13.65	2.77E-05	0.002493
Add2; Ank1; Ank2; Ank3; Camsap1; Camsap3; Kif3a; Myo10; Myo7a; Sptan1; Sptbn4; Unc13a;	GO:0030507~spectrin binding	12	31	38.71	3.18E-05	0.002493
Abl1; Adcy6; Add2; Ap1b1; Aspm; Atp1a1; Cacnb3; Cadps; Ccnt1; Cdc5l; Cdk12; Cdk5; Cdk5rap2; Cenpe; Cep152; Cep250; Cltc; Cspg4; Dab2ip; Daxx; Dctn1; Dnm1; Dnm2; Dvl1; Eef1a2; Elp2; Ep300; Gcn1l1; Golga2; Hdac7; Hsf1; Hsp90aa1; Iqgap1; Jak2; Jup; Kif13b; Map3k1; Mapk8ip2; Mtor; Nbea; Nefh; Nek9; Parp1; Pdgfrb; Pkd1; Plcg1; Pola1; Ppp1r12b; Ppp1r15a; Ptk2; Ptpn23; Rapgef2; Rasgrf1; Rbbp6; Rictor; Ryr2; Sipa1l1; Ski; Slc12a6; Srcin1; Stat3; Strip1; Trap1; Ulk1; Wnk1;	GO:0019901~protein kinase binding	65	482	13.49	3.32E-05	0.002493
Abca1; Abca2; Abca3; Abcc1; Abcc5; Abcf1; Abcf2; Atp13a1; Cenpe; Ddx39b; Dync1h1; Dync2h1; Hsp90aa1; Hspa5; Ino80; Kif13a; Kif13b; Kif1a; Kif20b; Kif21a;	GO:0016887~ATPase activity	34	194	17.53	3.37E-05	0.002493

Kif21b; Kif26a; Kif3a; Lonp1; Macf1; Myh9; Myo9b; Rad50; Ralbp1; Smarca4; Smchd1; Stard9; Vcp; Vwa8;						
Als2; Arhgef2; Dock4; Dock7; Dvl1; Eps8; Farp1; Flna; Iqgap1; Iqgap2; Map3k11; Pkn1; Ralbp1; Srgap2; Tiam1;	GO:0048365~Rac GTPase binding	15	50	30.00	4.05E-05	0.002766
Aars; Aars2; Acin1; Ankrd17; Ascc3; Cherp; Cpsf1; Ddb1; Ddx10; Ddx21; Ddx24; Ddx27; Ddx39b; Ddx41; Ddx42; Ddx5; Ddx54; Dhx29; Dhx36; Dhx40; Dhx57; Dhx8; E4f1; Eif3b; Enox1; Fxr2; Gli1; Gli2; Gpatch1; Hivep1; Hnrnpl; Igf2bp1; Ighmbp2; Marf1; Mcm3ap; Mex3d; Nynrin; Pcbp1; Pdcd11; Peg3; Pola1; Prdm10; Pspc1; Raver1; Rbbp6; Rbm26; Rbm28; Rbm33; Rbm5; Rev3l; Rexo1; Rnpc3; Safb; Safb2; Sall2; Sall3; Sart3; Scrt1; Sf3b3; Sfpq; Skiv2l2; Slu7; Snrnp200; Snrnp70; Son; Spen; Srsf7; Supt6; Tfip11; Tnrc6a; Tnrc6c; Trerf1; Tshz1; Tshz3; Wbp4; Xrn2; Zcchc11; Zcchc17; Zcchc6; Zcchc8; Zfhx3; Zfp287; Zfp316; Zfp318; Zfp335; Zfp512; Zfp521; Zfp57; Zfp579; Zfp592; Zfp598; Zfp608; Zfp622; Zfp638; Zfp804a; Zfp821; Zfp830; Zrsr1; Zscan2;	GO:0003676~nucleic acid binding	99	837	11.83	4.46E-05	0.002824
Acap2; Als2; Ankrd27; Arap2; Arhgap18; Arhgap21; Arhgap23; Bcr; Dab2ip; Dlc1; Dock4; Fam13b; Gapvd1; Gmip; Jun; Lars; Myo9b; Nf1; Ophn1; Rab3gap1; Rab3gap2; Ralbp1; Ralgapa1; Ralgapa2; Ranbp2; Rapgef2; Rasa3; Rgs12; Sgsm1; Sipa1l1; Sipa1l3; Srgap2; Stxbp5; Tbc1d10b; Tbc1d8; Tbc1d9; Tbc1d9b; Tsc2;	GO:0005096~GTPase activator activity	38	238	15.97	7.18E-05	0.004247
Atrx; Baz1b; Baz2a; Brd1; Brd7; Chd2; Chd8; Daxx; Ipo9; Jak2; Kdm5a; Kdm5b; Mysm1; Ncapd2; Noc2l; Phf12; Pkn1; Sart3; Smarca4; Supt16; Supt6; Tonsl; Zmynd11; Zmynd8;	GO:0042393~histone binding	24	120	20.00	8.12E-05	0.004499
2700049A03Rik; Aars; Abca1; Abl1; Acaca; Acap2; Actn1; Actn4; Adam11; Adar; Adcy5; Adgrv1; Afdn; Agrn; Ahi1; Akap6; Akap8; Akap9; Als2; Amotl2; Anapc1; Ank2; Ank3; Ankrd24; Ankrd26; Ankrd27; Anks3; Ap1b1; App; Arhgef2; Arid4b; Arvcf; Asxl1; Atg16l1; Atm; Atp1a1; Atp6v1e1; Atp8b2; Atpif1; Atr; Atrx; Atxn7; Basp1; Baz1b; Baz2a; Bbs1; Bcl9l; Bcr; Birc6; Bmp1; Boc; Bop1; Brd4; Brd7; Brwd1; Bsn; C2cd3; Cacna1a; Cacna1d; Cacna1h; Cacnb3; Cadps; Camsap3; Cand1; Ccar2; Ccdc88a; Ccdc88c; Ccnl2; Ccnt1; Cdc42bpb; Cdh13; Cdk5; Cdk5rap2; Celsr1; Celsr2; Cenpc1; Cep104; Cep152; Cep162; Cep164; Cep350; Chd2; Chd3; Chd5; Chd7; Chd8; Cherp; Cic; Cit; Clcn7; Clip1; Clip2; Cltc; Crebzf; Crocc; Cspg4; Ctdp1; Ctr9; Cyth3; Dab2ip; Dapk1; Daxx; Dbn1; Dctn1; Ddb1; Ddx21; Ddx41; Ddx5; Dgkz; Dhx36; Dicer1; Dlg5; Dlgap4; Dmd; Dnm1; Dnm2; Dnmt1; Dock3; Dock7; Drp2; Dscam; Dst; Dtx1; Dvl1; Dync1h1; E4f1; Edc4; Edem2; Eftud2; Ehmt1; Eif2s2; Eif3a; Eif3b; Eif4g3; Elp2; Ep300; Epha8; Eps15l1; Eps8; Exoc7; Ezr; Fat1; Fat4; Fbf1; Fbln2; Fbn1; Fbn2; Flcn; Flii; Flna; Flnb; Fn1; Fnbp4; Fras1; Frem2; Fryl; Fxr2; Gabbr2; Ganab; Gapvd1; Gcn1l1; Gigyf1; Gigyf2; Gli1; Gli2; Golga2; Golga3; Gprasp1; Gtf2f1; Hcfc1; Hdac7; Heatr5b; Hectd1; Hip1; Hip1r; Hist1h1a; Hist1h1b; Hist1h1c; Hist1h1d; Hist1h1e; Hivep1; Hk1; Hnrnpl; Hsp90aa1; Hspa5; Htt; Ift172; Igf2r; Ipo5; Iqce; Iqgap1; Iqsec3; Jag2; Jak1; Jak2; Jun; Jup; Kalrn; Katnb1; Kdm5a; Kdm5b; Kif13a; Kif13b; Kif20b; Kif26a; Kif26b; Kif27; Kif3a; Kif5a; Klc1; Kmt2a; Kmt2c; Kmt2d; Kndc1; Ksr1; L1cam; Lamc1; Ldlr; Leo1; Lpin1; Lrch1; Lrp1; Lrp1b; Lrp4; Lrpprc; Macf1; Magee1; Magi1; Magi3; Map1a; Map3k1; Map3k11; Map3k4; Map4; Mapk11; Mapk8ip2; Mapkbp1; Mast1; Mast2; Mcf2l; Med25; Metap2; Micall1; Mtcl1; Mtor; Mybbp1a; Mycbp2; Myh9; Myo10; Myo16; Myo6; Myo7a; Myt1; Myt1l; Ncor1; Ncor2; Neb; Nedd4; Nf1; Nfasc; Ngef; Nin; Nipbl; Nolc1; Notch1; Notch2; Notch3; Npc1; Nsd1; Nup153; Nxf1; Ophn1; P3h3; Palmd; Parp1; Paxbp1; Paxip1; Pcbp1; Pcdh15; Pclo; Pcnt; Pde4dip; Pdgfrb; Pdzrn3; Pelp1; Per2; Phc1; Phf12; Phip; Pik3c2b; Pik3c3; Pik3r2; Pitpnm2; Pja1; Pkd1; Pkn1; Plcg1; Plekhm1; Plxna1; Plxna2; Plxnb1; Plxnb2; Plxnd1; Pola1; Polr1a; Polr1b; Ppfia1; Ppfia2; Ppp1r10; Ppp1r9b; Ppp5c; Prickle1; Prkdc; Pspc1; Ptk2; Ptpn13; Ptpn23; Ptprs; Rab11fip3; Ralbp1; Ralgapa1; Ranbp2; Rasgrf1; Reln; Rere; Rev1; Rgs12; Rictor; Rif1; Rims2; Rnf31; Rock1; Rock2; Rufy1; Ryr2; Safb; Sbno2; Scn8a; Scrib; Scrt1; Scyl1; Secisbp2; Setdb1; Sf3b1; Sf3b2; Sfpq; Sgsm1; Sh3d19; Sh3pxd2a; Sik3; Sin3b; Ski; Slc12a6; Slc44a2; Slk; Smarca4; Smarcc2; Smc1a; Smc3; Son; Sorl1; Spen; Sptan1; Sptbn1; Sptbn4; Srcin1; Srgap2; Srpk1; Srsf7; Stat2; Stat3; Stip1; Stk25; Stxbp5; Suds3; Supt6; Syne1; Syne2; Tab1; Taf1; Taf3; Tfip11; Thbs1; Thoc2; Thoc5; Tiam1; Tjp2; Tln1; Tln2; Top2a; Trip11; Trpm7; Trrap; Tsc2; Tsc22d1; Tshz1; Tshz3; Ube2o; Ube4b; Ubqln2; Ubr1; Ubr2; Ubr4; Ubr5; Ubtf; Uggt1; Ulk1; Unc13a; Unc79; Unc80; Uqcrc1; Usp4; Usp5; Usp7; Usp8; Utp3; Vav2; Vcp; Vps41; Vti1b; Wbp11; Wbp4; Wnk1; Xrn2; Zcchc11; Zdhhc8; Zfp318; Zfp335; Zfp57; Zfp592; Zmym3; Zmynd11;	GO:0005515~protein binding	432	4799	9.00	0.000101	0.005244
Cenpe; Dync1h1; Dync2h1; Kif13a; Kif13b; Kif1a; Kif20b; Kif21a; Kif21b; Kif26a; Kif26b; Kif27; Kif3a; Kif5a; Klc1; Stard9;	GO:0003777~microtubule motor activity	16	64	25.00	0.000142	0.007007
Actn1; Actn4; Add2; Ccdc88a; Coro7; Crocc; Daam2; Dbn1; Dmd; Dst; Epb41l3; Eps8; Ezr; Fhod3; Flii; Flna; Flnb; Fmnl2; Hip1; Hip1r; Ino80; Limch1; Macf1; Map1a; Mib2; Mical2; Mical3; Mprip; Myh9; Myo10; Myo16;	GO:0003779~actin binding	48	343	13.99	0.00016	0.007481

Myo6; Myo7a; Myo9b; Ophn1; Ppp1r9b; Ptk2; Sptan1; Sptb; Sptbn1; Sptbn4; Syne1; Syne2; Tln1; Tln2; Triobp; Trpm7; Whamm;						
Aacs; Aars; Aars2; Abca1; Abca2; Abca3; Abcc1; Abcc5; Abcf1; Abcf2; Abl1; Acaca; Acsbg1; Actr1b; Adcy5; Adcy6; Ascc3; Atm; Atp13a1; Atp1a1; Atp8b2; Atp9b; Atr; Atrx; Baz1b; Bcr; Cad; Cdc42bpb; Cdk12; Cdk5; Cenpe; Chd2; Chd5; Chd6; Chd7; Chd8; Cit; Clcn7; Dapk1; Dclk2; Dclk3; Ddx10; Ddx21; Ddx24; Ddx27; Ddx39b; Ddx41; Ddx42; Ddx5; Ddx54; Dgkz; Dhx29; Dhx36; Dhx40; Dhx57; Dhx8; Dicer1; Dnm1; Dnm2; Dync1h1; Dync2h1; Eef1a2; Eftud2; Epha8; Ephb6; Eprs; Fam20c; Gnl2; Hist1h1e; Hk1; Hsp90aa1; Hspa5; Hunk; Iars; Ighmbp2; Ino80; Jak1; Jak2; Kalrn; Kif13a; Kif1a; Kif20b; Kif21a; Kif21b; Kif26a; Kif26b; Kif27; Kif3a; Lars; Lig1; Lonp1; Magi1; Magi3; Map3k1; Map3k11; Map3k4; Map3k9; Mapk11; Mark1; Mast1; Mast2; Mast3; Mcm3; Mink1; Mki67; Mtor; Myh9; Myo10; Myo16; Myo18a; Myo6; Myo7a; Myo9b; Nat10; Nek9; Nin; Nvl; Pdgfra; Pdgfrb; Peak1; Pfkl; Pfkp; Pi4ka; Pik3c2a; Pik3c3; Pkn1; Plk2; Pola1; Prag1; Prkdc; Prpf4b; Psmc3; Psmc4; Ptk2; Rabl6; Rad50; Rev3l; Rock1; Rock2; Sars; Scn8a; Shprh; Sik3; Skiv2l2; Slk; Smarca4; Smc1a; Smc3; Smc5; Smg1; Snrnp200; Speg; Srpk1; Stard9; Stk10; Stk25; Taf1; Taok2; Taok3; Top2a; Trap1; Trio; Trpm7; Ube2m; Ube2o; Ulk1; Vars; Vcp; Vwa8; Wnk1;	GO:0000166~nucleotide binding	170	1666	10.20	0.000176	0.007799
A230050P20Rik; Aars; Aars2; Aco1; Adar; Ankrd17; Aqr; Atxn2; Atxn2l; Baz2a; Caprin2; Cdc5l; Cherp; Cpsf1; Ddx10; Ddx21; Ddx24; Ddx39b; Ddx41; Ddx42; Ddx5; Ddx54; Dhx29; Dhx36; Dhx37; Dhx38; Dhx40; Dhx57; Dhx8; Dicer1; Dis3; Dnmt1; Eif3a; Eif3b; Eif3c; Eif3d; Eif4g3; Eprs; Fam120a; Fxr2; Hnrnpl; Hnrnpul1; Igf2bp1; Ighmbp2; Ilf3; Jakmip1; Kin; Larp1; Lrpprc; Mapkbp1; Marf1; Mex3d; Nol6; Nom1; Nxf1; Pcbp1; Pcp4; Pdcd11; Ppp1r10; Ppp5c; Prpf8; Pspc1; Pum3; Ranbp2; Raver1; Rbm26; Rbm28; Rbm5; Rnpc3; Safb; Safb2; Sart3; Scaf1; Secisbp2; Sf3b1; Sf3b3; Sfpq; Skiv2l2; Snrnp70; Son; Spen; Srrm1; Srsf7; Thoc2; Thoc5; Tnrc6a; Tnrc6c; Ubr5; Xpo5; Zcchc17; Zfp638; Zrsr1;	GO:0003723~RNA binding	92	798	11.53	0.000188	0.007935
Actn4; Atm; Carmil1; Cdc42bpb; Cdk5rap2; Cep131; Cog2; Dab2ip; Ddb1; Ddx39b; Dnm1; Dnm2; Ep300; Ercc6; Ezr; Fbn1; Flcn; Flna; Golga2; Hk1; Iqgap1; Kif3a; Kif5a; Lca5; Lrp1; Mapk8ip2; Mthfr; Myo7a; Mysm1; Ncor2; Numa1; Pcdh15; Pdgfra; Pfkp; Plk2; Ppfia2; Ppp1r9b; Ptk2; Ptprf; Sf3b3; Sipa1l1; Smarca4; Smc1a; Smc3; Sptan1; Sptbn1; Tab1; Tln1; Ulk1; Uqcrc1; Vcp;	GO:0032403~protein complex binding	51	388	13.14	0.000391	0.015747
Abl1; Actn1; Actn4; Add2; Camsap3; Dbn1; Ezr; Flii; Flna; Hip1; Hip1r; Iqgap2; Map1s; Myh9; Myo10; Myo18a; Myo6; Myo7a; Myo9b; Ppp1r9b; Sipa1l1; Sptb; Syne1; Syne2; Tln1; Tln2; Triobp;	GO:0051015~actin filament binding	27	163	16.56	0.00046	0.017736
Akap6; Akap8; Akap8l; Akap9; Arfgef1; Arfgef2; Ezr; Ryr2;	GO:0034237~protein kinase A regulatory subunit binding	8	20	40.00	0.000562	0.020787
Plxna1; Plxna2; Plxna3; Plxnb1; Plxnb2; Plxnd1;	GO:0017154~semaphorin receptor activity	6	11	54.55	0.000814	0.02887
Abl1; Atm; Atr; Brd4; Cad; Camkv; Cdc42bpb; Cdk12; Cdk5; Cit; Dapk1; Dclk2; Dclk3; Epha8; Ephb6; Hk1; Hunk; Ikbkap; Jak1; Jak2; Kalrn; Ksr1; Map3k1; Map3k11; Map3k4; Map3k9; Mapk11; Mark1; Mast1; Mast2; Mast3; Mink1; Mtor; Nek9; Nrbp2; Pdgfra; Pdgfrb; Peak1; Pik3c3; Pkn1; Plk2; Ppp1r9b; Prag1; Prkdc; Prpf4b; Ptk2; Rock1; Rock2; Scyl1; Sik3; Slk; Speg; Srpk1; Stk10; Stk25; Taok2; Taok3; Trio; Trpm7; Ulk1; Wnk1;	GO:0004672~protein kinase activity	61	514	11.87	0.001186	0.04047
Add2; Aspm; Cacna1a; Camkv; Camsap1; Camsap3; Cdk5rap2; Dapk1; Ddx5; Iqgap1; Iqgap2; Myh9; Myo10; Myo6; Myo7a; Myo9b; Pcnt; Pcp4; Plcb3; Rasgrf2; Ryr2; Scn3a; Sptan1; Sptbn1; Ubr4; Unc13a; Unc13b; Unc13c;	GO:0005516~calmodulin binding	28	185	15.14	0.001262	0.041457
Als2; Arhgef2; Bcr; Dock9; Farp1; Kalrn; Mcf2l; Ngef; Prex1; Rasgrf1; Rasgrf2; Tiam1; Trio; Vav2;	GO:0005089~Rho guanyl-nucleotide exchange factor activity	14	67	20.90	0.001651	0.052305
Ash1l; Dot1l; Ehmt1; Kmt2a; Kmt2c; Kmt2d; Nsd1; Setd2; Setdb1;	GO:0018024~histone-lysine N-methyltransferase activity	9	32	28.13	0.002034	0.062206
Als2; Arhgef2; Farp1; Kalrn; Prex1; Tiam1;	GO:0030676~Rac guanyl-nucleotide exchange factor activity	6	15	40.00	0.002788	0.082421

Chapter 3: AUTS2 Regulates Hippocampal Interconnectivity and Establishment of the Adult Neurogenic Niche

3.1: INTRODUCTION

Various abnormalities in hippocampal neurodevelopment, neural activity, and circuit integration have been reported in many genetic models of Autism and associated neurodevelopmental syndromes (Hulbert and Jiang, 2016). Indeed, patient studies have identified alterations in hippocampal morphology in Autism, such as reductions in the area dentata (Saitoh, 2001), and reduced functional connectivity (Cooper et al., 2017). Major reorganization and expansion of the dentate gyrus occurs during the first postnatal week in mice. During this period, and the period immediately preceding birth, neural stem cells, and intermediate neuronal progenitors migrate around the early hippocampal formation establishing a transient subpial neurogenic compartment. From this subpial neurogenic zone progenitors migrate inward to produce early born hippocampal neurons and to establish the adult neurogenic niche in in the subgranular zone (Hodge and Hevner, 2011; Hodge et al., 2013; Li et al., 2009a). During human neurodevelopment, this process largely occurs during the second trimester (Ge et al., 2015; Yang et al., 2014). Insults in this period, particularly related to infections and fever, are associated with ASD risk (Hornig et al., 2018; Zerbo et al., 2015), and hippocampal development is impaired in ASD (Raymond et al., 1995; Saitoh, 2001). Similar insults have been found to impair hippocampal development in mice (Malaeb et al., 2014). Previous work in our lab explored the developmental expression

patterning of Auts2, a gene linked to a distinct autism/intellectual disability syndrome. This work determined that, in mice, Auts2 exhibits transient developmental expression in maturing cortical neurons, and is prominently and perpetually expressed in hippocampal dentate gyrus granule neurons (DGNs) and cerebellar Purkinje neurons throughout life. Expression of AUTS2 was determined to be regulated downstream of an Autism linked transcription factor, T-Box Brain 1, (TBR1) which directly controlled activation of AUTS2 transcription, and identified it as a marker of predominantly rostral, upper cortical layer specification (Bedogni et al., 2010b). Through ChIP-seq studies of TBR1, these experiments found that TBR1 regulates AUTS2 expression by directly binding to and activating the AUTS2 promoter. Mice which had TBR1 deleted exhibited loss of Auts2 expression in the cortex. This study implicated Auts2 as a late part of the PAX6-TBR2-TBR1 transcriptional cascade which regulates the production of glutamatergic pyramidal neurons from progenitors and, in part, contributes to proper lamination and regionalization of the neocortex (Englund, 2005). This transcription factor cascade represents a conserved program of neurodevelopment which regulates the genesis of glutamatergic excitatory neurons in multiple brain regions, including the neocortex, hippocampus, and cerebellum (Hevner et al., 2006). In further dissecting this cascade of neuronal fate specifying factors, we previously described a mouse model of deletions in the gene Autism Susceptibility Candidate 2 (AUTS2) which, in addition to targeting the full-length transcript, also disrupts independently expressed isoforms originating from the 3' end of the locus. We determined that this deletion alters gene expression pathways in neonatal mouse frontal cortex including Rho GTPase activity, cell adhesion, and axon guidance pathways. These pathways

are consistent with previous studies of AUTS2's molecular action as a regulator of cytoskeletal assembly (Hori et al., 2014). We were unable to identify any gross morphological alterations in the cortical plate neurons, however, these previous studies identified transient alterations in cortical neuron migration and axon outgrowth which are consistent with our transcriptional profiling. We additionally identified altered gene expression in the RELN expressing Cajal-Retzius (CR) cells of cortical layer 1. CR cells are involved in determining layer specification in the cortex, and in regulating migration of progenitors in the developing hippocampus (Badea et al., 2007). We hypothesized that CR cell-dependent processes may be altered in the Auts2 cKO hippocampus during postnatal development. Unlike in the cortex, Auts2 expression in the dentate gyrus and cerebellum does not appear to be downregulated with maturation. This indicates that the molecular function of AUTS2 may be necessary for ongoing biological processes that are not developmentally restricted in these brain regions as they are in the cortex. Previously described models of AUTS2 deletion separately ablated expression of AUTS2 isoforms containing exons 7 and 8, impacting the full-length isoform, and one of the two short c-terminal isoforms (Gao et al., 2014; Hori et al., 2014). However, additional studies identified a c-terminal isoform of Auts2 originating from Exon 9 which is prominently expressed in developing neurons and was capable of the functional rescue of Auts2 deficiency in zebrafish (Beunders et al., 2013). Recently, a behavioral study was published reporting behavioral abnormalities in heterozygous animals containing this Exon 8 deletion (Hori et al., 2015). In this analysis mice carrying a heterozygous deletion of Exon 8 impacting the full-length isoform and c-terminal isoform variant 1 reproduced behavioral abnormalities with relevance for phenotypes exhibited by

AUTS2 patients. These partially AUTS2 deficient mice exhibited impairments in novel object recognition and cued associative memory tasks. These tests are thought to dependent on hippocampal functional activity (Broadbent et al., 2010; Yoon et al., 2011). As these animals still expressed the exon 9 variant from the disrupted locus and all Auts2 isoforms from the unaffected locus, hippocampal processes appear highly sensitive to perturbations of AUTS2 levels. Despite this, no examination of the hippocampus of these AUTS2 deficient animals was performed either cellularly or by transcriptional profiling. As AUTS2 is highly expressed in the hippocampal formation, not developmentally downregulated, and defects in hippocampal morphology are associated with other autism syndrome genes, we hypothesized that fully Auts2 deficient mice may exhibit substantial abnormalities in hippocampal development. We investigated this hypothesis through RNA-sequencing of neonatal Auts2 deficient hippocampus and immunohistochemical staining of various neuronal markers to track cell populations as the hippocampus matures.

3.2: RESULTS

3.2.1: Auts2 expression is not altered in the hippocampus of TBR2 or TBR1 knockout mice

Auts2 exhibits developmentally regulated transcriptional downregulation in the cortex of mature animals. The cortical expression of Auts2 appears tightly regulated by the transcription factor TBR1. Our lab previously reported that deletion of Tbr1 results in the loss of *Auts2* expression in the cortical plate of TBR1 knockout animals (Bedogni et al., 2010b). Hippocampal excitatory neurons are thought to follow broadly the same developmental transcription factor cascade as cortical pyramidal neurons, however, while Auts2 expression is developmentally downregulated in the cortical plate, this is not the case in the hippocampus, where neurons continue to express Auts2 throughout life (Bedogni et al., 2010a). To determine if the expression of *Auts2* in the hippocampus follows the same TBR1 dependent developmental cascade as in the cortex we performed immunohistochemistry against AUTS2 in the hippocampus of Tbr1 knockout animals. Contrary to our expectations, we found that despite distinct morphological alterations in TBR1 knockout hippocampi, AUTS2 expression was maintained **(Figure 1A, B)**. Dentate gyrus granule neurons, as well as a population of hilar neurons, expressed Auts2 normally at P14 in the TBR1 knockout mouse, an age when the dentate gyrus has reached a predominately mature architecture. However, Bedogni et al. reported that in the hippocampus a population of TBR2+ intermediate neuronal progenitors appeared to express Auts2. As TBR2 is the upstream transcription factor which regulates proliferation and maintenance of intermediate progenitors, a neural progenitor population which is

committed to the production of excitatory neurons, we additionally investigated whether knockout of TBR2 affects Auts2 hippocampal expression. Despite significant morphological abnormalities in the hippocampus of Tbr2 conditional knockout animals, as previously reported (Arnold et al., 2008), these hippocampi also exhibited normal Auts2 expression in their remaining granule neurons at P2 **(Figure 1C, D)**. These data suggest that despite major conservation of the transcriptional program of hippocampal and cortical excitatory neurons, regulation of the Auts2 locus appears to have undergone substantial divergence. Additional research is needed to identify the pathway of transcriptional control of AUTS2 in the hippocampus. Likewise, Purkinje neurons, some thalamic neurons, and some deep brain nuclei including a region of the pontine nucleus also appear to express Auts2 perpetually thorough life. Transcription factors which regulate the expression of AUTS2 in these brain regions may represent new autism genes, as well as genes for which AUTS2 dependent molecular functions should be investigated. To determine which isoforms of Auts2 are responsible for maintaining this expression, we compared expression of AUTS2 isoforms using in-house antibodies to the AUTS2 N-terminus and AUTS2 C-terminus. We found that the C-terminus of AUTS2, not the N-terminus that is persistently expressed in hippocampal neurons with only the C-terminal epitope detected at P37 **(Figure 2A-F)**. This isoform has previously been reported as a developmentally enriched isoform (Hori and Hoshino, 2017). The combination of these factors indicates that, in the hippocampus, AUTS2 is controlled by a separate transcriptional cascade than AUTS2 in the cortex and that it is the C-terminal isoform, traditionally described as developmentally upregulated, which is persistently expressed in the hippocampus throughout life.

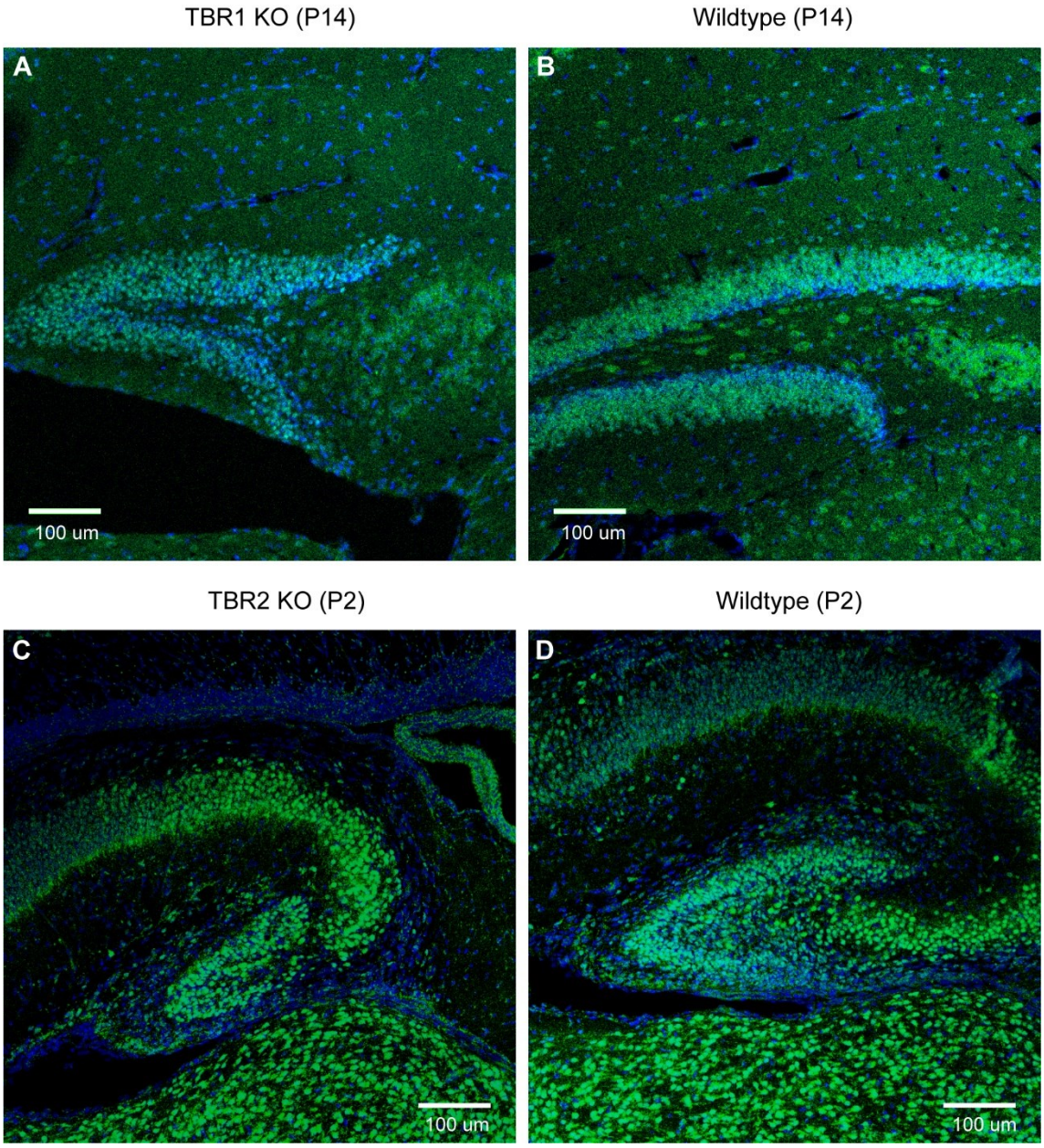

Figure 1: Expression of AUTS2 in TBR1 and TBR2 knockout hippocampus

(A) P14 TBR1 KO anti-AUTS2 Immunohistochemistry (20x Confocal) **(B)** P14 Wildtype anti-AUTS2 Immunohistochemistry (20x Confocal)

(B) P2 TBR2 cKO anti-AUTS2 Immunohistochemistry (20x Confocal) **(B)** P2 Wildtype anti-AUTS2 Immunohistochemistry (20x Confocal)

AUTS2 Expression is maintained in TBR1 and TBR2 knockout dentate gyrus

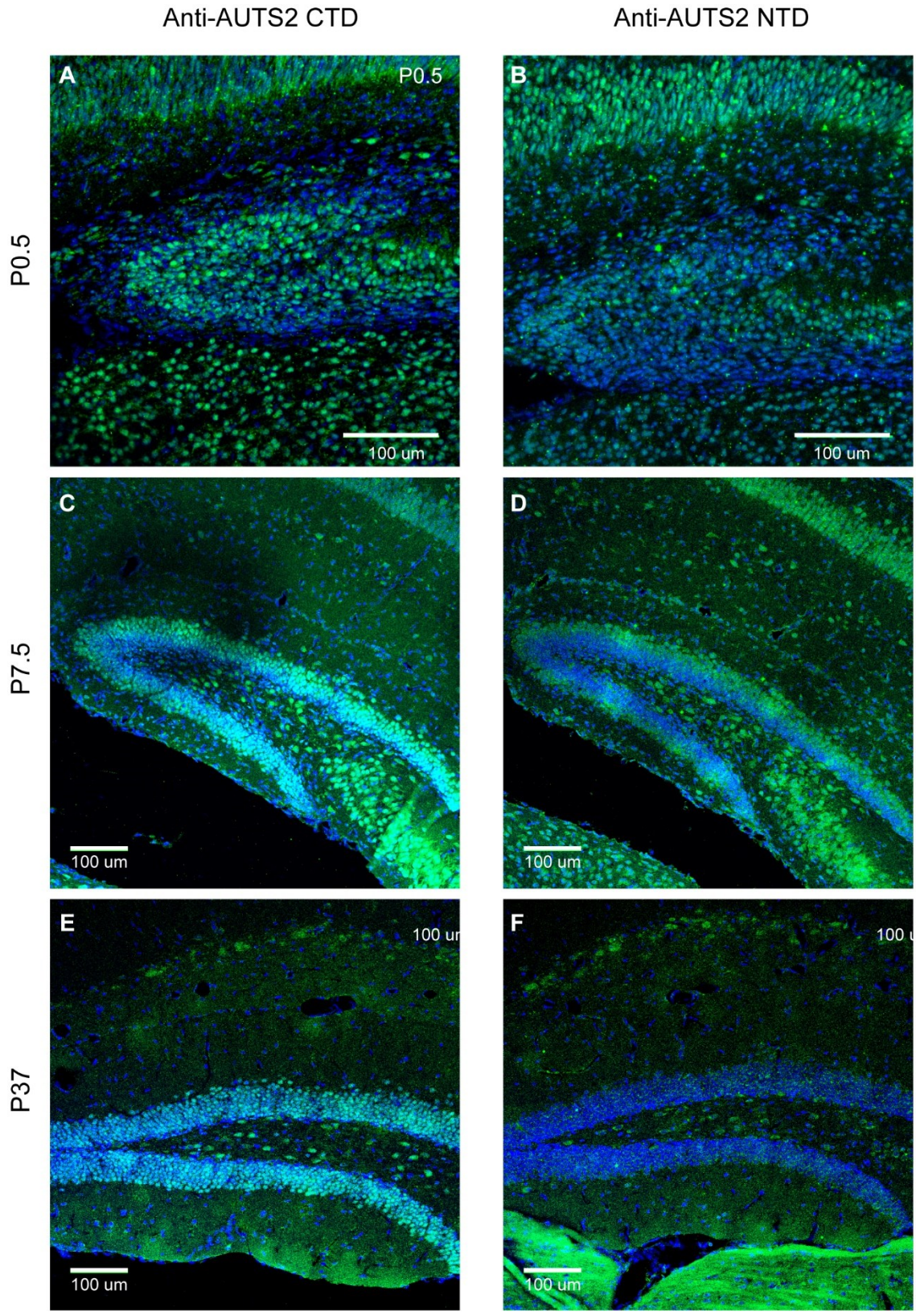
Anti-AUTS2 CTD
Anti-AUTS2 NTD
P0.5
P7.5
P37
A
P0.5
B
C
D
E
F
100 um

Figure 2: Expression of AUTS2 n- and c-terminus in developing dentate gyrus

(A) P0.5 anti-AUTS2 c-terminus immunohistochemistry (20x confocal)

(B) P0.5 anti-AUTS2 n-terminus Immunohistochemistry (20x confocal)

(C) P7.5 anti-AUTS2 c-terminus immunohistochemistry (20x confocal)

(D) P7.5 anti-AUTS2 n-terminus Immunohistochemistry (20x confocal)

(E) P37 anti-AUTS2 c-terminus immunohistochemistry (20x confocal)

(F) P37 anti-AUTS2 n-terminus Immunohistochemistry (20x confocal)

AUTS2 n-terminus is only transiently expressed during hippocampal development **(B, D, F)**, while c-terminal AUTS2 expression is maintained **(A, C, E)**

3.2.2: Regulation of hippocampal transcriptional programs by AUTS2

In order to determine the underlying molecular abnormalities which may drive pathogenesis of these hippocampus-dependent processes, we performed RNA-sequencing and pathway analysis of neonatal hippocampus from our Auts2 knockout animals. Including Auts2 itself, 54 genes were significantly differentially expressed (FDR Q<0.05) **(Table 1)** in our hippocampal dataset, and 250 with a P-value <0.01 **(Table S1)**. We previously described a persistent alteration in the expression of Preproenkephalin (PENK) in the cortical plate Cajal-Retzius cells which was initially identified as an upregulated target gene in our cortical RNA-Sequencing data. RNA-sequencing of the Hippocampus of AUTS2 cKO mice also identified upregulation of Preproenkephalin. Unlike in the cortex, Cajal-Retzius cells of the developing hippocampus normally express low-moderate levels of PENK. At birth, this population appeared to express substantially more PENK in the AUTS2 cKO hippocampus **(Figure 3A, B)** and these neurons appeared to maintain this increased PENK expression through the first postnatal week **(Figure 3C, D)**. As in neocortex, although *Penk* was upregulated, the majority of transcripts in Auts2 cKO were downregulated, suggesting that AUTS2 mainly increases the expression of target RNAs.

We assessed how molecular pathways are altered in the AUTS2 cKO hippocampus using geneSCF to perform GO analysis (Subhash and Kanduri, 2016) and accompanying STRING analysis of the differentially expressed genes for both Q<0.05 and P<0.01 sets. Auts2 itself was excluded from this analysis in order to avoid skewing of GO terms. We identified a collection of proteins associated with the organization of extracellular matrix that were significantly downregulated (FDR Q-value <0.05) in the AUTS2 deficient hippocampus.

Within this gene set, we identified a gene interaction network which was enriched in a STRING network. This network had significantly more molecular interactions than would be expected for a randomly selected gene set (PPI enrichment p-value:< 2.22e-15) **(Figure 4A)** and contained several COL6 alpha subunits which were downregulated in the Auts2 cKO hippocampus. The function of this collagen type during neurodevelopment has not been studied extensively, however, some research on its function during aging indicates that neurons lacking Col6 may exhibit increased apoptosis and higher vulnerability to oxidative stress resulting in accelerated neurodegeneration (Cescon et al., 2016). These processes may also be involved in the developmental reorganization of the hippocampal formation's extracellular matrix more broadly as the structure undergoes its dramatic postnatal expansion. Expression of extracellular matrix molecules including collagens, laminins, proteoglycans, and integrins has been suggested to be involved in the maintenance of neural progenitor self-renewal in the germinal zones (Fietz et al., 2012). We additionally assessed the dataset of P<0.01 dysregulated genes and identified multiple pathways which have implications for how extracellular matrix is organized in the Auts2 cKO mice. Several additional potential molecular function pathways (GO:MF pathways) were dysregulated which include how cells bind to heparin-sulfate proteoglycans (HSPGs) (FDR = 9.9e-7), collagen (FDR = 0.0028), and the general extra cellular matrix (FDR = 0.0028) **(Figure S1, Table S2),** as well as related biological processes (GO:BP pathways) involved in neuron migration (FDR = 0.0320) axon guidance (FDR = 0.0182) and cell adhesion (FDR = 0.0135) **(Figure 4B, Table S3)**.

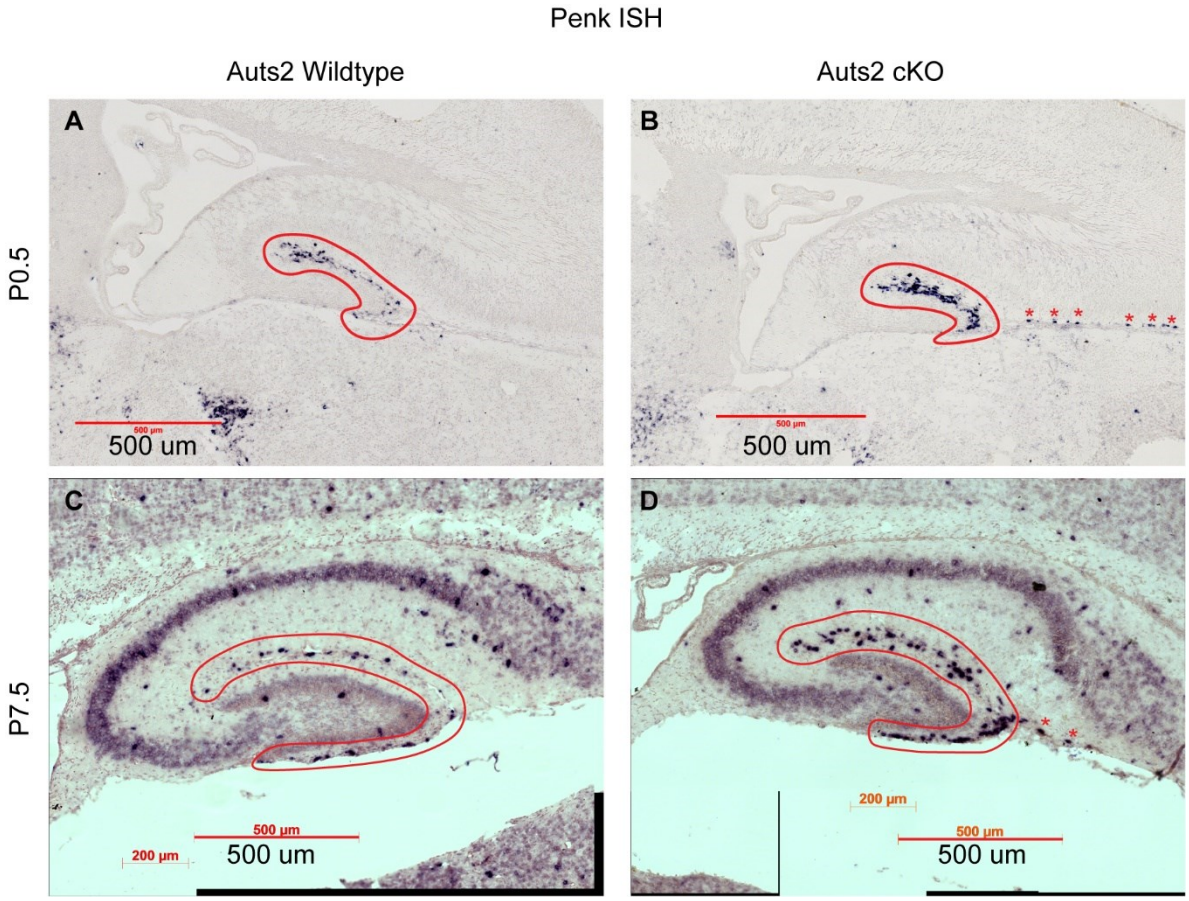

Figure 3: In-situ hybridization of *Penk* mRNA in Auts2 knockout and wildtype mouse hippocampus

Penk expressing cells in the subpial neurogenic zone of Wildtype **(A, C)** and Auts2 cKO **(B, D)** mice on P0.5 **(A, B)**. On P7.5 **(C, D)**

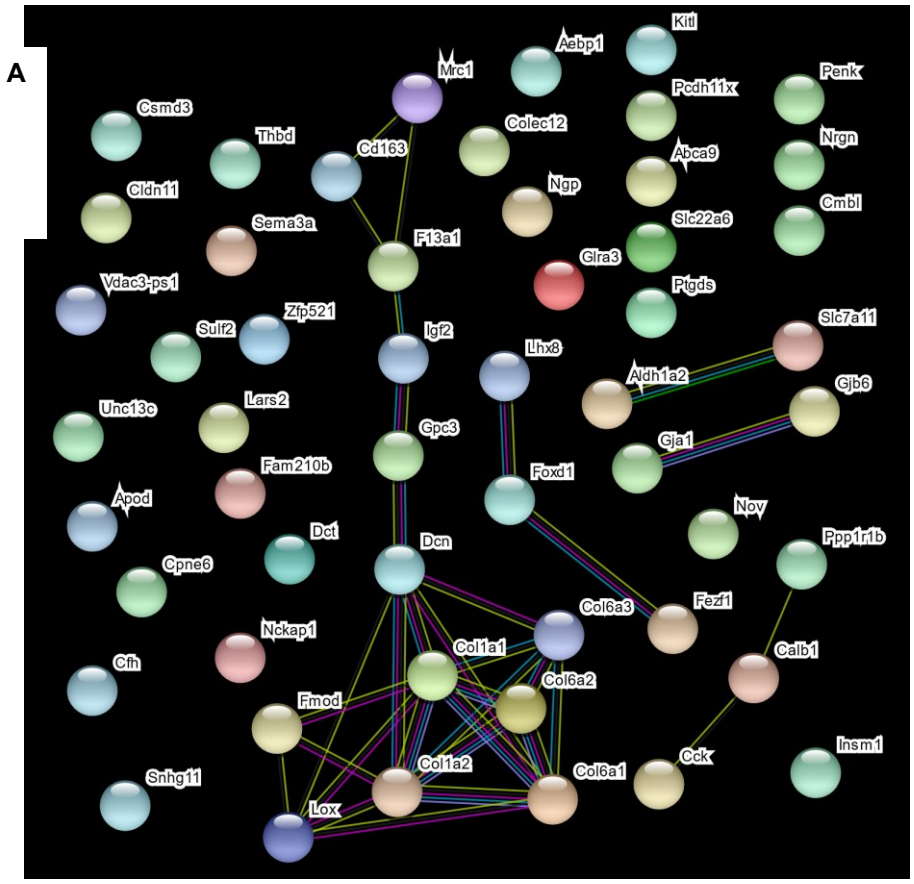
A
Kitl
Aebp1
Mrc1
Pcdh11x
Penk
Csmd3
Colec12
Thbd
Cd163
Nrgn
Abca9
Cldn11
Ngp
Cmbl
Slc22a6
Sema3a
F13a1
Clra3
Vdac3-ps1
Ptgds
Zfp521
Sulf2
Igf2
Slc7a11
Lhx8
Aldh1a2
Gjb6
Unc13c
Lars2
Gpc3
Gja1
Fam210b
Foxd1
Apod
Nov
Dct
Dcn
Ppp1r1b
Cpne6
Fezf1
Col6a3
Nckap1
Col1a1
Calb1
Cfh
Col6a2
Fmod
Insm1
Cck
Col1a2
Col6a1
Snhg11
Lox

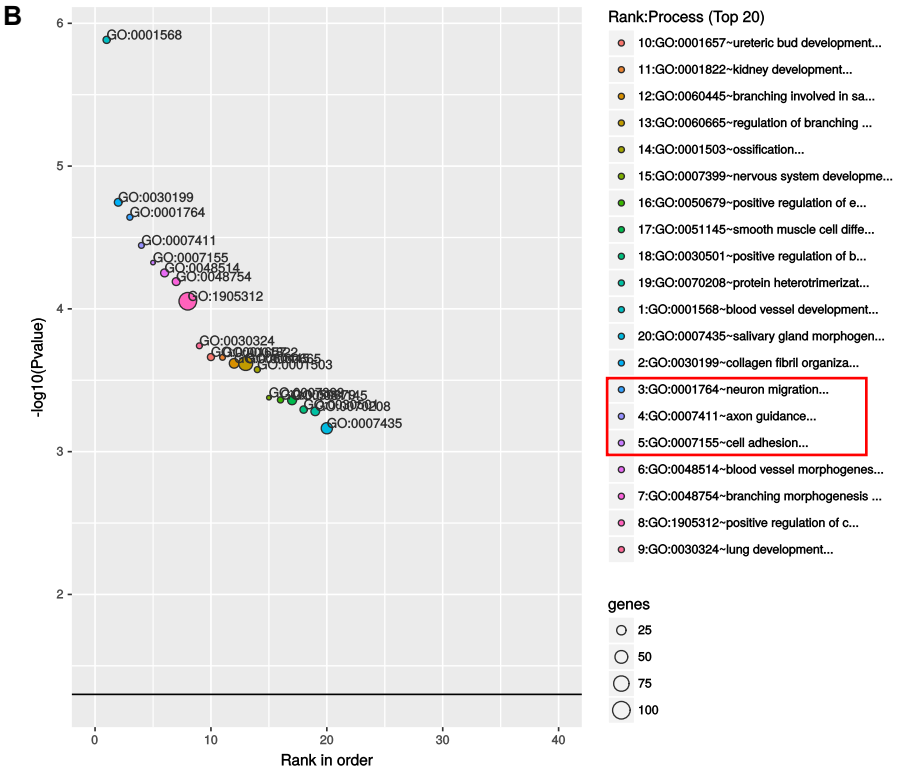
B
-log10(Pvalue)
Rank in order
GO:0001568
GO:0030199
GO:0001764
GO:0007411
GO:0007155
GO:0048514
GO:0048754
GO:1905312
GO:0030324
GO:0001503
GO:0007435
Rank:Process (Top 20)
10:GO:0001657~ureteric bud development...
11:GO:0001822~kidney development...
12:GO:0060445~branching involved in sa...
13:GO:0060665~regulation of branching ...
14:GO:0001503~ossification...
15:GO:0007399~nervous system developme...
16:GO:0050679~positive regulation of e...
17:GO:0051145~smooth muscle cell diffe...
18:GO:0030501~positive regulation of b...
19:GO:0070208~protein heterotrimerizat...
1:GO:0001568~blood vessel development...
20:GO:0007435~salivary gland morphogen...
2:GO:0030199~collagen fibril organiza...
3:GO:0001764~neuron migration...
4:GO:0007411~axon guidance...
5:GO:0007155~cell adhesion...
6:GO:0048514~blood vessel morphogenes...
7:GO:0048754~branching morphogenesis ...
8:GO:1905312~positive regulation of c...
9:GO:0030324~lung development...
genes
25
50
75
100

Figure 4: Molecular pathway alterations in the neonatal Auts2 cKO hippocampus

(A) STRING-DB network diagram for hippocampal differentially expressed genes (FDR Q<0.05) is enriched for an ECM related network. STRING PPI Enrichment P-value 2.22e-15. Expected number of edges for a random set: 6. Observed number of edges 33.

(B) geneSCF GO: biological process enrichment in the differentially expressed gene (P<0.01) in the AUTS2 cKO hippocampus.

Table 1: Differentially expressed genes in the AUTS2 cKO hippocampus (Q<0.05)

Gene Symbol	Wildtype (Average Count)	Knockout (Average Count)	Log_2(FC)	pValue	FDR qValue
Lhx8	0.261862	1.74526	2.73656	5.00E-05	0.017968
Ngp	0.152656	0.920655	2.59237	0.0001	0.030696
Vdac3-ps1	1.48968	7.15246	2.26344	5.00E-05	0.017968
Penk	4.51659	13.6084	1.59119	5.00E-05	0.017968
Dct	0.6134	1.49404	1.28432	5.00E-05	0.017968
Ppp1r1b	5.62458	11.3397	1.01157	5.00E-05	0.017968
Lars2	17.1119	32.8225	0.939684	5.00E-05	0.017968
Zfp521	4.27215	6.81402	0.673545	5.00E-05	0.017968
Cck	41.5953	64.182	0.625746	5.00E-05	0.017968
Sulf2	25.5733	37.1252	0.537758	0.00015	0.040928
Insm1	15.7763	22.709	0.525511	0.0001	0.030696
Fam210b	23.7564	33.4411	0.493306	0.0001	0.030696
Gja1	25.684	17.2046	-0.57808	5.00E-05	0.017968
Snhg11	118.845	79.4003	-0.58187	5.00E-05	0.017968
Csmd3	4.03685	2.6698	-0.5965	0.0001	0.030696
Sema3a	8.14514	5.29039	-0.62257	0.0001	0.030696
Auts2	46.7826	29.2098	-0.67952	5.00E-05	0.017968
Nrgn	91.6969	57.0828	-0.68382	5.00E-05	0.017968
Kitl	21.2097	13.086	-0.69669	5.00E-05	0.017968
Calb1	9.08265	5.49432	-0.72517	5.00E-05	0.017968
Apod	26.0164	15.1943	-0.77589	0.00015	0.040928
Slc7a11	3.07834	1.75847	-0.80784	0.0001	0.030696
Nov	11.2576	6.39866	-0.81506	5.00E-05	0.017968
Abca9	2.45127	1.3676	-0.84188	5.00E-05	0.017968
Unc13c	2.08545	1.14719	-0.86225	5.00E-05	0.017968
Gpc3	7.60042	4.15542	-0.87109	0.00015	0.040928
Colec12	5.70108	3.03319	-0.9104	5.00E-05	0.017968
Cpne6	7.14508	3.67995	-0.95726	5.00E-05	0.017968
Mrc1	3.01902	1.52782	-0.9826	5.00E-05	0.017968
H19	32.0735	16.1754	-0.98758	5.00E-05	0.017968
Col6a2	4.37957	2.1892	-1.00038	5.00E-05	0.017968
Cfh	4.74066	2.3486	-1.01329	5.00E-05	0.017968
Fezf1	4.63949	2.27262	-1.02961	5.00E-05	0.017968
Pcdh11x	9.76669	4.76822	-1.03442	5.00E-05	0.017968
Dcn	10.0747	4.78362	-1.07456	5.00E-05	0.017968
Col6a3	1.93944	0.899633	-1.10823	5.00E-05	0.017968
Igf2	48.4063	22.369	-1.1137	5.00E-05	0.017968
Col6a1	4.41883	2.00679	-1.13877	5.00E-05	0.017968
Thbd	3.1316	1.4114	-1.14978	5.00E-05	0.017968
Col1a2	12.0472	5.35717	-1.16916	5.00E-05	0.017968
Aebp1	4.02776	1.60786	-1.32483	5.00E-05	0.017968
Slc22a6	2.24547	0.884585	-1.34395	0.00015	0.040928
F13a1	2.99736	1.15616	-1.37435	0.00015	0.040928
Col1a1	5.04862	1.90162	-1.40866	5.00E-05	0.017968
Fmod	4.08637	1.5328	-1.41466	5.00E-05	0.017968
Lox	2.06956	0.759127	-1.44691	5.00E-05	0.017968
Glra3	0.964159	0.32964	-1.54838	5.00E-05	0.017968
Cmbl	4.13434	1.40124	-1.56096	5.00E-05	0.017968
Aldh1a2	4.44851	1.48484	-1.58301	5.00E-05	0.017968
Cd163	0.897557	0.265489	-1.75735	0.00015	0.040928
Ptgds	150.746	44.3613	-1.76475	5.00E-05	0.017968
Cldn11	4.64654	1.29085	-1.84784	5.00E-05	0.017968
Foxd1	0.754777	0.189825	-1.99138	5.00E-05	0.017968
Gjb6	2.41169	0.605251	-1.99444	0.0001	0.030696

3.2.3: Altered migration of TBR2+ intermediate neuronal progenitors in the developing Auts2 cKO hippocampus

Our RNA-sequencing analysis indicated dysregulation in several pathways involved in the process of neuronal migration into the nascent hippocampal formation. In order to assess if alterations in these processes resulted in measurable defects in hippocampal development, we examined the early post-natal development of the Auts2 cKO hippocampus by fluorescence immunohistochemistry. Establishment of the initial populations of neurons appeared largely unaffected in the Auts2 cKO hippocampus. The positioning of molecular layer resident Cajal-Retzius cells and the establishment of the initial shells of supra-pyramidal blade dentate granule neurons did not appear superficially altered in the knockout animals. Neither were gross alterations were observed in progenitor localization in the fimbrio-dentate junction and dentate migratory stream along the outer shell of the DG at P0.5 **(Figure 5A, B)**.

By P5, abnormalities in the migration of neuronal progenitors became dramatically more apparent. In wildtype mice, TBR2+ intermediate neuronal progenitors have begun to migrate into the hilar space **(Figure 5C)**. This occurs as a developmentally regulated transition from the immature sub-pial neurogenic zone to the adult sub-granular neurogenic zone (Li et al., 2009a). In the Auts2 cKO dentate gyrus, these TBR2+ progenitors failed to transition from the sub-pial neurogenic zone to colonize the hilus and subgranular zone **(Figure 5D)**. The absence of an established population of TBR2+ progenitors in the Auts2 cKO hilus persisted though P7.5 **(Figure 5 E-F)**. By P14.5 progenitors in the wildtype hippocampus had completely colonized the subgranular zone **(Figure 5G)**, fully

establishing the adult neurogenic niche, however, this colonization remained impaired in the Auts2 cKO **(Figure 5H)**. This failure of proper intermediate progenitor colonization is likely the underlying cause of the persistent morphological alterations that were apparent in the adolescent to adult dentate gyrus, as depletion of TBR2+ neural progenitors likely results in the production of fewer granule neurons. After postnatal day 7.5 development of the dentate infrapyramidal blade appeared disproportionately affected. Furthermore, at P14, dentate morphology in the Auts2 cKO appeared to resemble the morphology of a wildtype P7.5, this represents a substantial developmental delay in a key neurogenic window. Auts2 c-terminal cKO mice appear to exhibit a, primarily post-natal, developmental failure at a key transition point to adult hippocampal neurogenesis. This phenotype bears a remarkable resemblance to a specific phenotype of the dentate gyrus of Reeler mice (Li et al., 2009a). Notably, we found no deficit in RELN expression at P0.5 **(Figure S2A, B)**. Unlike the Reeler mice, migration of neural stem cells marked by SOX9 immunoreactivity did not appear appreciably affected by Auts2 cKO, although their number may be moderately reduced **(Figure S2C-H)**. In the Reeler mice, neural stem cells exhibited the same pattern of defective migration as the INPs, becoming stuck in the SPNZ and failing to migrate to the SGZ. However, in addition to marking neural stem cells, SOX9 also marks an abundant population of astrocytes. The prevalence of these cells, and the lack of molecular markers which clearly distinguish the NSCs may mask defects in NSC migration. Notably, we did not observe substantial cell death in the P0 and P7.5 timepoints analyzed **(Figure S3A-D)**. The lack of cleaved-caspase 3 staining in the knockout hippocampus indicated that the loss of TBR2+

progenitors from the hilar space is not likely a result of apoptosis, but rather a result of failed migration.

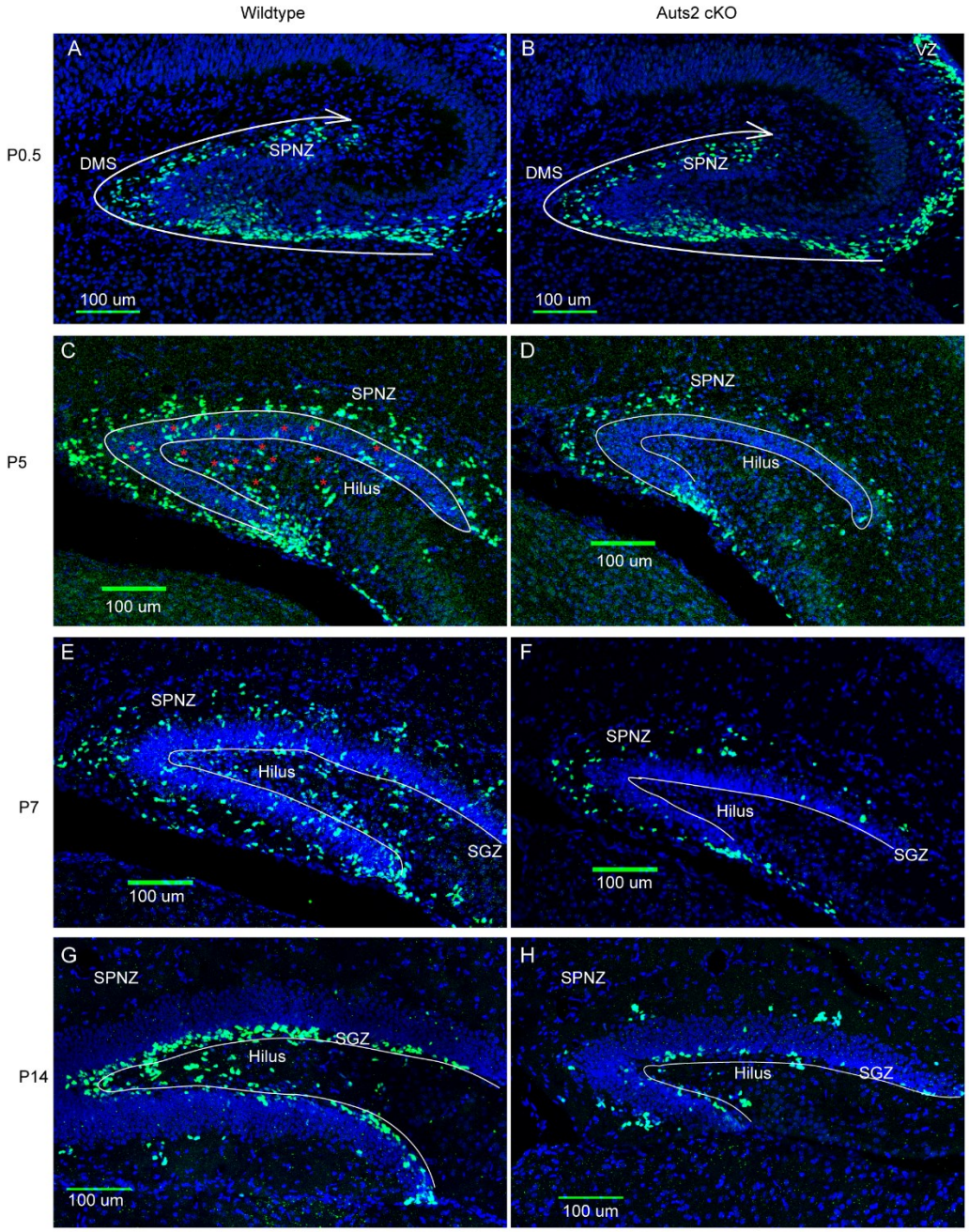

Figure 5: Impaired intermediate progenitor colonization of the neonatal dentate gyrus

TBR2+ Intermediate progenitors (INPs) (green) colonize the sub-pial neurogenic zone at P0.5 in both Wildtype **(A)** and Auts2 cKO **(B)** mice. INPs begin to migrate into the dentate blade and to colonize the hilus at P5 (indicated by *) in Wildtype **(B)** but not Auts2 cKO (C) mice. Dentate gyrus expansion continues in wildtype mice at P7 **(E)**, however, has not progressed in Auts2 cKO **(F)**. INPs have fully colonized the subgranular zone (SGZ) by P14 in wildtype **(G)**, however, colonization in AUTS2 cKO is reduced **(H)**.

3.2.4: Trans-hilar glial scaffolding necessary for neuroblast migration is not affected by Auts2 cKO

We observed multiple defects in neuronal populations which require migration into the hilar space. Migration into this niche from the dentate migratory stream and the fimbrio-dentate junction requires the establishment of a trans-hilar glial scaffolding which extends from the fimbrio-dentate junction into the sub-granular zone. This scaffolding is disrupted in both TBR2 knockout and Reeler mice (Brunne et al., 2013; Hodge et al., 2013). Our analysis of the Auts2 cKO hippocampus revealed a TBR2+ INP migration defect similar to the Reeler mice. As Reeler mice also exhibit defects in the organization of this hippocampal glial scaffolding as well as disorganization of radial glia processes in the dentate blades, we hypothesized that the Auts2 cKO hippocampus may exhibit a similar defect. We performed staining at P0.5 and P5 with Brain Lipid binding protein **(Figure 6A-B, E-F)**, as well as GFAP at P0.5 and P7 **(Figure 6C-D, G-H)** which label radial glial fibers, and at later ages, populations of astrocytes. In our observations, this scaffolding appeared to be present and normally organized in both knockout and wildtype hippocampus. This indicates that it is likely some property of the migrating neuroblasts themselves which is affected, such as their ability to bind the scaffolding, that results in their failure to colonize the hilar space rather than a defect in the scaffolding architecture.

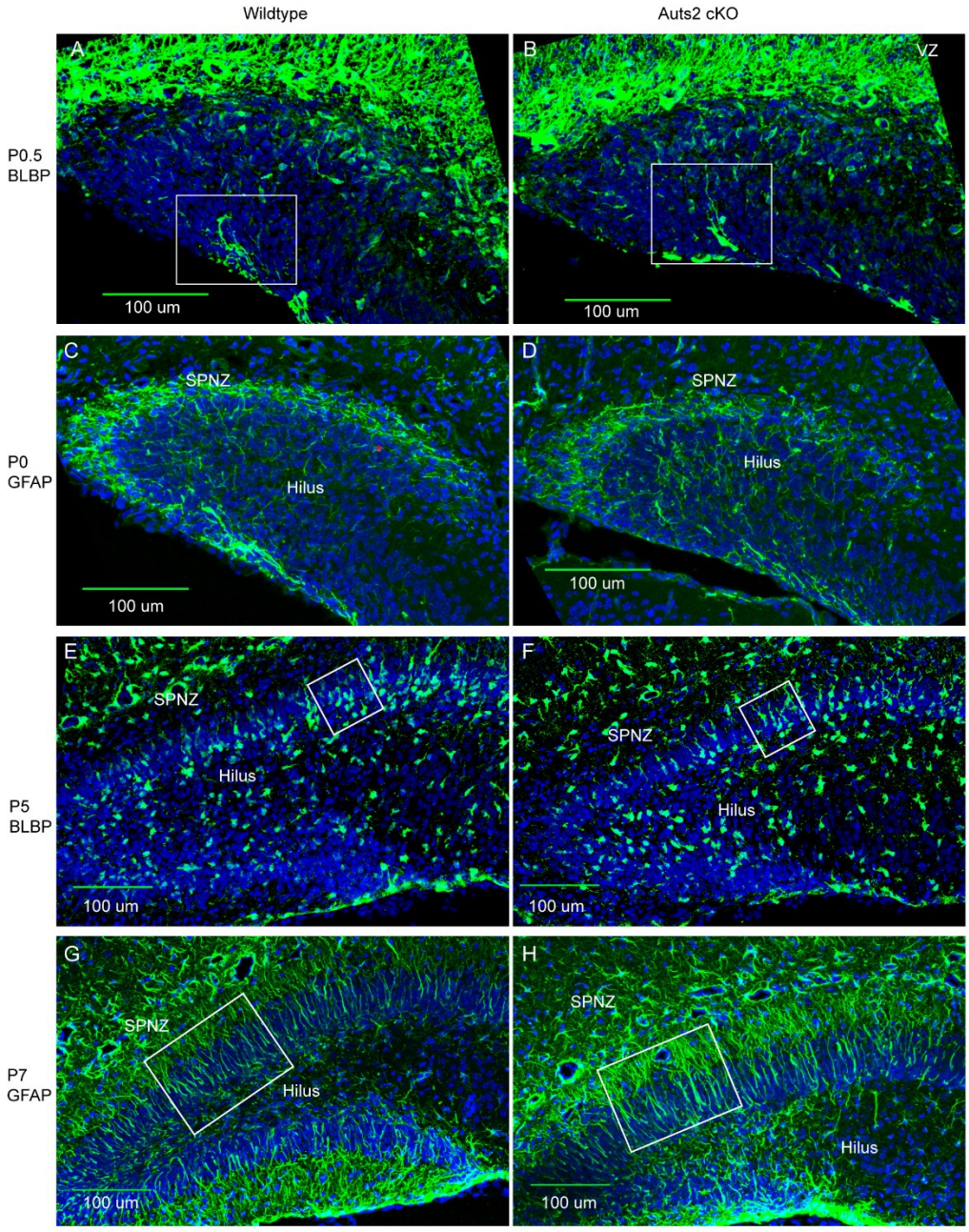

Figure 6: Dentate gyrus glial scaffolding is unaffected in Auts2 cKO

Brain Lipid Binding Protein (BLBP) labels trans-hilar glial scaffolding at P0.5 in Wildtype **(A)** and Auts2 cKO **(B)** (Boxed). Trans-hilar scaffolding is similarly labeled by Glial Fibrillary Acidic Protein (GFAP) at P0.5, as well as structure in the subpial neurogenic zone. This staining is present in both Wildtype **(C)** and Auts2 cKO **(D)**. BLBP labels a population of cells in the hilus, as well as radial glia in the dentate blade (box) in both Wildtype **(E)** and Auts2 cKO **(F)**. Radial glia fibers labeled by GFAP with characteristic architecture are clearly visible at P7 in both wildtype **(G)**, and Auts2 cKO **(H)** (box).

3.2.5: RNA-seq fingerprinting reveals hilar mossy neuron defects

While bulk, RNA-sequencing can provide insight into molecular pathway level alterations, and gross dissection of substructures (such as rostral cortex, or the hippocampal formation) can give information about region-specific processes, standard RNA-sequencing does not allow for analysis of changes in individual cell populations. In order to identify alterations in the transcriptional program of individual cells, single-cell sequencing using sorted dissociated cells, or captured single nuclei has become increasingly prominent. These techniques are both labor intensive, and for analysis of pathogenic processes in cells recapitulating a disease model, have the limitation that in the design of the experiment prior knowledge of the affected cell types is required to select the population which will be sequenced. However, these large single cell sequencing projects have produced an enormous amount of information on the transcriptional landscape of distinct neuronal populations. We hypothesized that these transcriptional signatures may be preserved to some degree in bulk sequencing data and that the alterations may be discernible with the GSEA methodology (Subramanian et al., 2005) to parse out particularly affected sub-populations for further analysis. In order to identify potential populations of neurons which may be affected in the AUTS2 cKO hippocampus, we constructed gene sets which uniquely identify individual neuronal populations in the Hippocampus from the HippoSeq database of single-cell RNA sequencing data (Cembrowski et al., 2016). The HippoSeq database consists of single-cell RNA-sequencing datasets constructed from dorsal and ventral populations of Hippocampal granule neurons, Hilar Mossy Neurons, CA1, CA2, CA3 pyramidal neurons, as well as some CA1 interneurons (http://hipposeq.janelia.org/). We constructed gene lists

from this repository which represent distinct molecular signatures for each of these cell populations. We then utilized this subpopulation identifying gene set as the query for GeneSet enrichment analysis (GSEA) using our Hippocampal RNA-sequencing. Using this methodology, we identified a significant downregulation in three gene sets in the Auts2 cKO hippocampus, these were the gene set which identifies Hilar Mossy Neurons, Granule Neurons, and Ventral CA1 neurons. The most significant, highest enriched pathway was the one which identified hilar mossy neurons (Normalized Enrichment score = -1.79, P-value = 0.000) **(Table 2)**. Based on this enrichment analysis, we hypothesized that Auts2 may regulate development of hilar mossy neurons in addition to the reported delays in granule neuron development.

Table 2: GSEA analysis of HippoSeq cell marker sets in the Auts2 cKO Hippocampus

Set Name	Size (Genes)	Enrichment Score (ES) In Knockout	Normalized ES	p-Value	FDR q-Value	Leading Edge
Mossy_Cell	69	-0.52	-1.79	0.000	0.004	tags=33%, list=16%, signal=40%
Ventral_CA1	16	-0.69	-1.76	0.003	0.003	tags=38%, list=4%, signal=39%
All_Granule_Cell	105	-0.43	-1.56	0.006	0.030	tags=31%, list=19%, signal=39%
CA2	46	-0.43	-1.39	0.061	0.095	tags=37%, list=19%, signal=46%
SST_CA1_Interneuron	357	-0.33	-1.34	0.012	0.115	tags=24%, list=17%, signal=28%
ALL_CA1	24	-0.45	-1.25	0.158	0.198	tags=29%, list=6%, signal=31%
PARLV_CA1_Interneuron	243	-0.28	-1.11	0.224	0.418	tags=27%, list=21%, signal=34%
Ventral_Granule_Cell	38	-0.33	-1.01	0.441	0.604	tags=37%, list=24%, signal=48%
Dorsal_CA1	11	-0.39	-0.90	0.606	0.830	tags=55%, list=20%, signal=68%
CA1_Proj_Postsubiculum	228	-0.22	-0.86	0.779	0.823	tags=21%, list=20%, signal=27%
CA1_Proj_Amydala	110	-0.18	-0.67	0.982	0.968	tags=15%, list=17%, signal=18%
Dorsal_Granule_Cell	244	0.19	0.90	0.897	0.671	tags=23%, list=19%, signal=28%
CA1_Proj_NAC	214	0.23	1.06	0.228	0.687	tags=22%, list=14%, signal=26%

3.2.6: The Auts2 cKO hippocampus lacks hilar mossy neurons

Disambiguation of our hippocampal bulk sequencing experiment using the HippoSeq gene set database identified a potential abnormality in hilar mossy neuron (HMN) development in the Auts2 cKO hippocampus. This finding was unexpected as, while thought to be born at E13.5, HMNs are not conventionally detectable in the hippocampus until the hilus becomes morphologically distinct at the end of the first post-natal week. Based on this finding in our P0.5 sequencing data, we sought to test the hypothesis that AUTS2 disruption alters Hilar Mossy neuron architecture. Hilar mossy neurons are conventionally detected by calretinin immunoreactivity which labels cell bodies in the temporal dentate gyrus, as well as the HMN axons which project to the inner molecular layer along the septotemporal extent of the DG **(Figure 7A)**. This inner-molecular layer axon band forms the Hippocampal Associational-Commissural pathway. Calretinin immunoreactivity is able to visualize these cells initially at the end of the first post-natal week with increasing intensity and distinction of the axon connectivity into adulthood. We initially selected an early adult (P52) timepoint in order to maximize our ability to visualize the axon connectivity of the HMNs across all dentate gyrus sections.

Examination of Calretinin immunoreactivity in our deletion of all AUTS2 isoforms revealed a dramatic abnormality in the connectivity of the hippocampus. These mice lacked the associational/commissural pathway marked by calretinin almost entirely **(Figure 7B)**. These axons, consisting of glutamatergic projections from hilar mossy neurons onto dentate granule neuron, and interneuron dendritic arbors. This forms a major pathway of interconnectivity in the hippocampus that is thought to be involved in associational

memory and encoding of sequences of information (Scharfman and Myers, 2013). In temporal sections as well, extreme depletion of calretinin-positive hilar mossy neuron cell bodies was apparent **(Figure 7C, D)**. However, some inner-molecular layer calretinin staining was still present, potentially innervating axons from another brain region or from HMNs which escaped EMX1-cre mediated Auts2 deletion. Calretinin is not a strong marker of HMNs only exhibiting immunoreactivity in the temporal dentate gyrus in mice and some primates and human hilar mossy neurons are not immunoreactive for calretinin at all (Seress et al., 2008). In order to determine if Hilar Mossy Neurons are truly absent in the Auts2 cKO hippocampus, we investigated other cellular markers for detection of this neuronal population which would identify cells across the septotemporal extent of the DG. In wildtype mice, we found that HMNs are immunoreactive for the transcription factor SATB1 at all levels of the DG (**Figure 7A, C** shown: PanSATB immunoreactivity) and for AUTS2 **(Figure S4)**. This labeling was present utilizing an antibody specific to SATB1 as well as a higher titer antibody which reacts to Satb1 and Satb2, it was not present with a specific antibody to SATB2 **(Figure S4).** When we examined the Auts2 cKO dentate gyrus, however, we found no hilar mossy neurons in the mature dentate gyrus, consistent with the observation of absent calretinin staining **(Figure 7B, D)**. These neurons are traditionally only identifiable in the dentate hilus at the end of the first postnatal week **(Figure 7E)**. Utilizing the pan-SATB antibody we were able to detect hilar mossy neurons in the nascent hilar space as early as P0.5 **(Figure 7G)**. However, even at this extremely early stage of hilar development the Auts2 mice still lacked this neuronal population **(Figure 7F, H)**. In addition to the specific expression of SATB1 by Hilar Mossy Neurons in the Dentate Gyrus.

SATB1 is also expressed by a subset of cortical pyramidal neurons where it regulates expression of immediate-early genes, and neuronal spine density (Balamotis et al., 2012). We previously reported a lack of gross morphological abnormalities in the Auts2 cKO cortical plate, however, the loss of a small sub-population of heterogeneously distributed neurons may not have been detectable. To determine if AUTS2 deficiency regulated development of SATB1+ neuronal populations globally rather than a specific effect on SATB1+ hilar mossy neurons in the hippocampus, we assessed immunostaining for SATB1 in AUTS2 cKO cortical plate. We found abundant expression of SATB1 in cortical plate neurons **(Figure S4)**. This indicates that the process that results in loss of Hilar Mossy Neurons is specific to that hippocampal neuronal population and not all SATB1 expressing excitatory neurons.

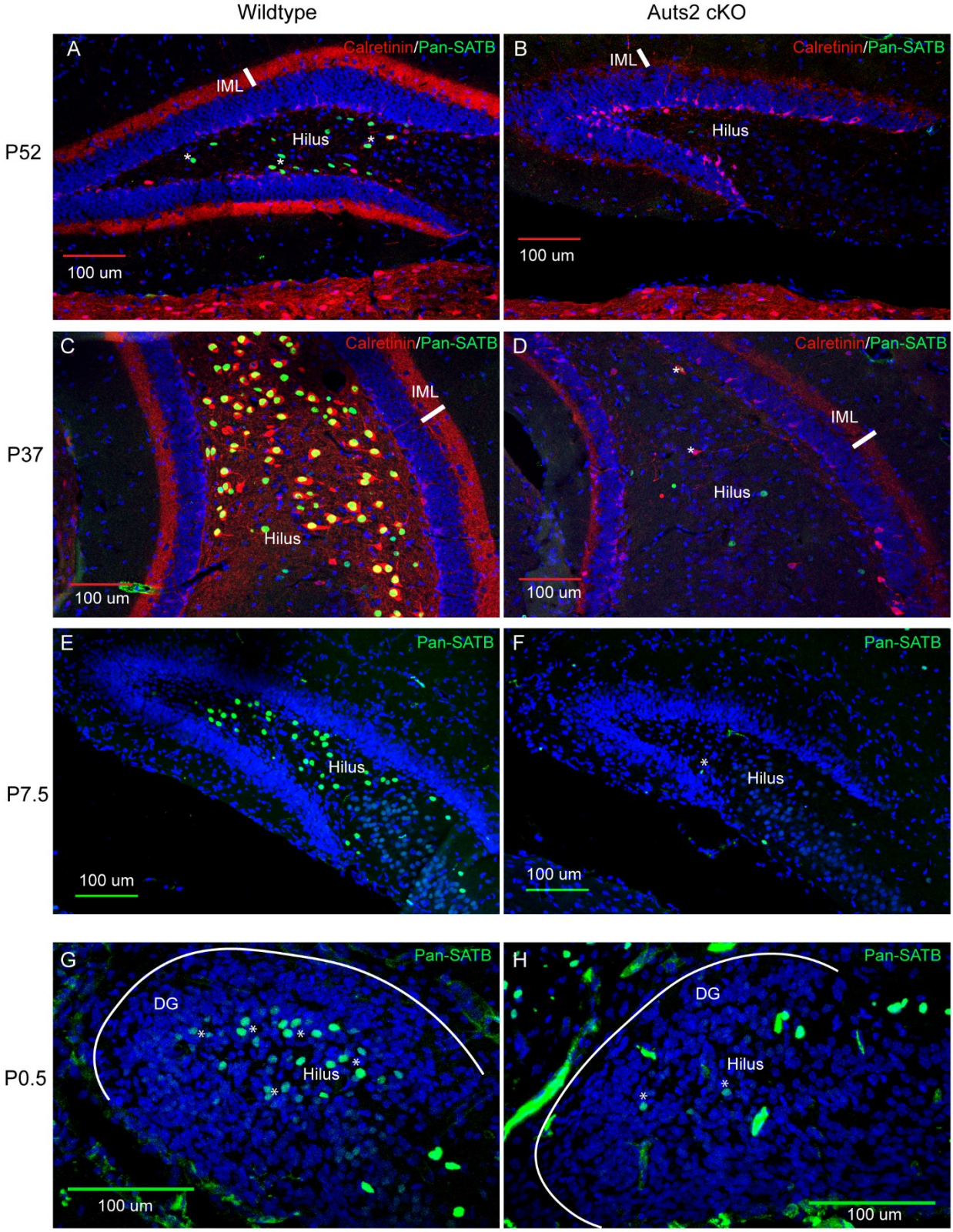
Wildtype
Auts2 cKO
P52
P37
P7.5
P0.5
A
B
C
D
E
F
G
H
Calretinin/Pan-SATB
Pan-SATB
IML
Hilus
DG
100 um

Figure 7: Hilar mossy neurons are absent from the Auts2 cKO dentate gyrus

Calretinin **(**red**)** marks Hilar Mossy Neuron (HMN) axons in the inner molecular layer (IML) which forms the hippocampal associational commissural pathway of the dentate gyrus in adult wildtype mice in **(A)** septal and (**C)** temporal sections. This immunoreactivity is markedly reduced in adult Auts2 cKO hippocampus **(B, D)**.

HMNs are labeled by Calretinin (Red), and SATB (Green) in Wildtype temporal hippocampus **(C)**. HMNs are labeled by SATB and not calretinin in the septal hippocampus **(A)**.

HMNs are absent in Auts2 cKO by both negative hilar calretinin (red) **(D)**, and SATB (green) **(D, B)**.

HMNs are traditionally detectable at P7.5 and are present in wildtype (SATB – green) **(E)**, but not Auts2 cKO **(F)** dentate.

HMNs are detectable at P0.5 by SATB (green) immunoreactivity in wildtype **(G)**, but absent in Auts2 cKO **(H)**.

3.2.7: TBR1 and TBR2 knockout does not result in absence of hilar mossy neurons

Hilar mossy neurons are believed to follow a broadly similar developmental program to other excitatory neuron populations (Li et al., 2008). Above, we described that, although dentate morphology is altered in TBR1 and TBR2 knockout animals, hippocampal neurons maintain their expression of AUTS2. To determine if the loss of Hilar mossy neurons was unique to the AUTS2 model we assessed their presence using calretinin and SATB immunoreactivity. We found that SATB+ cells are resident in the hilar space of both TBR1 and TBR2 knockout animals **(Figure 8A-D)** indicating that mossy neuron birth in these models is unaffected. Over all HMN number appeared reduced in the TBR2 cKO, however, this appeared proportional to the reduction in total dentate volume, in contrast to the Auts2 cKO hippocampus, in which HMNs were selectively and severely depleted. Additionally, a calretinin+ axon band was present in the inner molecular layer of both knockout animals indicating that the hilar mossy neuron axon outgrowth which forms the associational/commissural pathway innervating the dentate gyrus is also intact (not shown). Additionally, despite the similar defects in migration of TBR2+ progenitors in the hippocampus of Auts2 cKO and Reeler mice, previous research has shown that while HMNs are disorganized in Reeler mice they are not lost (Drakew et al., 2002). These data indicate that despite its relatively widespread expression in excitatory neurons and some progenitors in the hippocampus, AUTS2 may have a unique role in specifying the fate and integration of hilar mossy neurons. However, the molecular mechanism of this fate specification remains unclear.

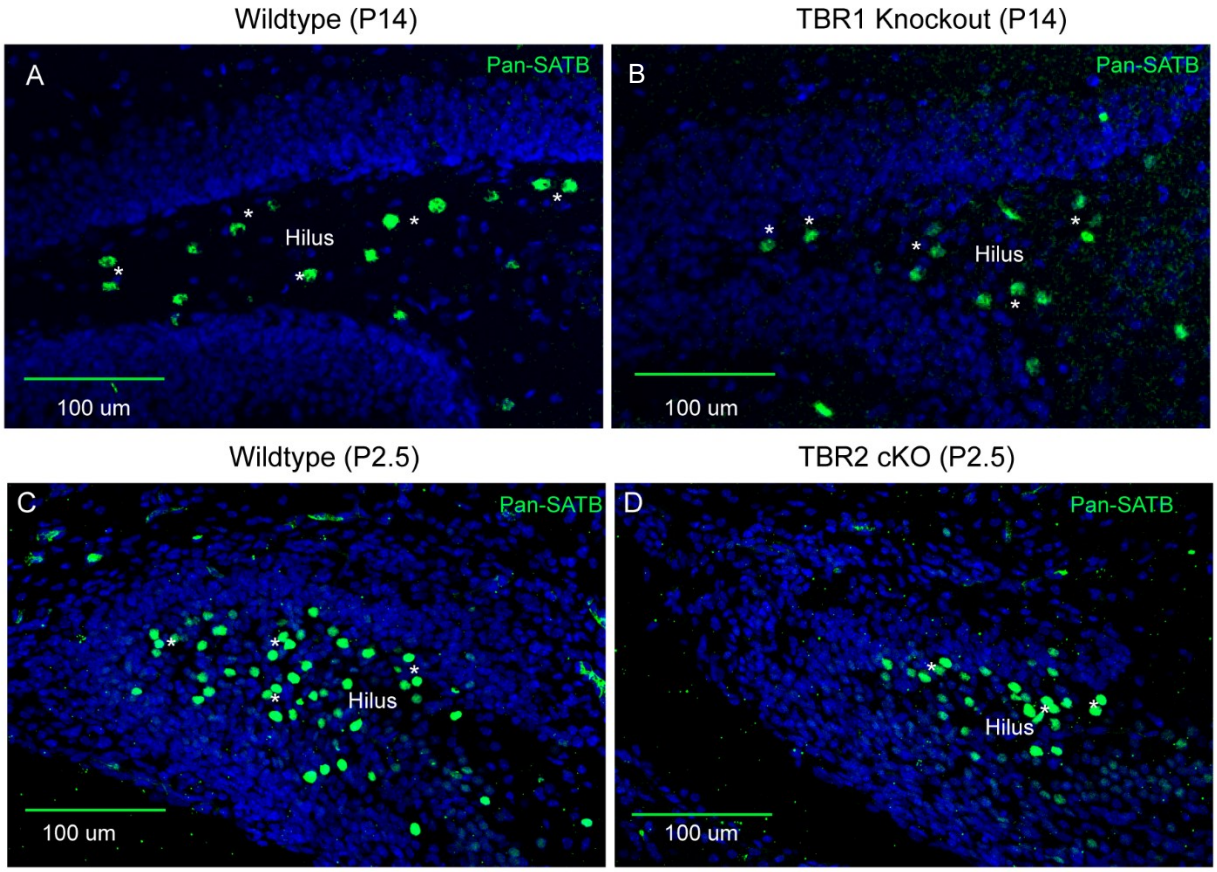

Figure 8: Hilar mossy neuron loss is specific to Auts2 cKO

Hilar mossy neurons are detectable by SATB immunoreactivity in wildtype **(A, C)** and in both TBR1 knockout **(B)** and TBR2 cKO **(D)** dentate gyrus.

3.3: DISCUSSION

3.3.1: Developmental delay of progenitor establishment in the developing Auts2 cKO dentate gyrus

We observed that while the initial phase of dentate progenitor colonization occurs normally in the Auts2 cKO hippocampus, this process breaks down within the first post-natal week in Auts2 cKO mice. This breakdown occurs during the primary initial expansion of hippocampal neurogenesis and a key transition point to establishing the adult neurogenic niche **(Figure 5)**. Neurogenesis in the adult hippocampus occurs from a population of neural stem cells, and TBR2+ intermediate progenitors which, in adults, reside on the boundary of the hilus and granule cell layer – the subgranular zone (Hodge et al., 2008). This neurogenic niche produces new hippocampal neurons throughout the lifetime of many mammals, and at a minimum, into adolescence in humans (Boldrini et al., 2018; Eriksson et al., 1998; Sorrells et al., 2018). The establishment of this niche occurs, in mice, near the end of the first post-natal week, a process which was dissected by previous research on Reelin and CXCR4 signaling (Li et al., 2009a). Briefly, this is the second stage of a process that is begun embryonically with the establishment of the Fimbrio-dentate junction (FDJ), a transient subpial niche at the junction of the dentate gyrus and fimbria, derived from the cortical hem. Migration of the progenitor population out of the FDJ occurs along the dentate migratory stream to establish a niche along an invagination of the neuroepithelium in the area that will become the dentate gyrus. Li et al. (2009) found that migration into this sub-pial neurogenic zone (SPNZ) is controlled by expression of Cxcl12 and Cxcr4 and dependent on the ligand-receptor interaction. In the Auts2 cKO mice, the initial stages of this process

occur without any gross defect. TBR2+ progenitors are established in the SPNZ at P0.5 along with the outer shell of the suprapyramidal blade and the SPNZ resident population of Cajal-Retzius cells. Signaling by Cajal-Retzius cells though RELN is necessary to complete the second phase of this transition. Reeler mice exhibited a phenotype where INPs and Nestin+ neural stem cells are delayed in their migration out of the SPNZ and into the hilus. Therefore, the RELN+ Cajal-Retzius cells appear to play a key role in the transition from a transient SPNZ to the permanent sub-granular neurogenic zone. In the Auts2 cKO mice, we observed a similar failure in the migration of TBR2+ intermediate neuronal progenitors (INPs) from the sub-pial neurogenic zone to the sub-granular neurogenic zone. In wildtype mice, by postnatal day 5, TBR2+ INPs have redistributed from the SPNZ across the entire dentate field. In the Auts2 cKO mice, this process had not occurred, TBR2+ cells remain clustered in the subpial zone. By P7.5, when TBR2+ progenitors have begun to form a recognizable ribbon of cells along the SGZ in wildtype mice, there are still no cells detected in this region in the AUTS2 cKO and these cells were almost entirely excluded from the hilar space in the knockout animals. At P14, the ribbon of progenitors was firmly established in wildtype mice spanning the entire SGZ, but this was incomplete in the cKO. Some progenitors did eventually colonize the SGZ as evidenced by staining on P14, however, appeared markedly reduced in quantity. Additional quantitative studies are necessary to determine the extent to which adult neurogenesis is impaired in the hippocampus of Auts2 cKO animals. This is a dramatic delay in the establishment of a key neurogenic population during a critical window of hippocampal development in which the primary postnatal construction and reorganization of the hippocampus occurs, and the life-long population of proliferative

progenitors is established. The stalling of this process in the Auts2 cKO hippocampus appears to result in a permanently stunted dentate gyrus with a depleted intermediate progenitor pool. This observation shares some similarity with the phenotype of the Reeler hippocampus which also exhibits an inability to transition from SPNZ to SGZ neurogenesis. Despite this, the Auts2 cKO mice appear to have normal RELN expression in the SPNZ space indicating that this process is molecularly distinct in Auts2 cKO mice from the disruption in Reeler. However, as we have shown, the RELN expressing Cajal-Retzius cells exhibit an abnormal molecular phenotype of upregulation of the endogenous opioid precursor peptide PENK. Exposure to processed enkephalins has been shown to reduce dendritic growth in cerebellar granule neurons and inhibit proliferation of cultured neural progenitors (Hauser et al., 2000) however the effect of these molecules on neuronal or neuronal progenitor migration in the hippocampus has not been clearly assessed. Additionally, unlike the Reeler mice which exhibited a migratory defect in both neural stem cells and INPs, the Auts2 cKO defect appears to be restricted to the INP population. Our RNA sequencing study on the early postnatal Auts2 cKO hippocampus identified an enrichment for the “neuronal migration” and “cell adhesion” Biological Process GO terms in the cKO dysregulated geneset. The underlying molecular function which appeared to mediate this dysregulation was related to heparin binding. Heparan-Sulfate proteoglycans (HSPGs) form a major component of the brain extracellular matrix, with the expression of the various heparinated proteins by neurons and neural progenitors. These HSPGs have been found to regulate growth factor response in NSCs, neurogenesis, synaptogenesis and axon guidance (Yamada et al., 2017; Yamaguchi, 2001). Future work assessing the expression patterns and molecular

functions of these genes may be able to determine the specific molecular mechanisms by which NSC and INP migration are differentially regulated in Reeler and Auts2 mice. We did not observe increased cell death at P0.5 or P7.5 nor upregulation of cell death associated pathways despite an apparent decrease in cell number and dentate volume. This suggests the possibility that in addition to a failure of neuronal migration, increased enkephalin signaling may play a role in suppressing proliferation of these progenitors leading to the observed reduction in the population without an induction of apoptosis. Based on these data, and the similarities to the hippocampus of the Reeler mutant, we conclude that the AUTS2 syndrome may involve a pathology of Cajal-Retzius cells in a manner that is similar to that caused by mutations in RELN but possibly through an independent molecular mechanism. This neuronal migration phenotype is also consistent with previously reported work by Hori et al (2014). This work identified transiently delayed neuronal migration in the Auts2 deficient cortex which was dependent on Rac signaling. Alterations in the Rac signaling pathway were not identified in our hippocampal sequencing data. However, this may be due to the different developmental stages of the cortex and hippocampus during the early post-natal period.

3.3.2: Identification of hilar mossy neuron defects by gene set enrichment analysis

Utilizing a collection of cellular markers curated from a hippocampal single-cell RNA-sequencing database (Cembrowski et al., 2016), Gene Set Enrichment Analysis (GSEA) of our P0.5 hippocampus RNA-sequencing dataset was able to conclusively identify the down-

regulation of Hilar Mossy Neuron marker genes at this early age when they are still believed to be immature (Pennucci et al., 2011). Downregulation of this gene set was validated experimentally by identifying loss of Hilar Mossy Neurons by immunohistochemistry in the AUTS2 knockout hippocampus. This analysis additionally provides a proof of concept that high-quality cellular identity marker Gene sets constructed from single-cell sequencing data can be utilized to parse out affected subpopulations of cells from bulk tissue sequencing data. While we have shown the utility of this data in parsing out a cell level phenotype from bulk-sequencing data, the gene sets utilized represent a preliminary selection of markers. Unfortunately, the single-cell sequencing database utilized only contained data from abundant adult neuronal populations. The utility of this approach could be improved through the inclusion of datasets from transient developmental populations of neuronal progenitors, immature neurons, sparser populations of developmentally important cells such as Cajal-Retzius cells, and additional interneuron populations. These cell-signature gene sets may enable the identification of defects in specific neuronal populations by parsing apart previously published and future bulk tissue RNA-sequencing experiments. Perhaps additional molecular profiling of earlier stages of the hippocampus using the genes from this dysregulated pathway will identify molecular markers of immature hilar mossy neuron that can be used for further tracing of these cells prenatally. This approach appears promising for the identification of specifically affected populations of cells within traditional “whole tissue” RNA-sequencing experiments and would benefit from the curation of marker sets from additional single cell databases to expand the repertoire of identifiable cells.

3.3.3: Loss of hilar mossy neurons from the AUTS2 deficient hippocampus

In investigating the alterations of neuronal population observed in our RNA-sequencing data filtered through the HippoSeq database, we identified and validated a profound loss of Hilar Mossy Neurons (HMNs) in the Auts2 knockout hippocampus. Loss of HMNs is a phenotype typically identified in association with seizure disorders (Blümcke et al., 2000), and depletion of these neurons is suspected to contribute to disinhibition of the hippocampal circuit (Zappone, 2004). However, unlike these disorders which typically result in progressive loss of HMNs, in our model loss of these neurons is apparent from birth. While the Auts2 cKO mice did not appear to exhibit spontaneous seizures, the possibility of electrophysiological abnormalities due to the loss of this neuronal population merits further study. The hippocampal disinhibition resulting from the loss of this population may predispose patients to the development of severe epilepsy. This is of particular interest considering the prevalence of epilepsy as a comorbidity of autism syndromes (Gabis et al., 2005). Developmental tracing of immature HMNs has been a historically difficult problem with very little data on their embryonic origin. Birth dating experiments have shown that these cells are born during the extremely proliferative E12-E14 window (Angevine, 1965). However, they are virtually indistinguishable from other migrating calretinin positive neurons until the hilus becomes distinct at the end of the first post-natal week. Using antibodies against the transcription factor SATB1, we are able to identify these neurons on P0.5, which is, to our knowledge, the earliest age these neurons have been conclusively observed. However, this is insufficient for understanding the pathology of HMN loss in the AUTS2 mice, as we observed these cells to be absent even at this early time point. This severe

and specific loss of HMNs in the Auts2 cKO mouse represents the first known implication of these cells in an intellectual disability syndrome model. Loss of HMNs has also been reported in Lef1 and NeuroD mutant mice, however, this is likely a consequence of near complete agenesis of the dentate gyrus (Li et al., 2008). The Auts2 model, while exhibiting substantially reduced DG volume, affects HMNs much more specifically. This selective loss of HMNs in the Auts2 cKO mouse more closely mirrors defects observed in Rac1/Rac3 mutant mice (Pennucci et al., 2011) which also observed selective loss of HMNs in double, but not single mutant mice. The authors of this study suggested that loss of HMNs in Rac mutant mice may be a result of failed migration of HMN precursors into the hilus. Auts2 has also been shown to be involved in regulating RAC1 signaling through Prex1 both in our cortical sequencing data, and previously (Hori et al., 2014). Although we did not detect transcriptomic alterations in Rac signaling specifically in the P0.5 Auts2 deficient hippocampus, other cell migration pathways were affected. Alterations in Auts2 dependent Rac1 signaling resulting in failed migration of HMN precursors at earlier time points may still underlie the absence of these cells in the AUTS2 deficient hippocampus and warrants further investigation at earlier embryonic ages.

Supplementary Data

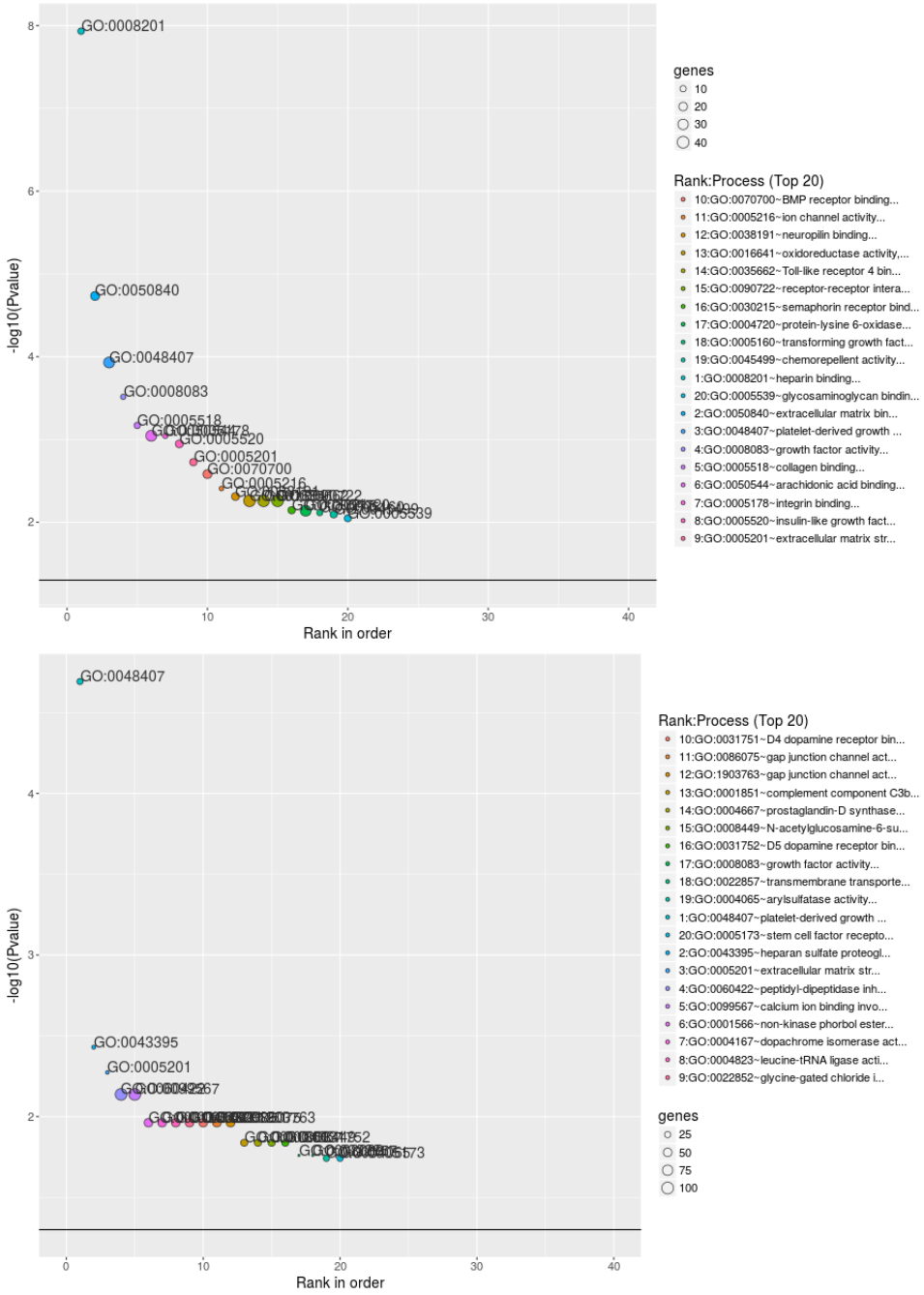

Figure S1, Related to Figure 4: GO: molecular function pathways enriched in the AUTS2 cKO hippocampus

(A) Pathways enriched in the dysregulated (P<0.01) genes.

(B) Pathways enriched in the dysregulated (Q<0.05) genes.

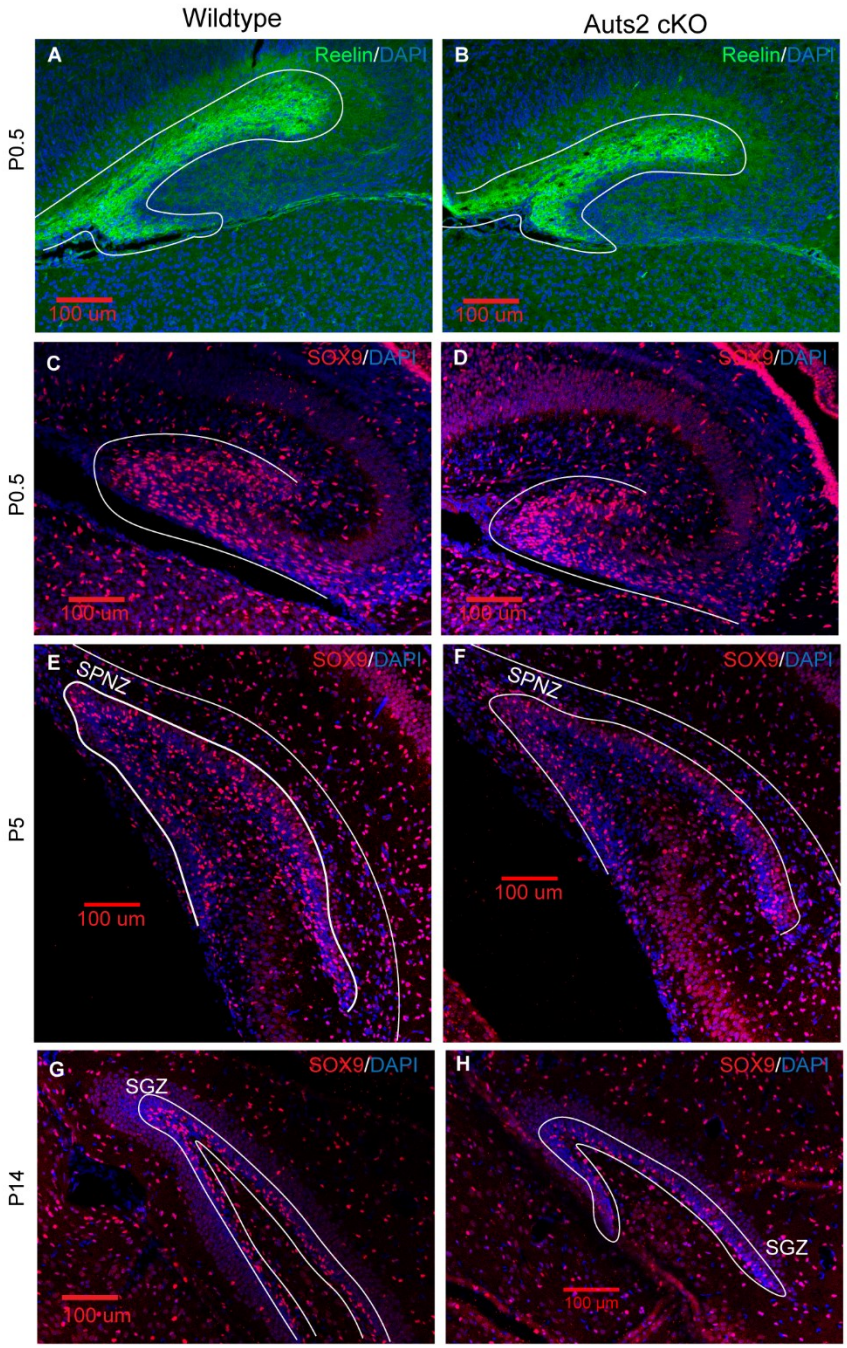

Figure S2, Related to Figures 5,6: Expression of RELN and SOX9 in the AUTS2 cKO hippocampus

(A, B) Expression of RELN in the marginal zone of the P0.5 dentate gyrus is unaffected by Auts2 cKO

(C-H) Migration of SOX9+ NSCs is unaffected in Auts2 cKO at P0 **(C-D)**. P5 (migration into the dentate blade out of the Subpial neurogenic zone (SPNZ) **(E-F)**. At P14 during colonization of the Subgranular zone (SGZ) **(G-H)**.

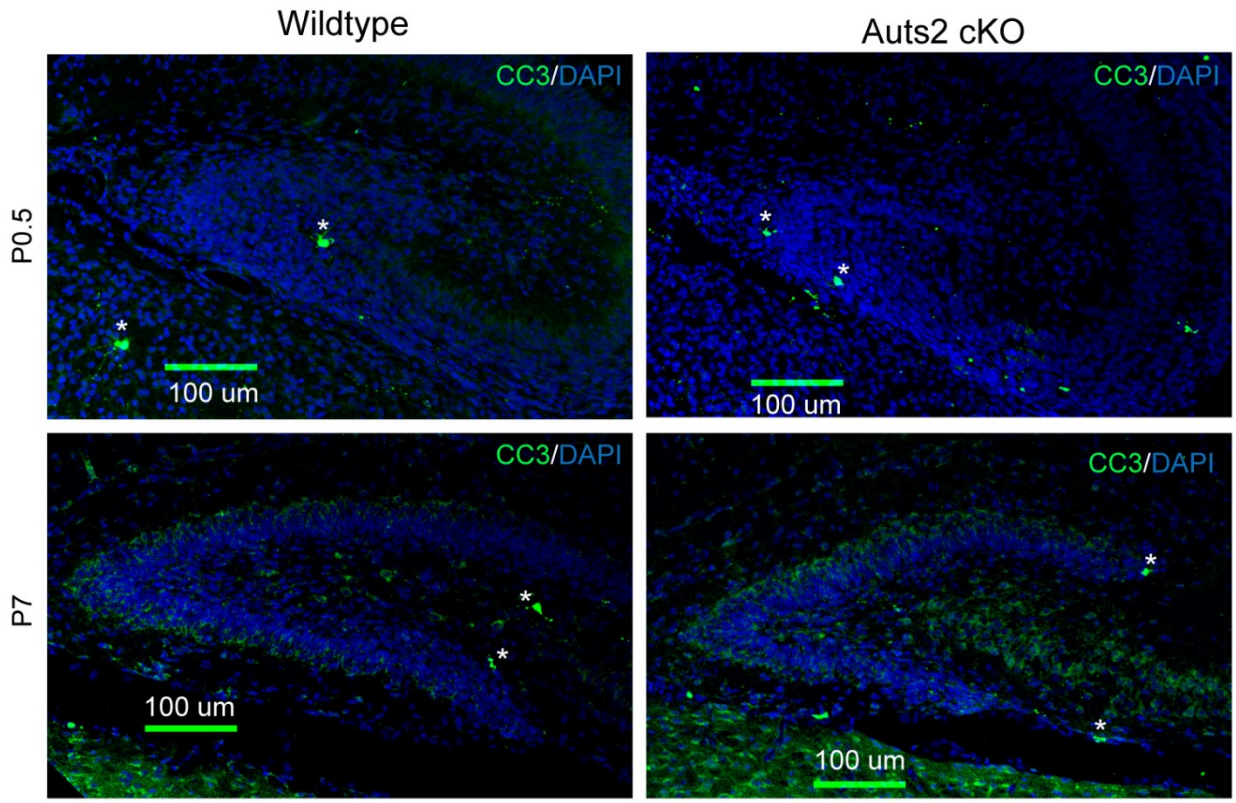

Figure S3, Related to Figures 5,6: No increased cell death in Auts2 cKO dentate gyrus

Immunohistochemistry for Cleaved Caspase 3 (CC3) labeling apoptotic cells in the dentate gyrus. Apoptotic cells indicated by (*). **(A, B)** Postnatal day 0.5. **(C,D)** Postnatal day 7.

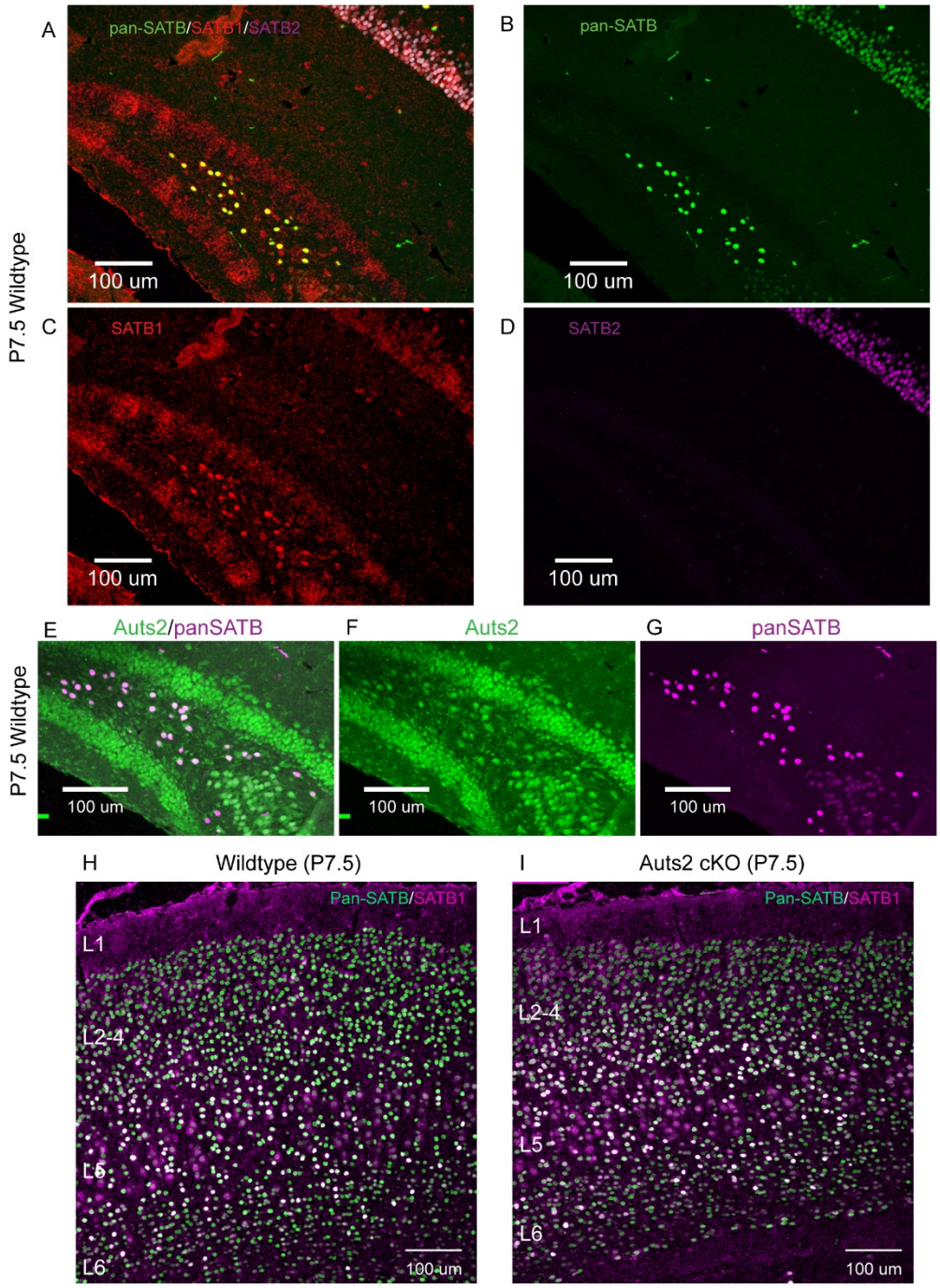

Figure S4, Related to Figure 7: AUTS2+ hilar mossy neurons are marked by SATB1, however, Auts2 cKO does not affect SATB1+ cortical plate neurons

(A-D) SATB1 **(C)** but not SATB2 **(D)** is specific for hilar neurons. Both antigens are detected by pan-SATB **(B)** Merge **(A)**
(E-G) AUTS2 **(F)** is expressed in SATB+ Hilar Neurons **(G)** Merge **(E)**

(H, I) SatB1+ neurons are present in both Wildtype **(H)** and Auts2 cKO **(I)** cortical plate

Table S1, Related to Table 1: Expression profiling of Auts2 cKO hippocampus

– See additional files –

Table S2, Related to Figure 4: GO: molecular function enrichment analysis on Auts2 cKO differentially expressed (P<0.01) genes (shown: pathway FDR <0.1)

Genes	Process~Name	# Genes	Gene group	percentage	P-value	Benjamini and Hochberg (FDR)
Adamts15; Bmp4; Bmp7; Cfh; Col25a1; Ctgf; Fgf10; Fgfr1; Fn1; Gpnmb; Grem2; Pcolce; Pf4; Postn; Vtn; Nov;	GO:0008201~heparin binding	16	145	11.03448	1.17E-08	4.60E-06
Adamts15; Bgn; Dcn; Spp1; Tgfbi; Vtn;	GO:0050840~extracellular matrix binding	6	28	21.42857	1.85E-05	0.003637
Col1a1; Col1a2; Col3a1; Col6a1;	GO:0048407~platelet-derived growth factor binding	4	12	33.33333	0.000118	0.015441
Bmp4; Bmp6; Bmp7; Ctgf; Fgf10; Igf2; Inhbb; Kitl; Nov; Bdnf;	GO:0008083~growth factor activity	10	147	6.802721	0.000306	0.030139
Dcn; Lum; Mrc2; Pcolce; Tgfbi; Vtn;	GO:0005518~collagen binding	6	58	10.34483	0.000678	0.05091
S100a8; S100a9; Stx3;	GO:0050544~arachidonic acid binding	3	9	33.33333	0.000903	0.05091
Col3a1; Ctgf; Fn1; Gpnmb; Igf2; Nov; Tgfbi; Vtn;	GO:0005178~integrin binding	8	112	7.142857	0.000904	0.05091
Ctgf; Igfbp6; Igfbpl1; Nov;	GO:0005520~insulin-like growth factor binding	4	24	16.66667	0.00113	0.055662
Col1a1; Col1a2; Col3a1; Lama1;	GO:0005201~extracellular matrix structural constituent	4	28	14.28571	0.001884	0.082477

Table S3, Related to Figure 4: GO: biological process enrichment analysis on Auts2 cKO differentially expressed (P<0.01) genes (shown: pathway FDR <0.05)

Genes	Process~Name	# Genes	Gene group	percentage	P-value	Benjamini and Hochberg (FDR)
Aldh1a2; Bmp4; Col1a1; Col1a2; Col3a1; Foxc1; Lox; Shb; Sphk1; Loxl1;	GO:0001568~blood vessel development	10	74	13.51351	1.31E-06	0.002133
Col1a1; Col1a2; Col3a1; Foxc1; Lox; Lum; Loxl1;	GO:0030199~collagen fibril organization	7	43	16.27907	1.79E-05	0.01243
Auts2; Cck; Cntn2; Fezf1; Gja1; Met; Nr2f1; Nr2f2; Ntn1; Robo3; Sema3a;	GO:0001764~neuron migration	11	129	8.527132	2.28E-05	0.01243
Bdnf; Bmp7; Cntn2; Epha4; Fezf1; Foxd1; Ngfr; Ntn1; Robo3; Sema3a; Sema3c;	GO:0007411~axon guidance	11	136	8.088235	3.59E-05	0.014679
Cdh12; Cldn11; Cntn2; Cntn3; Col6a1; Col6a2; Ctgf; Epha4; Flrt1; Fn1; Gpnmb; Itga8; Kitl; Lama1; Ncam2; Negr1; Nuak1; Postn; Spp1; Tgfbi; Vtn; Nov; Pcdh17;	GO:0007155~cell adhesion	23	525	4.380952	4.74E-05	0.015036
Fgf10; Fgfr1; Gja1; Lox; Nr2f2; Shb;	GO:0048514~blood vessel morphogenesis	6	35	17.14286	5.60E-05	0.015036
Bmp4; Bmp7; Fgf10; Met; Mgp; Wnt4;	GO:0048754~branching morphogenesis of an epithelial tube	6	36	16.66667	6.44E-05	0.015036
Bmp4; Bmp7; Sema3c;	GO:1905312~positive regulation of cardiac neural crest cell migration involved in outflow tract morphogenesis	3	3	100	8.84E-05	0.018063
Aldh1a2; Bmp4; Ctgf; Fgf10; Fgfr1; Foxp2; Gpc3; Lox; Mgp;	GO:0030324~lung development	9	111	8.108108	0.000181	0.030361
Bdnf; Bmp4; Bmp7; Fgfr1; Foxc1; Osr1;	GO:0001657~ureteric bud development	6	46	13.04348	0.000218	0.030361
Bmp4; Bmp6; Bmp7; Foxc1; Foxd1; Gpc3; Itga8; Pou3f3; Sulf2;	GO:0001822~kidney development	9	114	7.894737	0.000219	0.030361
Bmp7; Fgf10; Fgfr1; Lama1;	GO:0060445~branching involved in salivary gland morphogenesis	4	15	26.66667	0.000241	0.030361
Fgf10; Fgfr1; Met;	GO:0060665~regulation of branching involved in salivary gland morphogenesis by mesenchymal-epithelial signaling	3	5	60	0.000242	0.030361
Bmp4; Bmp6; Bmp7; Ctgf; Foxc1; Igf2; Mgp; Spp1;	GO:0001503~ossification	8	92	8.695652	0.000266	0.031088
Bdnf; Chodl; Cntn2; Cntn3; Epha4; Fezf1; Insm1; Itga8; Ngfr; Nr2f1; Otp; Pou3f3; Robo3; Sema3a; Sema3c; Sema3d; Zic1;	GO:0007399~nervous system development	17	384	4.427083	0.000419	0.04198
Bmp4; Bmp6; Fgf10; Foxp2; Osr1; Scn5a; Tbx18;	GO:0050679~positive regulation of epithelial cell proliferation	7	75	9.333333	0.000434	0.04198
Bmp4; Fgf10; Tbx18; Wnt4;	GO:0051145~smooth muscle cell differentiation	4	18	22.22222	0.000437	0.04198
Bmp4; Bmp6; Bmp7; Osr1; Wnt4;	GO:0030501~positive regulation of bone mineralization	5	35	14.28571	0.000507	0.044876
Col1a1; Col1a2; Col6a1; Col6a2;	GO:0070208~protein heterotrimerization	4	19	21.05263	0.000522	0.044876

Chapter 4: Auts2 and NonO Syndrome Models Share Pathway Dysregulation with Other Neuropsychiatric Disorders

4.1: INTRODUCTION

Autism syndromes are diagnosed clinically though identification of characteristic social and behavioral phenotypes. Autism syndrome disorders are commonly accompanied by a diagnosis of at least one additional psychiatric condition. These are most commonly anxiety and mood disorders, obsessive-compulsive disorder, attention deficit hyperactivity disorder, and oppositional defiant disorder (Rosen et al., 2018). Moreover, there is increasing evidence that Autism may exhibit substantial co-occurrence with schizophrenia (Chisholm et al., 2015). Autism and schizophrenia have long been recognized to have an underlying genetic connection which may contribute to this comorbidity (Canitano and Pallagrosi, 2017; Khanzada et al., 2017; Sundararajan et al., 2018). This most recent study identified neurotransmitter receptor genes and synaptic transmission pathways which were enriched in these disorders (Sundararajan et al., 2018). The finding of dysregulated neurotransmitter signaling pathways common to these disorders is relevant for identifying potential targets for pharmacological intervention in autism syndromes and for understanding which, if any, existing pharmaceuticals may be strong candidates for repurposing for ASD. Another recent study used transcriptomic profiling to more broadly assess molecular pathway alterations in common between autism syndromes and other neuropsychiatric disorders (Gandal et al., 2018). This study analyzed the gene expression patterns of a large number of post-mortem

brain tissue samples from autism, schizophrenia, bipolar disorder and alcoholism patients along with control tissue. In addition to identifying expected alterations in signaling receptor and synaptic pathways, enrichment of pathways involving mitochondrial function, extracellular matrix organization, and vascular development were also identified. Like many autism syndrome genes, *AUTS2* has also been linked to other neuropsychiatric conditions, typically through SNP linkage analysis, including schizophrenia (Zhang et al., 2014), suicide under the influence of alcohol (Chojnicka et al., 2013), response to antidepressants (Myung et al., 2015), and epilepsy (Mefford et al., 2010). In order to understand how Auts2 mutations fit into this broader molecular landscape of neuropsychiatric disorders, we mined our previously described RNA-sequencing experiments for additional altered molecular pathways utilizing Gene Set Enrichment Analysis (Subramanian et al., 2005). Gene Set Enrichment Analysis (GSEA) is a powerful, well-established, method for assessing transcriptome-wide regulatory alterations in clusters of genes with known relationships curated from known molecular pathways, gene expression networks and computational predictions (Liberzon et al., 2011, 2015). This analysis identified substantial molecular overlap between the Auts2 syndrome molecular pathology and the reported alterations in transcriptomes from neuropsychiatric patient samples. Auts2 polymorphisms have also been previously reported to be associated with increased suicide risk under the influence of alcohol and decreased response to SSRI antidepressants (Chojnicka et al., 2013; Myung et al., 2015). Utilizing our sequencing datasets from Auts2 deficient brain regions, along with drug target information from the DrugBank database (Law et al., 2014) we identified molecular pathways which may underlie these aberrant responses. Our data indicate that

the signaling pathways antagonized by these molecules may be downregulated in the Auts2 deficient hippocampus. These alterations may contribute to the pathological responses associated with these SNPs. We previously described molecular interactions between AUTS2 and the multifunctional RNA-processing protein NONO. Mutations in Nono, like Auts2, are associated with distinct neurological defects. Both syndromes exhibit distinct phenotypes of intellectual disability, developmental delay and feeding difficulties. A previous study performed RNA-sequencing on the hippocampus of adult mice with disrupted expression of Nono (Mircsof et al., 2015). Utilizing gene expression data retrieved from this paper, we performed an integrative expression analysis between the Nono deficient hippocampus and the Auts2 deficient hippocampus to identify shared dysregulation of molecular pathways. Additionally, we previously identified AUTS2 mRNA targets through RNA Immunoprecipitation sequencing (RIP-Seq). In order to further examine the interaction between AUTS2 and NONO we performed a pilot RIP-seq experiment against the NONO protein to, with the use of our previous AUTS2 RIP-seq data, identify co-targeted transcripts between AUTS2 and NONO in the cortex. This approach identified a pathway centered on several Notch family proteins, which is consistent with our previously reported targeting of the Auts2 complex. Finally, we report on physiological abnormalities observed in Auts2 mutant animals which have not been previously identified. We had identified that the Auts2 deficient hippocampus lacks hilar mossy neurons during all stages of post-natal development. Hilar mossy neurons are believed to regulate the excitability of dentate granule neurons through an indirect circuit which involves the activation of inhibitory interneurons. Loss of these neurons, a phenotype observed in epilepsy (Blümcke et al.,

2000), has been found to result in disinhibition of the hippocampal circuit (Jinde et al., 2012; Zappone, 2004). Several AUTS2 syndrome patients have been diagnosed with epilepsy (Beunders et al., 2013; Oksenberg et al., 2013) and epilepsy is a common comorbidity of Autism syndromes (Gabis et al., 2005). Based on these data, we performed EEG recordings from Auts2 cKO mice to determine if abnormal electrical activity potentially indicative of epilepsy was detectable in these brains. Additionally, previous reports indicated that mice with Auts2 deleted in the whole CNS exhibited P0.5 lethality (Gao et al., 2014), we produced mouse models with all isoforms of Auts2 deleted in both the whole CNS using Nestin-cre, or forebrain only using EMX1-cre. We observed that these Nestin-cre driven deletions were lethal on P0.5. We previously observed that AUTS2 cKO mice exhibited upregulation of Preproenkephalin transcripts in Cajal-Retzius cells along the cortical and hippocampal surface. Processed enkephalin peptides exert a number of physiological effects on the brain. Among these, studies have found that application of enkephalins may suppress respiratory rhythm. A study which performed infusion of enkephalin in neonatal rabbits found reduced ventilation, and periodic breathing with apneas (Grunstein and Grunstein, 1982). A likely cause of early post-natal mortality is failure to generate a stable respiratory rhythm (Turgeon and Meloche, 2009). To perform a preliminary assessment of this possibility, we performed plethysmographic recordings of respiratory rhythms in our AUTS2 deficient mouse models. These data provide context for understanding how the Auts2 syndrome phenotypes relates to other neurodevelopmental syndromes, and how underlying neurodevelopmental abnormalities may contribute to autism syndrome comorbidities.

4.2: RESULTS

4.2.1: Molecular pathways altered in the Auts2 cKO hippocampus overlap with those altered in the cortex, and in other neurodevelopmental syndromes

We previously performed expression analysis of frontal cortex and hippocampus from mice which carry recombination induced deletions of all Auts2 isoforms in the forebrain. Gene ontology analysis of these altered transcriptomes identified a number of molecular pathways involved in neuronal migration, cytoskeletal assembly, and extracellular matrix reorganization which were dysregulated on Auts2 deletion in both the hippocampus and frontal cortex, however only a minority of genes were significantly differentially expressed in both datasets. This lack of overlap may be due to the different developmental stage of the neurons, therefore, we hypothesized that AUTS2 may still be regulating the same molecular pathways in those separate brain regions. To assess this possibility we performed Gene Set Enrichment Analysis (GSEA) and Enrichment Map co-clustering of the frontal cortex and hippocampal RNA-seq datasets to compare the molecular pathway profiles of these two brain regions. We identified a downregulation in gene clusters involving extracellular matrix organization which was consistent with our previously reported data. Additionally, we observed the downregulation of pathways involved in CREB mediated synaptic receptor signaling, G-alpha(i) GPCR signaling, and transcriptional control of the circadian clock. Substantial upregulation was observed in pathways involved in mRNA processing, DNA synthesis and repair, and several mitochondrial pathways involving both mitochondrial protein production and electron transport **(Figure 1)**. Prior work from our lab had reported that AUTS2 interacts with the RNA-regulatory protein NONO by Co-immunoprecipitation

experiments, as well as co-expression analysis in neurons. NONO is a known factor for regulation of the circadian clock and coupling of the circadian clock to the cell cycle (Kowalska et al., 2013), a pathway which appeared dysregulated in the Auts2 deficient brain. A previous study performed RNA-sequencing analysis of the hippocampus of animals in which NONO had been rendered non-functional through insertion of a gene-trap into the locus (Mircsof et al., 2015). To assess whether the AUTS2 and NONO interaction partners also regulate the same molecular pathways, we performed Gene Set Enrichment Analysis between these two hippocampal datasets. These two independent experiments appeared to exhibit a strong correlation in the differentially expressed pathways and these pathways appeared to be largely inversely regulated (**Figure 2)**. These data indicate that AUTS2 and NONO co-regulate molecular pathways during development, but that the directionality of the regulation may be inverted.

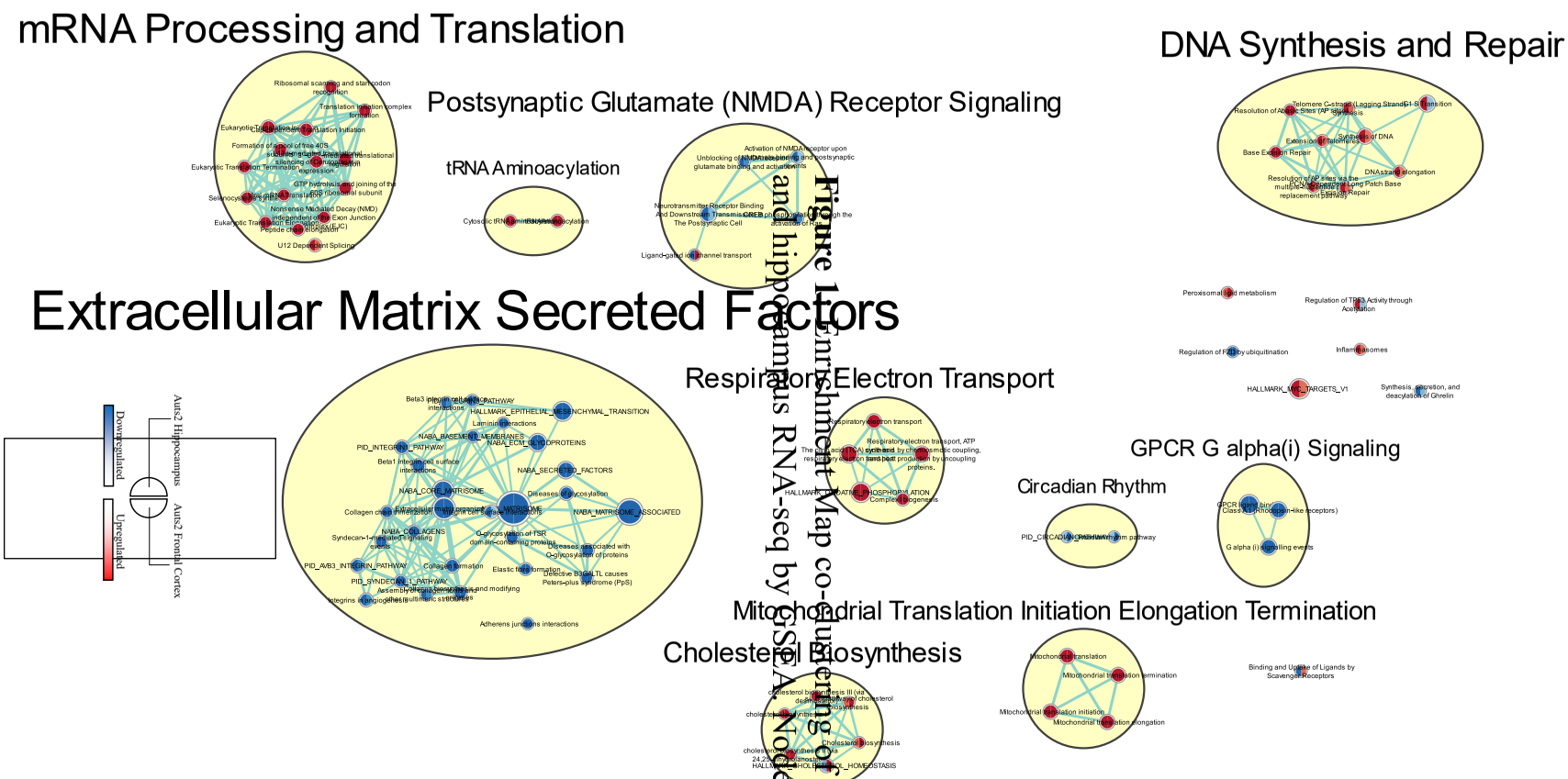

Figure 1. Enrichment Map co-clustering molecular pathways perturbed in P0.5 and hippocampus RNA-seq by GSEA. Node cutoff: GSEA Q<0.05.

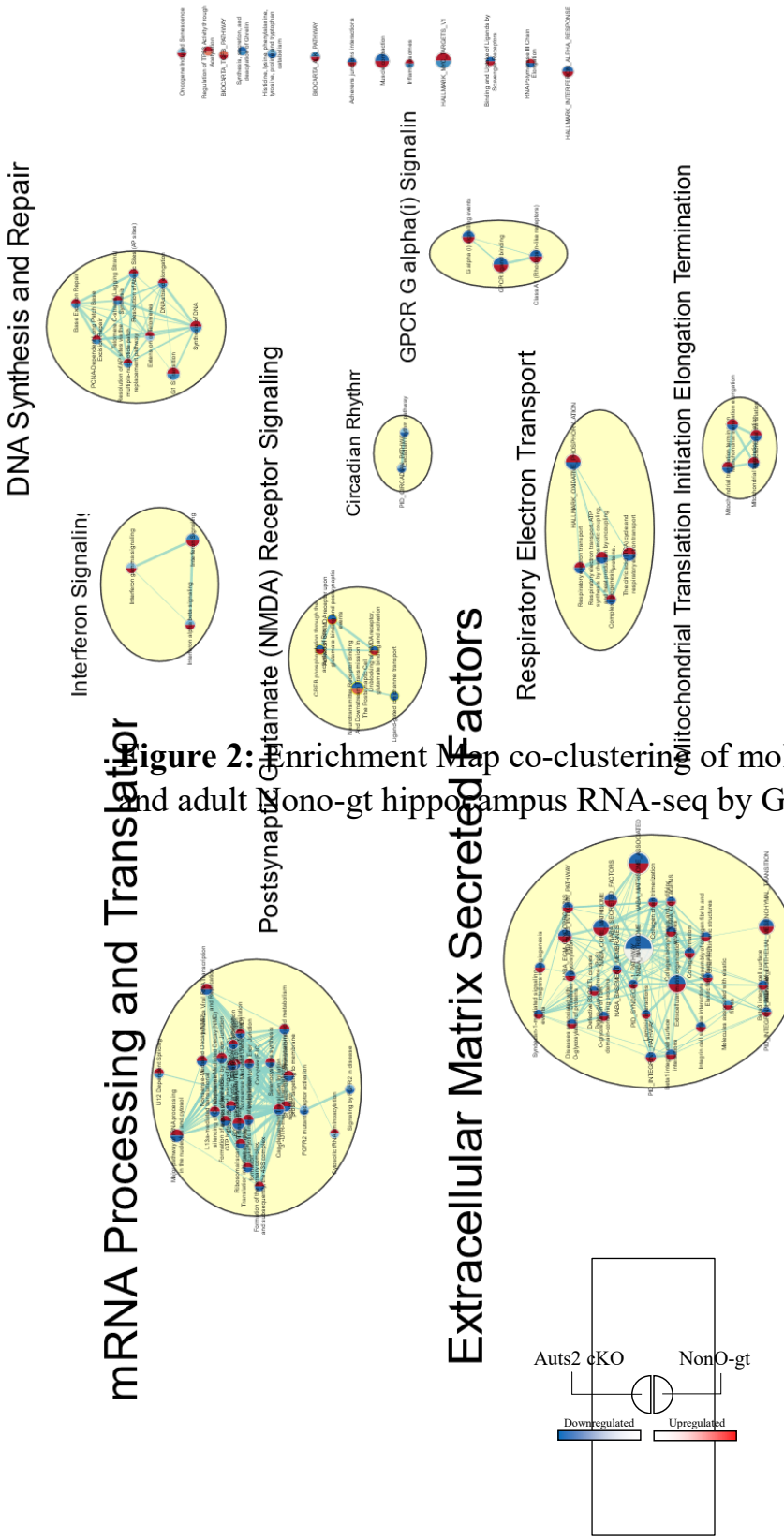

Figure 2: Enrichment Map co-clustering of molecular pathways perturbed in P0.5 Au and adult Nono-gt hippocampus RNA-seq by GSEA. Node cutoff: GSEA Q<0.05.

4.2.2: Co-targeting of mRNA transcripts and molecular pathways by AUTS2 and NONO

Our data indicated that AUTS2 and NONO physically interact in neurons and integration of RNA-sequencing datasets indicated that AUTS2 and NONO co-regulate molecular pathways in the hippocampus, albeit in opposite directions. In order to determine if AUTS2 and NONO physically target the same RNA transcripts, we performed a pilot RIP-seq experiment against NONO to complement our previously reported AUTS2 RIP-seq experiment **(Table S1)**. We identified 122 transcripts which were enriched (P<0.05) over IgG control upon RNA-immunoprecipitation of NONO from cortical lysate. 39, (32%) of the significant transcripts targeted by NONO were also targeted by AUTS2. Enrichment analysis in STRING identified that this transcript network was significantly enriched for protein functional connections (PPI enrichment p-value: 6.09e-06). **(Figure 3)** These connections contained a Notch signaling related pathway (KEGG:04330 FDR=0.00548) and a calcium ion binding pathway (GO:0005509 FDR=7.12e-5), as well as an enrichment for transcripts for membrane-bound vesicle proteins (GO:0031988 FDR=0.000139). These pathways support previously identified targets of AUTS2 regulation and co-regulatory action of AUTS2 and NONO.

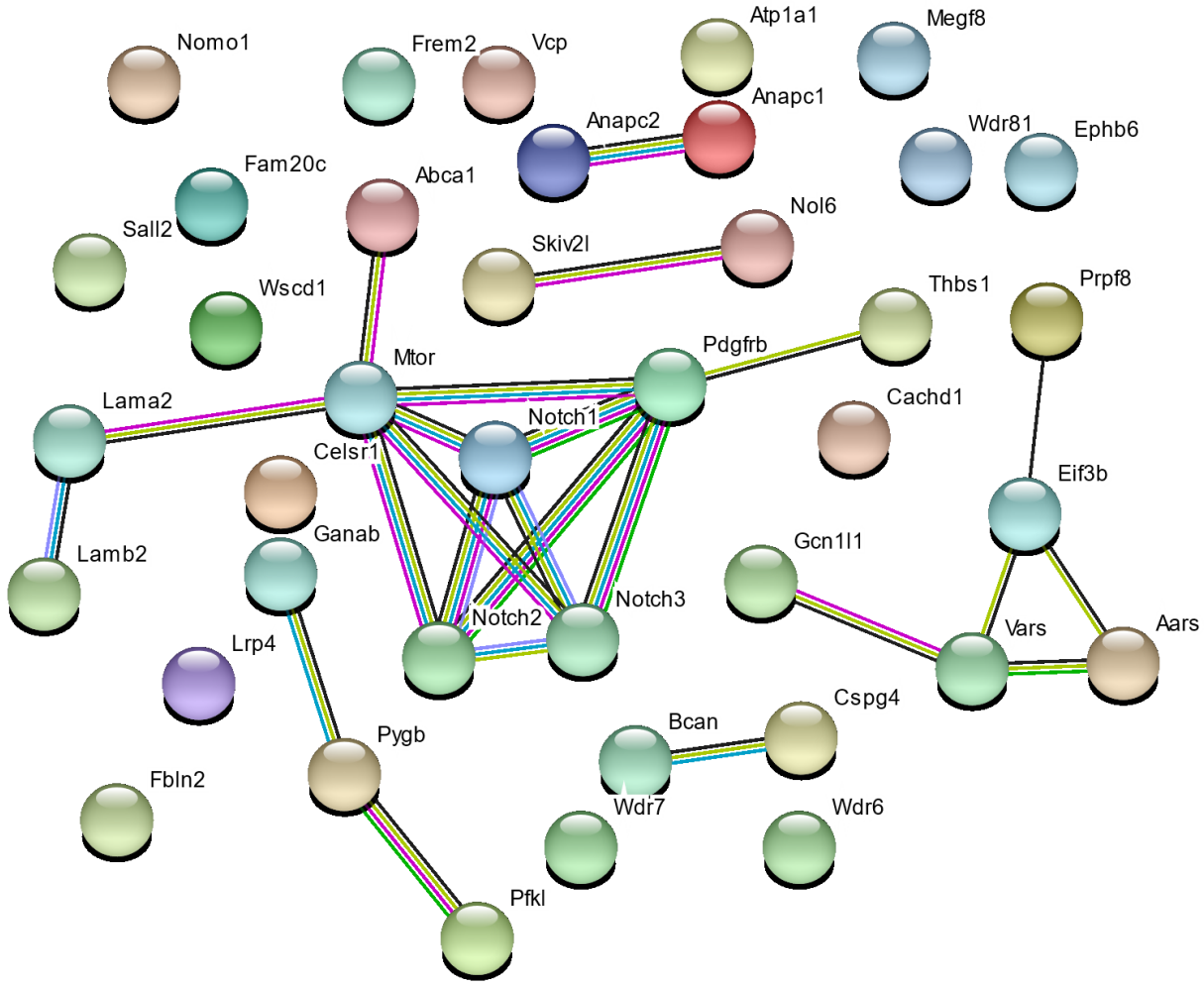

Figure 3: STRING-DB network of transcripts co-targeted by AUTS2 and NONO RIP

Target transcripts were enriched (Log2(FC)>0) in both N=2 Anti-AUTS2 RIP (FDR Q<0.05) and N=1 Anti-NONO RIP (P<0.05).

4.2.3: Dysregulated drug target pathways may underlie Auts2-linked abnormal drug responses

Polymorphisms in the *AUTS2* locus have been linked to several abnormal phenotypes related to substance response. A 2015 study in a Korean population found that individuals carrying polymorphisms in the Auts2 locus exhibited significantly reduced responses to SSRI antidepressants (Myung et al., 2015). Separate studies have found that AUTS2 polymorphisms in humans as well as lower levels of Auts2 in mouse brain are associated with reduced consumption of alcohol (Schumann et al., 2011), additionally, the human polymorphisms are associated with increased rate of suicide under the influence of alcohol (Chojnicka et al., 2013). These data suggest that decreased Auts2 may be involved in increased adverse effects of alcohol consumption.

Our GSEA analysis of Auts2 deletion model RNA-sequencing suggested several molecular pathways which might mediate these observed effects. To determine whether genes dysregulated in these samples were significantly enriched for drugs which target these pathways we performed additional GeneSet Enrichment against the DrugBank database (Law et al., 2014) which we then integrated with our dysregulated pathways using EnrichmentMap (Merico et al., 2010). As we previously identified that hippocampus development is most severely affected in Auts2 mutant models, we focused on this dataset for drug target identification. We identified two clusters of compounds which were significantly enriched for target genes in the Auts2 deficient hippocampus (FDR Q-value <0.05) **(Figure 4)**. These drug clusters shared target genes with two non-overlapping molecular pathway clusters involved in neurotransmitter signaling events. Drug cluster A

consisted primarily of atypical antipsychotics which antagonize their target dopamine and serotonin receptors. The target receptors of these drugs which were dysregulated in the hippocampus consisted primarily of *Htr2c* (Log_2FC=-0.6158, P=0.0041), *Htr1a* (Log_2FC=-0.4931, P=0.00885), and *Drd1* (Log_2FC=0.5554, P=0.03765) Drug cluster B consisted of Benzodiazepine class drugs which are commonly used to treat anxiety, insomnia, and seizures. Additionally, this cluster contained Ethanol, which exhibits similar functional effects. These drugs antagonize GABA and Acetylcholine receptors which were enriched in the targeted pathway (e.g. *Gabra1* (Log_2FC=-0.5124, P=0.0023) and *Chrna3* (Log_2FC=-0.538524, P=0.0235)) and which were downregulated in the sequencing dataset.

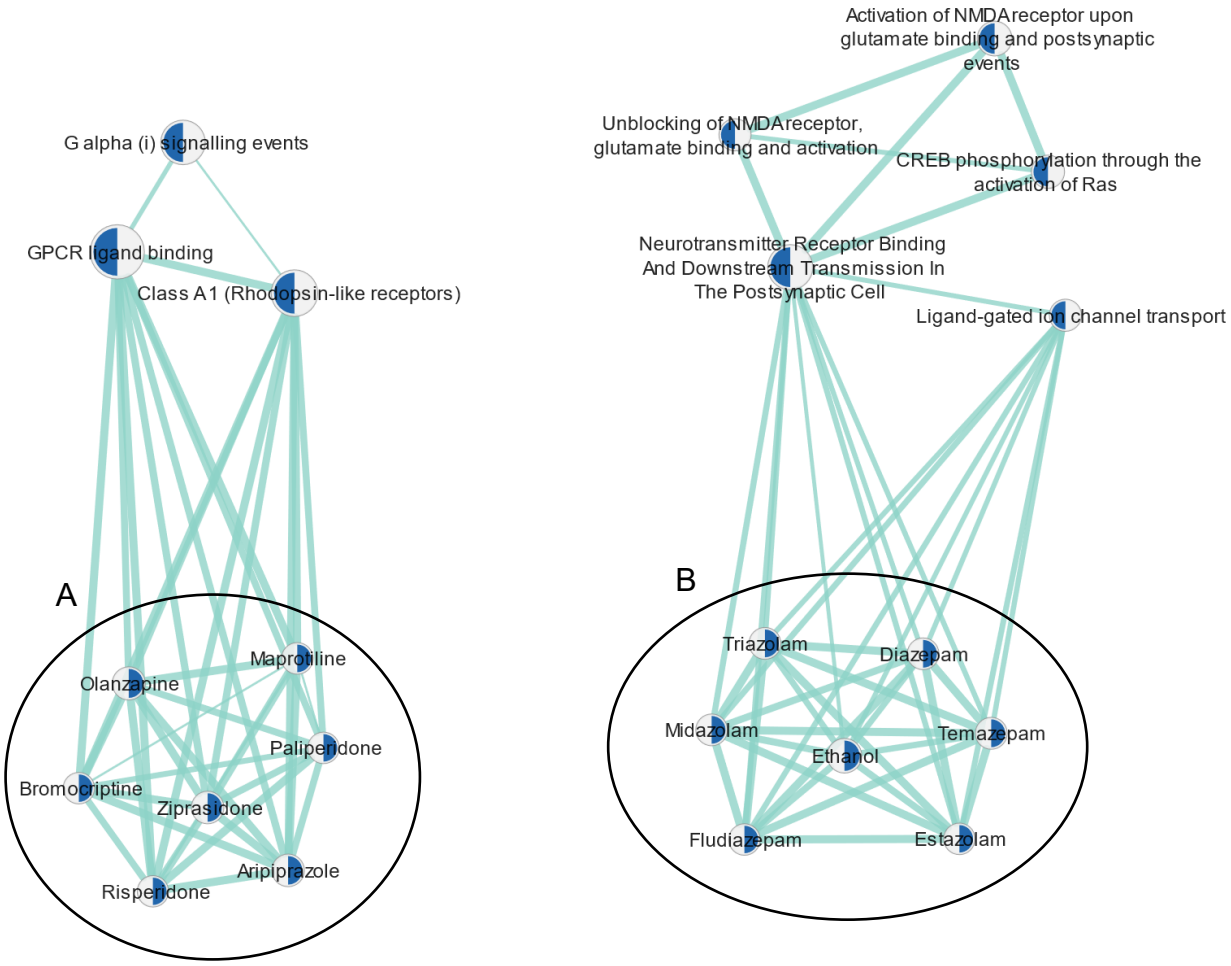

Figure 4: Drug and drug target networks enriched in Auts2 cKO hippocampus dysregulated pathways

EnrichmentMap co-cluster of GSEA dysregulated pathways in Auts2 cKO hippocampus and DrugBank enriched targets. Drug cluster **(A)** consisted primarily of atypical antipsychotics. Drug cluster **(B)** consisted of Benzodiazepines

4.2.3: Auts2 cKO EEG recordings exhibit potential pre-epileptic activity

Patient mutations in *AUTS2* have previously been associated with epilepsy (Oksenberg et al., 2013). We identified that mice carrying our deletion of AUTS2 exon 15 lack hilar mossy neurons in the hippocampus from birth. Hilar mossy neurons are believed to contribute to suppression of granule neuron excitability through synapses with GABAergic interneurons, and loss of hilar mossy neurons has been shown to result in disinhibition of the hippocampus (Zappone, 2004). We performed EEG recordings from adolescent AUTS2 deficient mice to determine if these mice exhibited hallmarks of either neuronal disinhibition, or epileptogenic processes. These EEGs identified significant increases in Delta peak power (93% increase) and Theta peak power (50% increase) **(Figure 5A).** Additionally, Beta frequency activity was increased in these recordings **(Figure 5B)**. Finally, mutant mice exhibited evidence of interictal spikes at rest and during NREM sleep **(Figure 5C**.

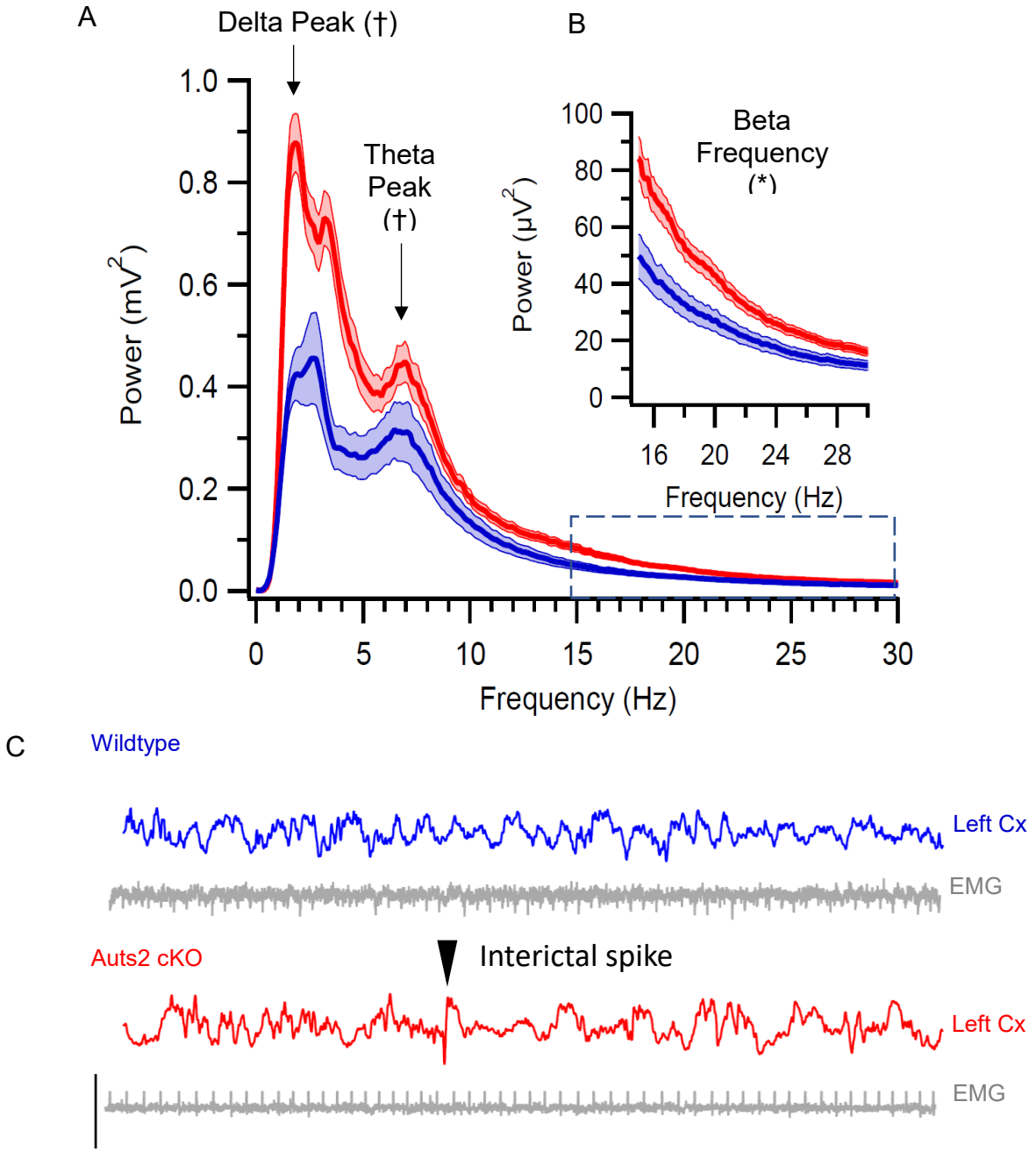

Figure 5: EEG recordings from adolescent Auts2 cKO mice

(A) Power spectrum of Auts2 cKO (n=3) and Wildtype (n=5) EEG recordings. Wildtype Delta Power: 0.45 ± 0.00009 mV^2 Auts2 cKO Delta Power: 0.87 ± 0.00006 mV^2 Wildtype Theta Power 0.30 ± 0.00006 mV^2 toAuts2 cKO Theta Power 0.45 ± 0.00004 mV^2. (†=P<0.001)
(B) Increased power was also observed in the Beta rhythm frequency range (*=P<0.05).
(C) EEG traces from Wildtype (top) and Auts2 cKO (bottom). Inter-ictal spike annotated in Auts2 cKO

4.2.4: Neonatal Auts2 mice exhibit respiratory complications with CRE driver dependent viability

Mice carrying homozygous constitutive exon 8 deletions driven by CAG-cre mediated recombination using were found to be neonatally lethal despite compensatory upregulation of the Auts2 isoform originating from Exon 9 (Hori et al., 2014). In order to further assess this early neonatal death phenotype, we developed two mouse lines in which Auts2 Exon 15 is excised. A line in which recombination mediated excision is restricted to the telencephalon driven by EMX1-cre which was described in an earlier chapter and Nes11-cre mediated excision of Exon 15 in the whole central nervous system. We found that cre-mediated recombination excising Exon 15 in the whole CNS resulted in total early neonatal lethality. (100% on P0.5, the day of birth), in contrast, EMX1-cre mediated deletions were viable. To investigate the possibility of respiratory rhythm dysregulation causing early neonatal death in these animals, we performed plethysmographic recordings of both NES11-cre **(Figure 6A, representative traces)** and EMX1 driven Auts2 deletion lines. Auts2 NES11 cKO mice exhibited significantly fewer breaths per minute **(Figure 6B)**, and these breaths were both significantly larger, indicating potential gasps or sighs **(Figure 6C)** and exhibited significant irregularity in the frequency potentially indicating apneas **(Figure 6D)**. Additional quantification metrics supported these findings **(Figure S1).** The significantly reduced respiratory rate was also observed in the EMX1-cre driven Auts2 deletion **(Figure S2)** however this did not appear to affect the viability of the neonates.

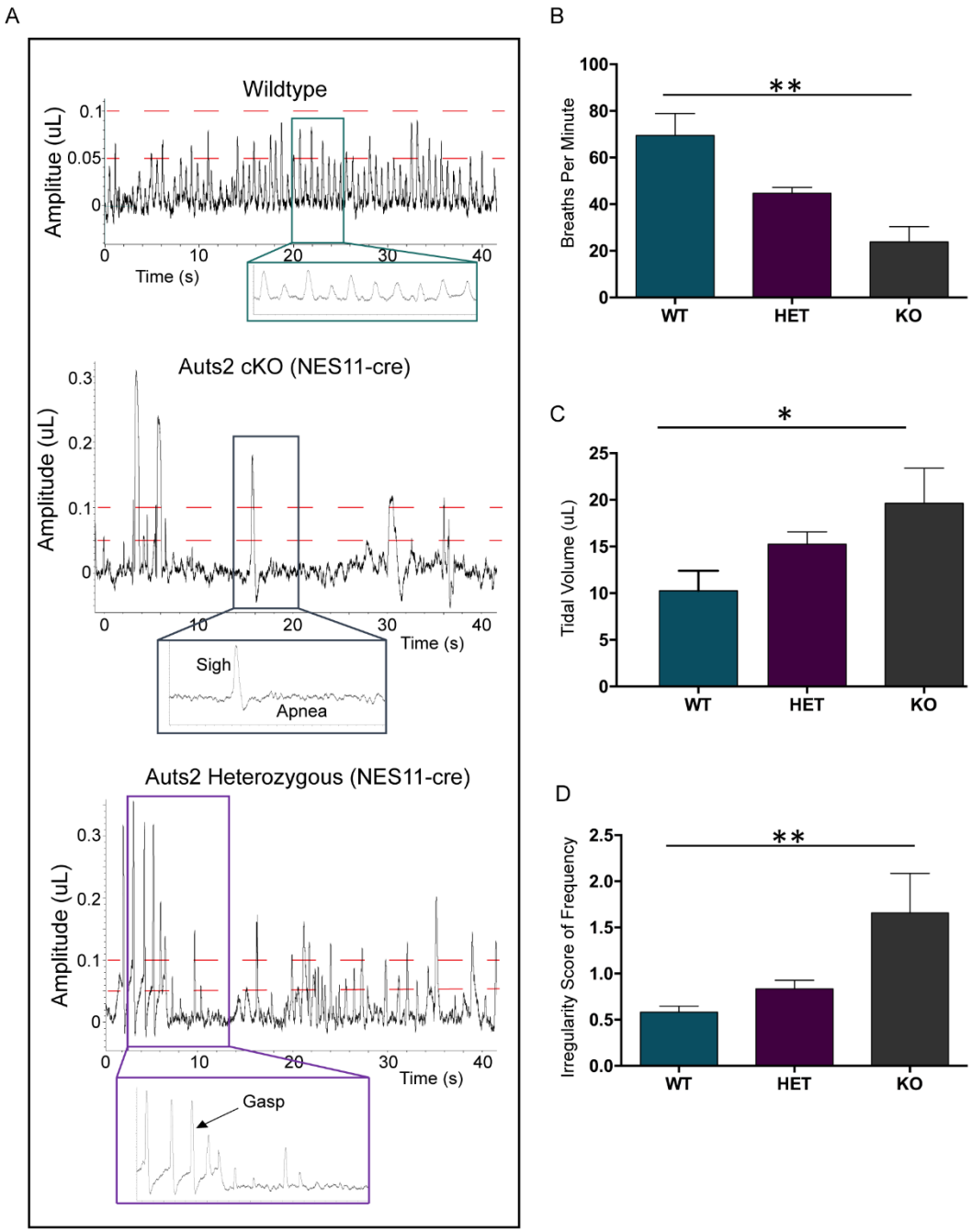

Figure 6: Respiratory rhythm analysis of NES11-cre driven Auts2 cKO neonates on P0.5

(A) Representative traces from Wildtype (top), heterozygous (middle), and Knockout (bottom) animals on P0.5. **(B)** The frequency of breaths (BPM) was significantly reduced in Auts2 deficient Animals (One-way ANOVA P=0.0045). **(C)** Event volume was significantly larger (One-way ANOVA P=0.0406). **(D)** Auts2 deficient animals exhibited significant irregularity in their respiratory rhythm (One-way ANOVA P=0.0018). Data represented as mean + S.E.M.

4.3: DISCUSSION

4.3.1: AUTS2 exerts an opposing regulatory effect to other ASD and ID linked developmental factors

In this study, we utilized previously generated gene expression datasets from studies of Auts2 deficiency model mice to further characterize the molecular pathways altered in the brains of these animals. We found that, despite the different developmental stages and different differentially expressed genes, the broad molecular pathways altered in the frontal cortex and hippocampus of Auts2 deficient mice are consistent between the two tissues. We found that AUTS2 deficient mice exhibited dysregulation in molecular pathways which regulate GPCR signaling, extracellular matrix organization, and mitochondrial biology. Furthermore, these pathways substantially overlapped with those identified as perturbed in a large study of molecular dysregulation in psychiatric disorders. A previous study performed gene expression analysis of human cortical tissue from post-mortem psychiatric disorder patients including samples from individuals affected by autism, schizophrenia, bipolar disorder, depression, and alcoholism (Gandal et al., 2018). This study identified several core molecular pathways which were altered in these patient brains, including extracellular matrix organization, synaptic transmission pathways, and regulation of mitochondrial biology. Unexpectedly however, while the mitochondrial biology pathways appeared to be downregulated in the psychiatric disorder patient cohorts, we found that they were upregulated in the Auts2 model. Inverse regulation in molecular pathways was also observed in the dataset integration with gene-set enrichment analysis of hippocampal RNA-sequencing from mice deficient in the AUTS2 interaction partner NONO (Mircsof et

al., 2015). All major pathway clusters were inversely regulated between AUTS2 and NONO deficient hippocampi. This may be indicative of fundamental opposition in the molecular functions of these interacting proteins. However, one complicating factor is that the hippocampal sequencing study by Mirscof et al., was performed on the adult hippocampus, and our AUTS2 sequencing was performed on the neonatal hippocampus. However, cortical neurons are broadly mature at P0.5 and exhibited identical regulatory directionality to the hippocampus, and in the hippocampus, Auts2 is perpetually expressed throughout life. Additionally, we previously noted that, in some respects, phenotypic features of the NONO syndrome appear to oppose those in the Auts2 syndrome (e.g.: microcephaly in *AUTS2*, macrocephaly in *NONO* syndrome; round or square face in *AUTS2*, long face in *NONO* syndrome; outgoing demeanor in *AUTS2*, shy demeanor in *NONO* syndrome). The combination of these factors leads us to believe that the directionality observed in these studies is unlikely to be an artifact of age at sequencing, however additional follow-up expression analysis of adult AUTS2 deficient hippocampus would be necessary for confirmation. Interestingly, molecular pathways involved in regulation of circadian rhythm were downregulated in both NONO and AUTS2 deficiency. This was one of the few exceptions to the general state of inverse regulation. We reported that AUTS2 may function as an RNA-binding protein which appeared to bind Per2 mRNA in the cortex, which was downregulated in the Auts2 cKO. Cry1, a transcriptional repressor which is a core component of the circadian clock complex was also downregulated, although it's transcript did not appear to be bound directly by AUTS2. NONO has also been reported previously a regulator of the circadian clock (Kowalska et al., 2013). We performed additional experiments to

identify which mRNAs are co-targeted by AUTS2 and NONO. These experiments identified gene networks, predominantly involved in Notch signaling which appear to be co-regulated by transcript co-binding of AUTS2 and NONO. Previous work found that Auts2 levels oscillate with other Notch signaling genes (Dequéant et al., 2006; William et al., 2007). Circadian clock regulation has also been found to be important for regulating the production of new hippocampal neurons (Bouchard-Cannon et al., 2013) and that Notch signaling may function in this process to prevent depletion of neural stem cells (Imayoshi and Kageyama, 2011). A growing body of research has indicated that circadian rhythm dysregulation may be a prominent feature of Autism Spectrum disorder (Glickman, 2010), bipolar disorder (Harvey et al., 2006), and schizophrenia (Wulff et al., 2012), furthermore, a recent study identified a cluster of polymorphisms in an intergenic region approximately 1 Mb upstream from AUTS2 which was significantly linked to insomnia disorder (Stein et al., 2018). These findings implicate AUTS2 in circadian regulation of Notch signaling during neurodevelopment.

Finally, we identified two clusters of genes which may provide avenues of further research into pharmacological interventions for the AUTS2 syndrome. A cluster of dysregulated serotonin and dopamine receptors was identified in the Auts2 cKO hippocampus. This cluster appeared to contain drug targets for atypical antipsychotics. Interestingly, the drug cluster which targeted these receptors contained Risperidone and Aripiprazole, the only drugs currently approved for treatment of behavioral disorders in patients with autism (Aman et al., 2015). This analysis additionally identified a second cluster of receptors, primarily GABA and Acetylcholine receptors which were downregulated in the Auts2 cKO

hippocampus. Downregulation of GABA receptors is a feature which has previously been identified in the brains of ASD patients (Fatemi et al., 2009). Among the drugs which targeted this receptor cluster were benzodiazepines and alcohol. Further antagonism of these already downregulated targets may underlie the observed association between Auts2, alcohol consumption and suicide (Chojnicka et al., 2013). Moreover, benzodiazepines themselves are associated with increased suicide risk (Dodds, 2017). These data provide a word of caution for the use of the use of these drugs in some subtypes of ASD.

4.3.2: Dysregulated respiration through altered opioid signaling may underlie AUTS2 whole CNS cKO lethality and feeding defects

Previous studies have identified deficits in the ability of AUTS2 Exon 8 cKO mice to vocalize and to feed (Gao et al., 2014). Patient studies have also identified speech deficits and feeding defects in AUTS2 patients (Amarillo et al., 2014; Beunders et al., 2015). We identified additional deficits in the ability of Auts2 Exon 15 cKO mice to generate a stable respiratory rhythm. When this Auts2 deletion was driven homozygous by NES11-cre, which exhibits recombinase activity in the entire CNS, including respiratory centers of the brainstem (Finger et al., 2017), the resultant homozygous mice were non-viable on the first postnatal day. We believe this to be a result of the severe lack of a stable respiratory rhythm in these animals. Coordination of respiration into the feeding reflex is a critical component of early survival (Lau, 2015) and may be disrupted by the gasping phenotype in the heterozygous animals. Unexpectedly, a similar, albeit not as severe, reduction in respiratory rate was observed in EMX1-cre driven deletions of Auts2 exon 15 and the resultant mice were viable.

EMX1-cre is not expected to be expressed in the brainstem (Finger et al., 2017). This indicates that AUTS2 may be involved in respiratory rhythm generation indirectly.

We previously reported increased expression of Preproenkephalin in both cortical and hippocampal Cajal-Retzius neurons of EMX1-CRE driven deletions of AUTS2. Secretion of this peptide into the CSF by Cajal-Retzius cells may result in suppression of respiratory rhythm, a feature of Enkephalin signaling which has previously been reported (Grunstein and Grunstein, 1982). An effect in these cells alone would not explain why the phenotype is more severe in NESl1-CRE driven deletions as Cajal-Retzius cells are not present in the hindbrain. However, PENK is expressed in a subset of hindbrain neurons (Allen Institute for Brain Science, 2015) and a population of neurons in the respiratory centers expresses Reelin like CR cells (Tan et al., 2012). Increased PENK expression in this population of hindbrain neurons in NESl1-CRE driven AUTS2 deletion may compound with the increased PENK secretion by the cortical CR cells further suppressing respiratory rhythm. Future work on the effects of brainstem deletion of AUTS2 is necessary to test this hypothesis. Additionally, enkephalin mediated respiratory repression is relieved by application of naloxone (Grunstein and Grunstein, 1982), future work should test the ability of naloxone to restore respiratory rhythms in AUTS2 deficient mice.

4.3.3: Auts2 cKO EEG abnormalities resemble ASD and epilepsy: contributions of hilar mossy neurons and the circadian clock

Our research found that AUTS2 cKO mice appeared to lack hilar mossy neurons in their dentate gyrus from birth. Severe depletion of these neurons has been reported to result in disinhibition of dentate gyrus excitability (Jinde et al., 2012; Zappone, 2004). Loss of hilar mossy neurons is also a consistent finding in epilepsy (Blümcke et al., 2000), and epilepsy has been diagnosed in a subset of Auts2 Syndrome patients (Oksenberg et al., 2013). To assess the possibility of a contribution of AUTS2 deficiency to the pathogenesis of epilepsy we performed initial EEG recordings of adolescent AUTS2 deficient mice. These EEGs indicated significant electrical abnormalities, including several which are considered potential biomarkers for epilepsy. We observed substantial increases across the EEG frequency spectrum, as well as inter-ictal spiking. Inter-ictal spiking is a well-established indicator of epileptic activity (Staley and Dudek, 2006) and is promoted by sleep deprivation (Díaz-Negrillo, 2013). The most notable increases in EEG power in the AUTS2 cKO mice were in the Delta and Theta peaks. Increases across the EEG power spectrum particularly delta, theta, and high-frequency activity are also a known finding in ASD (Cornew et al., 2012). The Theta rhythm is produced by the hippocampus and is indicative of hippocampal excitatory network activity (Pernía-Andrade and Jonas, 2014). Disinhibition of the hippocampal circuit through loss of HMNs may be the cause of this theta power increase. We also observed a substantial increase in delta power. Increased delta power is a known phenotype of autism spectrum disorder (Cornew et al., 2012). This finding indicates a degree of disinhibition of cortical network activity in the Auts2 cKO mice as well, however,

the cellular and molecular underpinnings of this finding are less clear. Delta oscillations are not considered a hippocampal rhythm and are rather thought to be produced by cortical neuron activity (Harmony, 2013). One hypothesis for this increased delta power may involve dysregulation of circadian cycling in the Auts2 deficient brain. Dysregulated circadian rhythms have been hypothesized to be a feature of ASD (Geoffray et al., 2017; Glickman, 2010) and an association between epilepsy and circadian cycles has been known for over 2,000 years (Cho, 2012). At least two AUTS2 syndrome patients have exhibited sleep disturbances (Amarillo et al., 2014; Beunders et al., 2016 - Supplementary Data). We previously reported that AUTS2 appears to regulate *Per2* mRNA, a core circadian clock gene which was downregulated in the Auts2 cKO in the frontal cortex and that AUTS2 interacts with NONO to regulate target genes, a protein which is also known to be involved in circadian clock regulation (Kowalska et al., 2013). Per2 levels have been shown to increase with time spent in the awake state and delta power was found to be increased in Per1/2 knockout mice following sleep deprivation (Curie et al., 2013). Increasing levels of PER2 may promote the transition to sleep phase and loss of PER2 (e.g. by the loss of Auts2) may prevent this transition, promote the awake state, and increase delta activity. These data identify classic ASD EEG findings in the AUTS2 deficient brain and provides evidence of epilepsy associated activity in the hippocampus which may be a direct physiological correlate of a neuroanatomical defect previously described in these mice. Future work is necessary to investigate the possible contribution of circadian rhythm dysregulation to epileptic activity in the AUTS2 deficient brain. Sleep deprivation has been identified to increase seizure risk

in epilepsy (Díaz-Negrillo, 2013) and a future study is necessary to address the possibility of sleep deprivation induced seizure susceptibility in AUTS2 deficient mice.

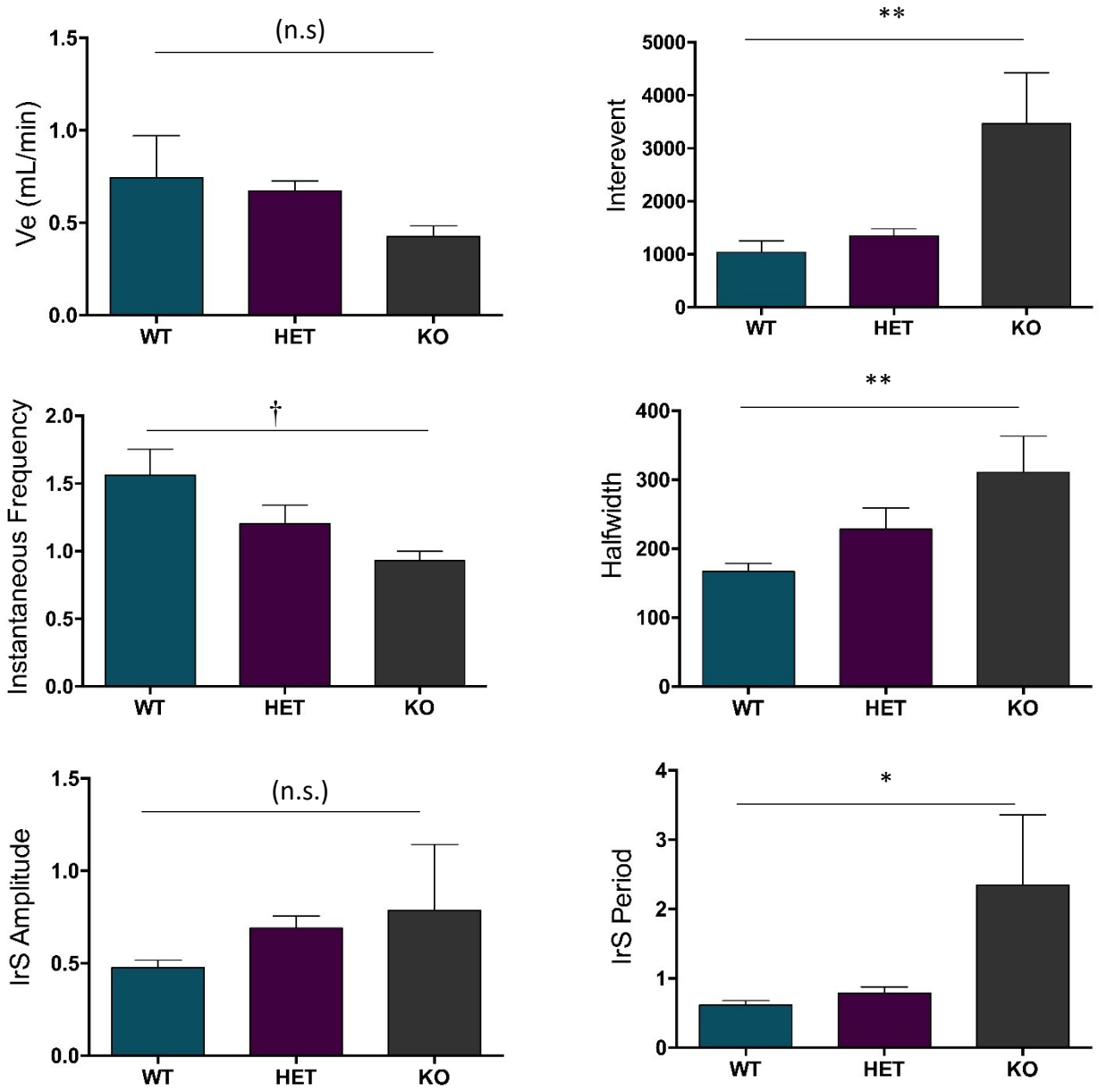

Figure S1 Related to Figure 6: Additional respiratory quantifications from NES11-cre deletion

Auts2 NES11-cre driven conditional knockouts exhibit reduced instantaneous breath frequency, and increased irregularity of the frequency. P-values calculated using ordinary one-way ANOVA testing. Error bars represent Standard error of the Mean. n.s. = Not Significant ($P>0.05$). = $P<0.05$, ** = $P<0.005$, † = $P<0.1$

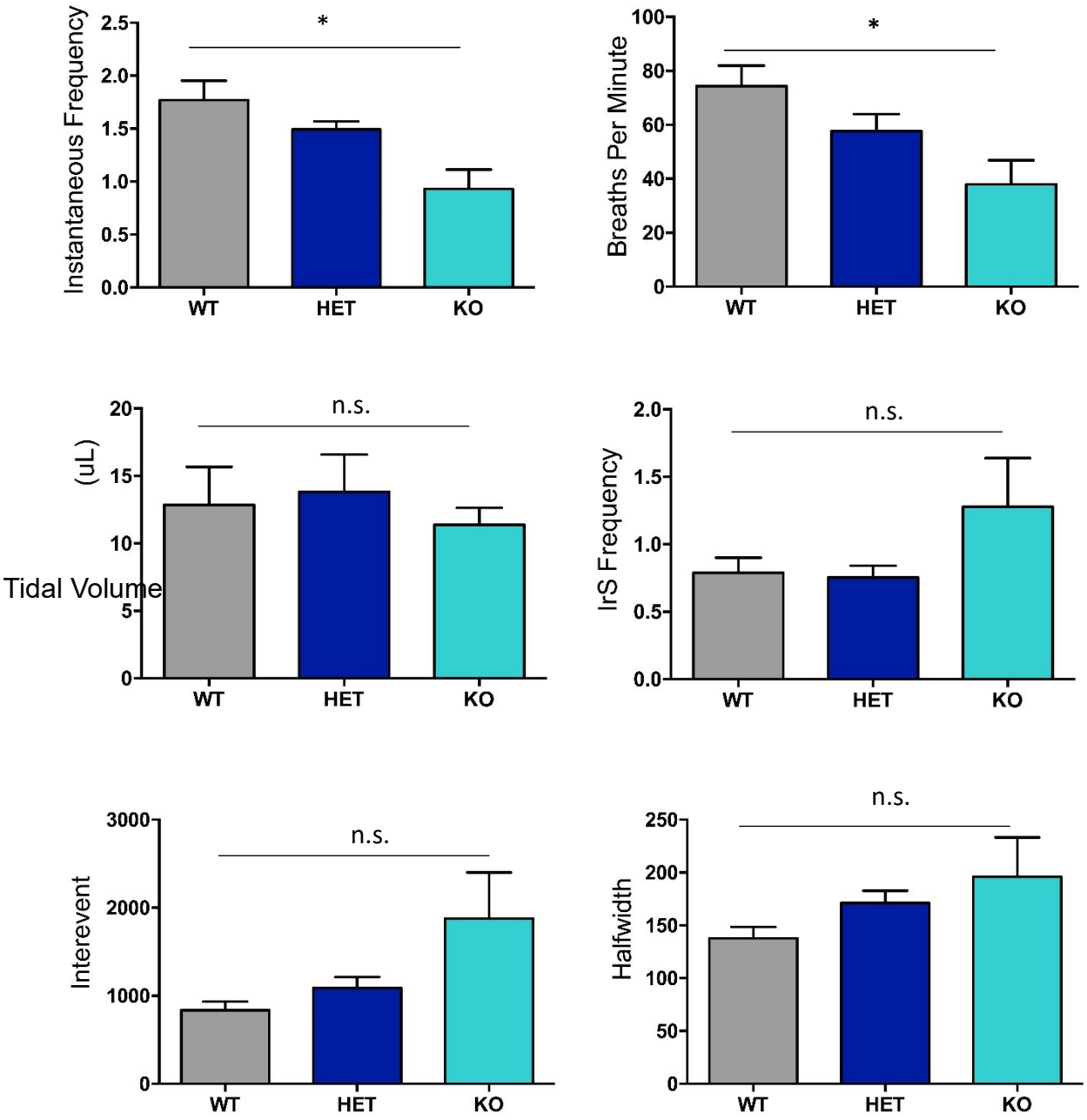

Figure S4, Related to Figure 6: Quantification of respiratory metrics from EMX1-cre driven Auts2 deletion

Auts2 EMX1-cre knockout mice exhibit reduced respiratory frequency. P-values calculated using ordinary one-way ANOVA testing. Breaths Per Minute; P=0.0412. Instantaneous Frequency; P=0.0234. Error bars represent the standard error of the mean. n.s. = Not Significant (P>0.05) * = P<0.05

Table S1, Related to Figure 3: Transcriptome-wide targeting of mRNAs by NONO RIP-seq

– See additional files –

Chapter 5: Conclusions and Future Directions

In this study, we identified numerous molecular, anatomical, and physiological findings which significantly expand our understanding of the etiology of AUTS2 Syndrome. Additionally, we identify features which connect the AUTS2 syndrome to other intellectual disability and autism syndromes, as well as pathologies associated with AUTS2 locus SNPs. Our data also identify connections between autism associated pathologies and common comorbidities, particularly to the pathogenesis of epilepsy (Gabis et al., 2005) and respiratory dysfunction (Ming et al., 2016).

5.1: AUTS2 dependent regulation of RNAs in neurodevelopment

Previous research focused largely on the ability of AUTS2 to bind chromatin (Gao et al., 2014; Oksenberg et al., 2014). However, they did not assess the ability of these binding events to directly impact gene regulation on the whole-transcriptome scale. Reanalysis of this data indicated that these events appeared unlikely to contribute to gene regulation directly. Additionally, new research has cast doubt on the contribution of AUTS2 to non-canonical Polycomb related transcriptional activation (Yan et al., 2017). We identified that AUTS2 participates in an RNA-binding complex, likely with the RNA-processing protein NONO. We found that loss of AUTS2 from this complex appears to predominantly result in downregulation of targeted RNAs. RNA binding has previously been implicated as a potential function of the Auts2-family protein FBRSL1 (Baltz et al., 2012). The ability for DNA binding proteins to exhibit a multifunctional role in binding RNA has become increasingly recognized (Cassiday, 2002; Hudson and Ortlund, 2014). In fact, core splicing

factors have been found to purify associated to chromatin (Allemand et al., 2016). We identified that RNA targeting appears to be a primary function of AUTS2 and that AUTS2 chromatin binding did not appear to specifically contribute to gene regulatory events. However, the specific molecular mechanism underlying how AUTS2 regulates its target RNAs, as well as both when, and how AUTS2 performs this targeting remain unclear. Many splicing factors, including NONO, are associated with gene promoters and are loaded onto nascent mRNAs through interactions with the RNA-polymerase tail (Amelio et al., 2007; Knott et al., 2016). We did not assess the specific mechanism by which AUTS2 is loaded onto mRNA transcripts. However, the identification of histone components in our Auts2 protein-protein interaction complex indicates that this may occur co-transcriptionally and that AUTS2 may require a transient step of chromatin association to become loaded onto nascent mRNAs. Additional work will be necessary to determine what, if any, impact AUTS2 chromatin association has on its transcript binding dependent regulatory activity. Furthermore, we did not directly determine the mechanism by which AUTS2 regulates its target mRNAs. One hypothesis is that AUTS2 may be involved in the co-transcriptional modification of RNAs. We identified a number of splicing factors other than NONO associated with the AUTS2 complex, as well as several histone subunits, and several small ribosomal subunits. Some ribosomal subunits including RPS3 which was identified in the AUTS2 complex have been found to associate to complexes near transcriptional start sites (Brogna et al., 2002; De et al., 2011) and histones have been found associated with the spliceosome and to influence RNA splicing activity (Allemand et al., 2016). Additionally, several new RNA-targeting processes have recently been identified with implications for

RNA-regulation specifically during neurodevelopment, in particular, m6A-RNA methylation, (Yoon et al., 2017) a process which seems to be, like the AUTS2 protein, highly specific to vertebrates. m6A-RNA methylation appears to be involved in regulating transcript stability and alternative splicing events (Yue et al., 2015). While we did not detect association of the core RNA methyl-transferase complex with AUTS2, one of the factors which is involved in regulating m6A-RNA methylation is HNRNPA2B1 (Alarcón et al., 2015) which was enriched in the AUTS2 complex. AUTS2 seems to be situated at the center of a highly diverse network which regulates chromatin architecture, splicing, and post-transcriptional RNA modification. The specific role of AUTS2 regulation of these processes requires further investigation, however, it appears that AUTS2 may contribute to regulation of transcript stability through some splicing associated process. Likely future experiments involved crosslinked RNA-immunoprecipitations separately from chromatin-associated fractions and cytoplasmic fractions, as well as direct sequencing of target RNAs on a platform which is able to detect RNA-base modifications, and CLIP-sequencing to determine AUTS2 RNA-binding motifs. Additional work is also necessary to confirm AUTS2-NONO co-targeted transcripts and transcript regulation using age-matched NONO mutant mice, as well as additional NONO RNA-immunoprecipitations.

5.2: Impairment of hippocampal neurogenesis in the AUTS2 syndrome

We identified molecular pathways altered in the hippocampus of neonatal AUTS2 deficient mice which indicated impairments in cell adhesion and migration pathways. Histological examination of these hippocampi during the first postnatal week identified a defect in

intermediate neuronal progenitor (INP) migration. This defect resembled, in some respects, the defect observed in REELER mice (Li et al., 2009a). Like AUTS2, Reelin mutations have been implicated in the pathogenesis of ASD, and schizophrenia (Bonora et al., 2003; Fatemi, 2002). Normally, during the first post-natal week, INPs migrate inward from the dentate migratory stream and the sub-pial neurogenic zone to colonize the hilus and the subgranular zone (Hodge et al., 2013; Li et al., 2009a). Establishment of neural progenitors in the subgranular zone is necessary for hippocampal adolescent and adult neurogenesis (Hodge et al., 2008). In both REELER and AUTS2 cKO mice, INPs were retained in the SPNZ and failed to migrate inward to colonize the hilus, only sparsely colonizing the SGZ at the tail end of the developmental window. Unlike REELER, this effect was not observed for SOX9+ neural stem cells in the AUTS2 cKO hippocampus which appeared to exhibit roughly normal migration. Further work is necessary to determine the specific mechanism of the INP migration delay in Auts2 cKO hippocampus. INPs are not known to prominently express Auts2 indicating that this may be a cell-nonautonomous phenotype, possibly through altered activity-dependent signaling by newborn hippocampal granule neurons. Enkephalin signaling has also been shown to impair neuronal proliferation (Hauser et al., 2000), which we have shown is altered in AUTS2 frontal cortex and hippocampus, the possibility of rescue of this phenotype through application of naloxone should be investigated. An additional area of future research is the effect this delay of colonization and apparent depletion of progenitors has on later adult neurogenesis.

5.3: Loss of hilar mosy neurons has implications for neurodevelopment, learning and memory, and epilepsy

We observed substantial loss of Hilar Mossy Neurons in the Auts2 cKO hippocampus, this loss was observable from birth, and persisted through all ages studied into adulthood. Hilar mossy neurons are a glutamatergic cell population which, as their name suggests, reside in the dentate gyrus hilar space. These cells project through the granule cell layer into the inner molecular layer. These axons project long-distances to other hippocampal regions, across the septotemporal extent of the dentate gyrus both ipsi- and contralaterally. This hilar mossy neuron axon projection innervates both inhibitory interneurons and excitatory granule neurons. The primary effect of mossy cell synaptic output on hippocampal circuits remains an ongoing area of research. However, the predominant hypothesis is that upon receipt of action potentials from their associated granule neurons, hilar mossy neurons activate GABAergic interneurons along the extent of the dentate to suppress additional granule neuron firings form the same initial input, called the “dormant basket cell hypothesis” (Scharfman, 2017). The net-inhibitory effects of HMN activation are believed to be important for the process of pattern separation, allowing distinct input events to propagate unique activity patterns. Pattern separation in the hippocampus is critical for the encoding and recall of episodic memory and memory context (Yassa and Stark, 2011). In addition to a tri-synaptic pathway of activity suppression through activation of GABAergic interneurons, HMNs form additional synapses on granule neuron dendrites in a direct excitatory circuit. This circuit is the first glutamatergic input that newborn granule neurons receive and is in addition to GABAergic input coordinated by HMN activity, which is also excitatory for these

newborn cells. These inputs, coordinated by HMNs appears to be essential for activity-dependent maturation of these adult-born granule cells (Chancey et al., 2014). These excitatory hilar neurons are extremely active, receiving a large number of monosynaptic inputs from many hippocampal granule cells, and are highly susceptible to excitotoxicity. HMNs are depleted in the brains of epileptic patients (Blümcke et al., 2000), and severely and selectively depleted in a study of kainic acid-induced excitotoxicity (Zappone, 2004). The *Sdy* mouse model of a mutation in Dysbindin-1C, an isoform of dysbindin-1 which is linked to schizophrenia has also been shown to result in loss of Hilar Mossy Neurons, and delayed hippocampal neuron maturation (Wang et al., 2014), however, the loss of HMNs in this model was relatively subtle (~17% decrease). Loss of Hilar mossy neurons, and the overall hippocampal phenotype was more severe in AUTS2 cKO than in in the *Sdy* animal, however this may be due to the more extensive expression of the knocked-out AUTS2 isoforms in the hippocampus than the Hilar neuron-specific isoform of Dysbindin disrupted in the *Sdy* mouse. Published linkage analysis of Auts2 locus polymorphisms indicated a connection between Auts2 and schizophrenia (Zhang et al., 2014). A severe loss of hilar mossy neurons is also a phenotype of Rac1/Rac3 double mutant mice (Pennucci et al., 2011). Previous research has indicated that Auts2 is involved in regulating RAC1 signaling during neurodevelopment through Prex1. Auts2 was shown to bind PREX1 protein (Hori et al., 2014) and in our data, bind the Prex1 mRNA which was downregulated in the Auts2 knockout. While Hori et al (2014) did not identify involvement of RAC3 in this pathway, PREX1 has also been shown to function as a GEF for this RAC (Waters et al., 2008). Unlike what we observed in cortical neurons, our hippocampal RNA-sequencing dataset did not identify

downregulation of RAC signaling pathways in the Auts2 deficient hippocampus at P0.5, however this may be a result of confounding factors. Either lack of sensitivity in the sequencing preparation or a dysregulation which occurs before P0.5 before these neurons would become established in the hilus may explain our inability to detect Rac signaling alterations in the hippocampus. As we've shown, at P0.5 these HMNs have either already reached their hilar niche in wildtype P0.5 mice, or been completely lost in the cKO, a transient migratory pathway may not be detectable in this window. For these reasons, a similar effect on Rac1 signaling in hilar mossy neurons as in cortical neurons cannot be entirely dismissed. Alterations in Prex1 dependent Rac1 signaling during earlier, embryonic, hippocampal development should be assessed in future research.

Multiple studies have shown that the functional consequence of HMN depletion is a disinhibition of granule neuron excitability that may contribute to a pro-epileptic feedback loop (Jinde et al., 2012; Zappone, 2004). Patient mutations in Auts2 have previously been associated with epilepsy (Beunders et al., 2016) and a general review of comorbidities of intellectual disability syndrome patients identified epilepsy in about 20% (Oeseburg et al., 2011). Considering the depletion of hilar mossy neurons observed in Auts2 cKO mice, as well as previously reported interactions between AUTS2 and other syndromic intellectual disability genes (Gao et al., 2014) developmental dysregulation of hilar mossy neuron development may play an important role in the pathogenesis of this common comorbidity.

We performed initial EEG experiments to assess if AUTS2 deficient brains exhibited epileptiform-like activity. We identified multiple pathological features including inter-ictal

spiking, a biomarker of epilepsy (Staley and Dudek, 2006) and increases across the power spectrum, particularly delta, theta, and beta bands which are a known finding in ASD (Cornew et al., 2012). However, despite EEG activity which resembles findings in epilepsy, AUTS2 mice do not appear to spontaneously seize. As sleep deprivation can increase seizure risk (Díaz-Negrillo, 2013), and our data indicate that AUTS2 may be involved in regulation of circadian pathways, additional work is needed to determine if AUTS2 deficient mice are susceptible to this insult. Additionally, increases in theta band power which we observed are a hallmark of hippocampal disinhibition. Electrophysiological recordings are necessary to determine how the loss of AUTS2 affects hippocampal network activity directly, either by slice, or in-vivo recordings. This should be accompanied by recording experiments in the presence of GABA and Glutamate receptor agonists and antagonists to determine if the altered hippocampal activity is an intrinsic property of hippocampal granule neurons which lack AUTS2, or a result of circuit level defects from loss of hilar mossy neurons.

5.4: Summary

In this study we identified multiple biological processes which are regulated by AUTS2 and carry implications for our understanding of the AUTS2 syndrome and associated pathologies. We found that AUTS2 participates in an RNA-binding complex which contains multiple canonical splicing factors as well as factors known to regulate post-transcriptional modification of RNAs. We then found that this novel AUTS2 containing complex directly targeted RNAs, including previously identified effectors of AUTS2 and proteins involved in multiple neurodevelopmental processes. These processes included neuron projection

development and Notch signaling. Transcripts targeted by this complex were predominantly downregulated in the absence of AUTS2 which we identified utilizing RNA-sequencing of the frontal cortex from a novel AUTS2 mutant mouse. This mouse carried a deletion which ablated expression of major 3' isoforms expressed from the Auts2 locus in an animal model for the first time. Downregulation of these targets indicates that AUTS2 likely is involved in promoting the production of its target genes, although the specific mechanism of this action remains an area for future study. Production of this mouse model also allowed us to identify substantial abnormalities in hippocampal development which resulted from absence of AUTS2. Hippocampal abnormalities are a known feature of ASD (Saitoh, 2001), schizophrenia (Heckers and Konradi, 2002), and epilepsy (Das et al., 2009). AUTS2 variants have previously been associated with all of these disorders (Beunders et al., 2016; Mefford et al., 2010; Zhang et al., 2014). We identified abnormalities in our Auts2 cKO mice which may contribute to our understanding of the pathogenesis of these disorders, including dysregulated expression of enkephalins in CR cells. CR cells which have been implicated in ASD and schizophrenia pathology previously though mutations in the reelin gene (Fatemi, 2002; Folsom and Fatemi, 2013) are involved in patterning neuronal migration in the cortex and hippocampus. Dysregulation of enkephalin signaling may also play a role in observed respiratory abnormalities in these mice, itself a finding with relevance for understanding the pathogenesis of respiratory dysfunction in children with ASD (Ming et al., 2016). Finally, we identified loss of the hilar mossy neuron circuitry, a major pathway of hippocampal interconnectivity. This pathway, which while known to be involved in hippocampal processing (Lysetskiy et al., 2005) and is implicated in both schizophrenia (Wang et al.,

2014) and epilepsy (Jinde et al., 2013) is not well studied. Our results indicate a potential role for this circuitry in the pathogenesis of intellectual disability as well. These findings contribute to understanding how AUTS2 dependent RNA processing regulates neurodevelopmental processes which are pathologically altered in AUTS2 syndrome patients resulting in intellectual disability, developmental delay, and microcephaly. These findings also supply cellular and molecular relationships which may aid in understanding the connections between ASD pathology and common neurological comorbidities.

Chapter 6: EXPERIMENTAL METHODS

6.1: Bioinformatic analyses of Auts2 structure and function

To perform this analysis novel AUTS2 domains were identified using ProDom (http://prodom.prabi.fr/prodom/current/html/home.php) a machine-generated library of domains built from PSI-Blast searches UniProt database (Bru et al., 2005) with an E-value cutoff of 10^-50 additional canonical domains were annotated using the NCBI Conserved Domain search tool (https://www.ncbi.nlm.nih.gov/Structure/cdd/wrpsb.cgi). To predict molecular function annotation of the identified domains, amino acid sequences were submitted to UniGOPred (Rifaioglu et al., 2018). UniGOPred is a machine learning methodology based on data from the UniProt knowledgebase which utilizes multiple modeling predictions to assign GO Molecular Function terms based on primary amino acid sequence and homology modeling.

6.2: Nuclear Complex Immunoprecipitation

Wildtype C57Bl/6 mice from Jackson labs were harvested at P0.5. The cortex was dissected in cold saline, weighed and flash frozen to prevent degradation. Nuclei were prepared from 1.0g pooled cortex and lysed for protein content in hypotonic buffer. Co-IP incubations were performed in accordance with the ActiveMotif Nuclear Complex Co-IP kit (Product Number 54001) for tissue using low stringency wash buffer to maximize candidate interactions and prevent loss of lightly bound complex members. Auts2 was immunoprecipitated from pooled P0.5 cortices using Prestige Antibodies® Anti-Auts2 produced in Rabbit

(Cat#HPA000390). Samples were run against negative control blank Protein A beads incubated with identical neuronal lysate. Whole eluted Co-IP reactions were trypsin digested and desalted for LTQ/Mass-spec in accordance with protocols obtained from the Goodlett lab (goodlettlab.org). Additional Co-IP reactions were run on a denaturing acrylamide gel, the gel was Coomassie stained, bands were excised, Trypsin digested and eluted for Mass-Spec. Gel Extraction was performed according to the Goodlett Lab Protocols (adapted from Shevchekno et al., 1996). Detection was performed on a ThermoScientific Linear Orbitrap Q Exactive spectrometer. Mass Spec fragment database searches were performed by University of Washington core facilities. Total independent spectra for each protein was normalized to the length of the protein, and these enrichment values were used to determine the top 25% of proteins enriched in both replicates. This list was subsequently submitted for String and GO analysis.

Western blotting for LTQ/MS validation was performed using 5 µg each of antibody to AUTS2 c-terminus (generated for this project) and commercial anti-NONO, and 500 µg whole nuclear lysate. The nuclear lysate was prepared through the ActiveMotif nuclear isolation protocol from 3 pooled cortices per replicate. Co-IP was performed using included alternative Active Motif high stringency wash buffer and immunoprecipitated using Protein G Beads, as Goat primary antibodies such as the NonO antibody used are not selected with high fidelity by Protein A. Westerns were run on BioRad Mini-Protean TGX 4-20% gradient gels, double probed with Donkey Anti-Rabbit AlexaFluor 488 and Donkey Anti-Goat AlexaFluor 647 diluted 1:5000 in blocking solution and imaged using the FluorChem R system (ProteinSimple).

6.3: Tissue Preparation for RNA-seq and Western Blotting

P0.5 neonates from EMX1-cre driven Auts2 cKO were rapidly decapitated into cold saline. Frontal cortex from eye socket forward was dissected, meninges and olfactory tract removed, and flash frozen on dry ice. All tissue was stored at -80˚C prior to RNA isolation. For immunological analysis or in situ hybridization neonates were cold-anesthetized. Postnatal mice were anesthetized with isoflurane. Animals were perfused with 4% paraformaldehyde in 1× PBS (pH 7.4). Brains were post-fixed by immersion in cold buffered (4 °C) 4% paraformaldehyde for 4–16 h. Brains were cryoprotected in 30% sucrose in 0.1 M sodium phosphate (pH 7.0), frozen in optimum cutting temperature compound (Sakura Finetek), cryosectioned at 12 µm, and mounted on Superfrost Plus slides (Thermo Fisher Scientific). Slides were stored at –8o °C until needed.

6.4: Immunohistochemistry

Antigen recovery was performed by boiling in 0.01M Sodium Citrate. Sections were blocked for 30 minutes at room temperature in 10% serum (Goat or Donkey depending on Primary antibody origin species), 3% BSA, 0.1% Triton X-100 in PBS. Primary Antibodies were diluted in blocking solution and incubated overnight at 4C. Tissue was washed 3x 5 minutes in 1X PBS before secondary application. Alexafluor conjugated secondary antibodies were diluted 1:400 in blocking solution and incubated for 2 hours at room temperature. Tissue was again washed 3x in PBS, incubated briefly in DAPI and mounted with SouthernBiotech Fluoromount-G and allowed to cure before imaging on a Zeiss LSM710 Confocal.

6.5: In-Situ Hybridization

Penk cDNA (Accession: BC049766) was subcloned into pBluescriptSK(+) (Stratagene). DIG-labeled riboprobes were prepared with Roche kit # 1l175025910 as previously described (Bedogni et al., 2010b; Elsen et al., 2013). The detailed hybridization protocol has been made available on OpenWetWare:

https://openwetware.org/wiki/In_Situ_Hybridization_on_Cryosectioned_Tissue

6.6: RNA Isolation

RNA was prepared from individual dissected frontal cortex and hippocampal tissue specimens using the Qiagen RNEasy Plus Universal Mini kit (Cat No.: 73404) according to the manufacturer's instructions with the exception that all reagent amounts were scaled to 1/3 of the indicated volume to account for small sample sizes. All samples were normalized to 3,500ng in 50 uL H2O (concentration 70ng/uL) and submitted to the Northwest Genomics Core (NWGC) at The University of Washington Department of Genome Sciences for quality control, poly-A selection, Illumina TruSeq library preparation, sequencing and mapping to the reference genome. http://nwgc.gs.washington.edu

6.7: RNA Sequencing

75 base pair paired-end reads were obtained on an Illumina HiSeq 4000 from frontal cortex and hippocampus RNA samples isolated from four wildtype and four knockout P0.5 neonates as described. Libraries were prepared by the Northwest Genomics Core using the Illumina TruSeq library preparation kit and sequenced to a depth of 30 million reads. Reads

were mapped to the mm10 (Gencode M11) mouse genome by the Northwest Genomics Core using STAR (Dobin et al., 2013) and received from the sequencing core as paired-end bam files.

6.8: RNA-Immunoprecipitation Sequencing

Magna RIP™ RNA-Binding Protein Immunoprecipitation Kit 17-700 from Millipore Sigma was used for RNA-Immunoprecipitations. Whole cortex was dissected from P0.5 C75BL/6J neonates generated from breeder pairs of Cre negative wildtype control littermates from the Auts2 cKO generation colony. Two cortices were pooled for each replicate. Two replicates (four cortices) were prepared for RIP according to the "For Tissue Sample" section of the Millipore 17-700 protocol. After lysate preparation, RNA-Immunoprecipitation was performed according to the Millipore protocol. RNA samples were submitted to the Northwest Genomics Core for sequencing. Sequence libraries were prepared using the Clonetech SMARTer® Stranded Total RNA Sample Prep for RIP-Sequencing library preparation (Zhao et al., 2010). Clonetech SMARTer stranded libraries were run on an Illumina NextSeq. Reads were mapped to the mm10 (Gencode M11) mouse genome by the Northwest Genomics Core using STAR (Dobin et al., 2013) and received from the sequencing core as paired-end bam files.

6.9: RNA Quantification and Differential Expression Analysis

Reference genome and transcriptome for the mouse was obtained from Gencode M14 annotation. Cuffdiff (Galaxy Version 2.2.1.3) (Trapnell et al., 2013) was run to calculate transcript level (frontal cortex) and gene level (hippocampus) differential expression with

the following deviations from the default parameters. RNA-Seq: --library-type fr-firststrand -dispersion-method per-condition --no-effective-length-correction

RIP-sequencing sample enrichment was also calculated in Cuffdiff with the following flags: --library-type fr-secondstrand -dispersion-method pooled --no-effective-length-correction. As RIP-Seq, unlike CLIP-seq does not fragment RNAs, we used CuffDiff 2.1 (Trapnell et al., 2013) to quantify enrichment at the whole transcript level rather than peak calling methods which are more appropriate for defined regions of sharp sequence enrichment.

RIP-sequencing analysis was run separately for each control type (IP vs IgG in one run, IP vs Input in a second run), transcript differential expression testing files were joined and only samples with a FDR Q<0.05 in both comparisons were considered significant hits.

A blacklist file containing Gencode m14 annotations for rRNA, tRNA, tRNA pseudogenes, mitochondrial genes and genes mapping to ChrY was also passed to the program for all analysis.

6.10: Gene Ontology Analysis

GeneSCF-v1.1-p2 from the Kanduri Lab (Subhash and Kanduri, 2016) was used for GO analysis, the background parameter (--bg) was set using the total number of transcripts (for frontal cortex) or genes (for hippocampus) that passed Cuffdiff significance testing thresholds (status=OK)

6.11: GeneSet Enrichment Analysis

For analysis of hippocampal neuronal populations, A GMX formatted GeneSets database was constructed from the HippoSeq repository http://hipposeq.janelia.org (Cembrowski et al., 2016). Expression lists were filtered for genes which were enriched 2.5-fold in one neuronal population vs. all other neuronal populations in the database. This resulted in the construction of 16 gene lists each uniquely identifying a neuronal population. For analysis of canonical genesets, the Bader Lab enrichments pathways were retrieved for Mouse_AllPathways_April_01_2017_symbol.gmt and Mouse_Human_DrugBank_all_symbol.gmt (Merico et al., 2010). A gene list filter threshold (Min Size: Exclude Smaller Sets) of 10 was set which excluded two of these datasets which marked CA3 neurons from the analysis. FPKM tables were extracted from the CuffDiff cummeRbund database produced from differential gene expression analysis of the Hippocampal RNA-sequencing study (as previously described). Count tables were filtered to select only genes which passed the CuffDiff thresholds for determining expressed genes for statistical testing. This resulted in the selection of 14,900 expressed genes for Gene Set Enrichment analysis for Hippocampus and 14,345 for Frontal Cortex. GSEA was run in gene_set permutation type mode with the “weighted” enrichment statistic, the “Signal2Noise” ranking metric, and the “meandiv” normalization mode (default parameters).

6.12: Video-EEG-EMG Recording.

1 month old mice (n=3), and wildtype controls (n=5) underwent survival surgery to implant EEG and EMG electrodes. The mice were anesthetized with 2-3% isoflurane gas and given bupivacaine analgesia (0.1 mg/kg, s.c.). Using aseptic technique, a midline incision was made anterior to posterior to expose the cranium. Fine silver wires were placed through small cranial holes created with a fine cutting needle and fixed in place with cyanoacrylate glue. EEG electrodes were placed at visually identified locations - bilateral frontal and bilateral posterior. EMG electrodes were placed in back muscles. A reference electrode was placed at the midline cerebellum and a ground electrode was placed subcutaneously over the back. Electrode impedances were typically < 25 kΩ. After electrode placement, the skin was closed with sutures and the mice were allowed to recover for at least 3 days to allow recovery from surgery and anesthetic effects. Simultaneous video-EEG-EMG records were collected in conscious mice on a PowerLab 8/35 data acquisition unit using LabChart 7.3.3 software (AD Instruments, Colorado Spring, Co). All bio-electrical signals were acquired at 1 KHz sampling rate. The EEG signals were processed off-line with a 1-80 Hz bandpass filter and the EMG signals with a 3-Hz high pass filter. Video-EEG-EMG data collected were analyzed using LabChart software. The analysis was conducted on one-hour segments of the EEG when the animal was immobile. To control for circadian influence on the EEG all analyses were conducted on data collected between 1 pm and 3 pm.

6.13: Plethysmography

Whole-body plethysmography was performed on P0.5 wild-type (N=7 Nestin experiment, N=3 EMX1 experiment), Heterozygous Auts2 Nes11-cre deletion (N=7) and Homozygous Auts2 Nes11-cre deletion (N=3), Heterozygous Auts2 EMX1-cre deletion (N=3), Homozygous Auts2 EMX1-cre deletion (N=3) animals. Animals were placed in a custom built barometric chamber and equilibrated to the chamber with open air flow. The chamber was sealed for a 60 s recording session, and the pressure difference was measured between the experimental and reference chamber with a differential pressure transducer. Only recording periods in which the animals were immobile were analyzed. Data were collected and analyzed using pCLAMP 10.5 software (Molecular Devices). All analysis was performed blinded to genotype.

6.14: ChIP-Seq Data Reprocessing

ChIP-seq of factors of interest and paired controls were obtained from EBI/GEO and imported into Galaxy for remapping to mm10. Auts2 ChIP data was obtained from Gao et al: GSE60411. Fastqsanger files were mapped to mm10 using (Bowtie2 Galaxy Version 2.2.6.2) (Langmead et al., 2009) with the --very-sensitive-local presets (-D 20 -R 3 -N 0 -L 20 -i S,1,0.50).

Mapped reads were processed in accordance with the methods described in the Galaxy ChIP-Seq tutorial for MACS2 (Zhang et al., 2008) peak calling using Galaxy Version 2.1.1.20160309.0 (https://galaxyproject.org/tutorials/chip/) Mapped reads were quality filtered for a MAPQ quality score >20 using SAMTools (Li et al., 2009b). Additionally, reads

overlapping regions in the ENCODE artifact blacklist (maintained by the Kundaje lab), marked with the PCR duplicate or QCfail flags were removed with the BAMfilter tool. MFOLD parameters were set at 5, 100. Band-width was set using fragment size from size-selection where available (Gao et al=350). Extension size parameter for peak calling was obtained by running the MACS2 predictd component.

6.15: Binding and Expression Target Analysis (BETA)

BETA 1.0.7 (Wang et al., 2013) binaries were retrieved from Cistrome.org and were configured on a local workstation. MACS2 peaks (bed) files were generated as described above. The inbuilt gene/transcript reference database corresponding to UCSC mm10 was replaced with an updated transcriptome file generated from the Gencode M14 release. BETA Minus was used with the Gencode M14 transcriptome to identify targeted transcript start sites within 5 kB of AUTS2 ChIP peaks (in accordance with the identification of ±5kB of a TSS as the region of AUTS2 genomic binding (Gao et al., 2014).

6.16: Mouse Strains

B6.129S2-Emx1tm1(cre)Krj/J (EMX1-cre) (Gorski et al., 2002) and B6.Cg-Tg(Nes-cre)1Kln/J (Nes11-cre) (Tronche et al., 1999) were obtained from The Jackson Laboratory (EMX1-ires-Cre JAX stock #005628 and Nes11-Cre JAX stock #003771). C57BL6/J derived Auts2 Exon 15 Floxed Mice were generated in collaboration with GenOway.

6.17: PCR Screening of Auts2 Exon Excision

Primer Name	PCR Product Size		
	Wildtype	LoxP Allele	Cre-excised
119467cre-HEV1	1440	3180 – Not Amplified under standard conditions	457
119470cre-HEV1			
119468cre-HEV1	148	226	

Reaction Conditions			
Step	Temp (C)	Time (s)	Cycles
Denaturing	94	120	1
Denaturing	94	30	30
Annealing	65	30	
Extension	68	60	
Final Extension	68	480	1

6.18: KEY RESOURCES TABLE

REAGENT or RESOURCE	SOURCE	IDENTIFIER
Antibodies		
Rabbit Polyclonal Anti-AUTS2 c-terminal	This paper	PAS#19228
Rabbit Polyclonal Anti-AUTS2 n-terminal	This paper	PAS#19226
Goat Polyclonal Anti-NONO/P54NRB	ThermoFisher	PA5-18514
Rat Monoclonal Anti-CTIP2	Abcam	AB18465
Rat Monoclonal Anti-TBR2	eBioscience	Dan11mag
Rabbit Anti-SOX9	Millipore Sigma	AB5535
Mouse IgG1 Anti-Reelin	Millipore Sigma	MAB5364
Rabbit Anti-Calretinin	Swant	CR 7697
Mouse IgG1 Anti-Calretinin	Millipore Sigma	MAB1568
Rabbit Anti-GluR2/3	Millipore Sigma	AB15062
Rabbit Monoclonal Anti-SATB2	Abcam	AB92446
Mouse Monoclonal Anti-PanSATB	Abcam	AB51502
Goat Anti-SATB1	Abcam	AB189372
Rabbit Anti-5HTT	Millipore Sigma	602-622

Bacterial and Virus Strains		
OneShot TOP10 Chemically Competent e. coli	Invitrogen	C4040
Chemicals, Peptides, and Recombinant Proteins		
In-Situ Hybridization Protocol and Complete Reagents	This paper	openwetware.org/mediawiki/index.php?title=In_Situ_Hybridization_on_Cryosectioned_Tissue
Critical Commercial Assays		
Nuclear Complex Co-IP Kit	ActiveMotif	54001
Magna RIP Kit	Millipore Sigma	17-700
DIG RNA Labeling Kit	Roche	11175025910
GoTaq Flexi DNA Polymerase	Promega	M929
RNEasy Plus Universal Mini kit	Qiagen	73404
TruSeq Stranded mRNA Library Prep	Illumina	20020594
SMARTer® Stranded Total RNA Sample Prep Kit	Clonetech	634836
Deposited Data		
AUTS2 Frontal Cortex RNA-Seq	This paper	
AUTS2 Cortex RIP-Seq	This paper	
Experimental Models: Organisms/Strains		
B6.129S2-Emx1tm1(cre)Krj/J	Gorski et al., 2002	JAX stock #005628
B6.Cg-Tg(Nes-cre)1Kln/J	Tronche et al., 1999	JAX stock #003771
Auts2 c-terminal cKO	This Paper	N/A
Oligonucleotides		
Auts2 Primer 119467cre-HEV1: TTGGCTGTCTGCTTCAAGTTGGACC	This paper	N/A
Auts2 Primer 119470cre-HEV1: CCAATAGGACCTGTGCTGGCTGGT	This paper	N/A
Auts2 Primer 119468cre-HEV1: TCAACGCTGAGAACACTGTGAGAATGAAG	This paper	N/A
Recombinant DNA		
pBluescriptSK(+)	Stratagene	GenBank X52325.1
MGC Mouse Penk cDNA Accession: BC049766 Clone ID: 6774387	Dharmacon	MMM4772-202843165
Software and Algorithms		

GeneSCF	Subhash et al., 2016	http://genescf.kandurilab.org/
BETA 1.0.7	Wang et al., 2013	http://cistrome.org/BETA/
Cuffdiff (Galaxy Version 2.2.1.3)	Trapnell et al., 2012	usegalaxy.org
Bowtie2 (Galaxy Version 2.2.6.2)	Langmead et al., 2008	usegalaxy.org
MACS2 (Galaxy Version 2.1.1.20160309.0)	Zhang et al., 2008	usegalaxy.org
SamTools (Galaxy Version 1.1.2)		usegalaxy.org
STAR (RNA-Seq: 2.5.2b. RIP-Seq: 2.5.3a)	Dobin et al., 2013	https://github.com/alexdobin/STAR
GSEA 3.0 Build 0160	Subramanian et al., 2005	http://software.broadinstitute.org/gsea/index.jsp
Other		
Gencode M14 Release	GenCode	https://www.gencodegenes.org/mouse_releases/14.html
Encode Artifact Blacklist	Kundaje lab	http://mitra.stanford.edu/kundaje/akundaje/release/blacklists/mm10-mouse/
AUTS2 ChIP-Seq	Gao et al., 2014	GSE60411
NONO Gene Trap Hippocampus RNA-sequencing	Mircsof et al., 2015	GSE62571
Auts2 Frontal Cortex RNA-Seq and AUTS2 RIP-Seq	This paper	GSE112792
Auts2 Hippocampus RNA-seq	This paper	Unpublished

REFERENCES

Alarcón, C.R., Goodarzi, H., Lee, H., Liu, X., Tavazoie, S., and Tavazoie, S.F. (2015). HNRNPA2B1 Is a Mediator of m6A-Dependent Nuclear RNA Processing Events. Cell *162*, 1299–1308.

Allemand, E., Myers, M.P., Garcia-Bernardo, J., Harel-Bellan, A., Krainer, A.R., and Muchardt, C. (2016). A Broad Set of Chromatin Factors Influences Splicing. PLOS Genet. *12*, e1006318.

Allen Institute for Brain Science (2015). Allen Mouse Brain Atlas. Allen Mouse Brain Atlas *2*, 1–13.

Aman, M., Rettiganti, M., Nagaraja, H.N., Hollway, J.A., McCracken, J., McDougle, C.J., Tierney, E., Scahill, L., Arnold, L.E., Hellings, J., et al. (2015). Tolerability, Safety, and Benefits of Risperidone in Children and Adolescents with Autism: 21-Month Follow-up After 8-Week Placebo-Controlled Trial. J. Child Adolesc. Psychopharmacol. *25*, 482–493.

Amarillo, I.E., Li, W.L., Li, X., Vilain, E., and Kantarci, S. (2014). De novo single exon deletion of AUTS2 in a patient with speech and language disorder: A review of disrupted AUTS2 and further evidence for its role in neurodevelopmental disorders. Am. J. Med. Genet. Part A *164*, 958–965.

Amelio, A.L., Miraglia, L.J., Conkright, J.J., Mercer, B.A., Batalov, S., Cavett, V., Orth, A.P., Busby, J., Hogenesch, J.B., and Conkright, M.D. (2007). A coactivator trap identifies NONO (p54nrb) as a component of the cAMP-signaling pathway. Proc. Natl. Acad. Sci. *104*, 20314–20319.

American Psychiatric Association (2013). Diagnostic and Statistical Manual of Mental Disorders, 5th Edition (DSM-5). Diagnostic Stat. Man. Ment. Disord. 4th Ed. TR. 280.

Angevine, J.B. (1965). Time of neuron origin in the hippocampal region. An autoradiographic study in the mouse. Exp. Neurol. Suppl. Suppl 2:1-70.

Arnold, S.J., Huang, G.J., Cheung, A.F.P., Era, T., Nishikawa, S.I., Bikoff, E.K., Molnár, Z., Robertson, E.J., and Groszer, M. (2008). The T-box transcription factor Eomes/Tbr2 regulates neurogenesis in the cortical subventricular zone. Genes Dev. *22*, 2479–2484.

Badea, A., Nicholls, P.J., Johnson, G.A., and Wetsel, W.C. (2007). Neuroanatomical phenotypes in the Reeler mouse. Neuroimage *34*, 1363–1374.

Balamotis, M.A., Tamberg, N., Woo, Y.J., Li, J., Davy, B., Kohwi-Shigematsu, T., and Kohwi, Y. (2012). Satb1 Ablation Alters Temporal Expression of Immediate Early Genes and Reduces Dendritic Spine Density during Postnatal Brain Development. Mol. Cell. Biol. *32*, 333–347.

Baltz, A.G., Munschauer, M., Schwanhäusser, B., Vasile, A., Murakawa, Y., Schueler, M.,

Youngs, N., Penfold-Brown, D., Drew, K., Milek, M., et al. (2012). The mRNA-Bound Proteome and Its Global Occupancy Profile on Protein-Coding Transcripts. Mol. Cell *46*, 674–690.

Bedogni, F., Hodge, R.D., Nelson, B.R., Frederick, E.A., Shiba, N., Daza, R.A., and Hevner, R.F. (2010a). Autism susceptibility candidate 2 (Auts2) encodes a nuclear protein expressed in developing brain regions implicated in autism neuropathology. Gene Expr. Patterns *10*, 9–15.

Bedogni, F., Hodge, R.D., Elsen, G.E., Nelson, B.R., Daza, R.A.M., Beyer, R.P., Bammler, T.K., Rubenstein, J.L.R., and Hevner, R.F. (2010b). Tbr1 regulates regional and laminar identity of postmitotic neurons in developing neocortex. Proc. Natl. Acad. Sci. *107*, 13129–13134.

Van Belzen, M., Bartsch, O., Lacombe, D., Peters, D.J.M., and Hennekam, R.C.M. (2011). Rubinstein-Taybi syndrome (CREBBP, EP300). Eur. J. Hum. Genet. *19*, 121.

Beunders, G., Voorhoeve, E., Golzio, C., Pardo, L.M., Rosenfeld, J.A., Talkowski, M.E., Simonic, I., Lionel, A.C., Vergult, S., Pyatt, R.E., et al. (2013). Exonic deletions in AUTS2 cause a syndromic form of intellectual disability and suggest a critical role for the C terminus. Am. J. Hum. Genet. *92*, 210–220.

Beunders, G., De Munnik, S.A., Van Der Aa, N., Ceulemans, B., Voorhoeve, E., Groffen, A.J., Nillesen, W.M., Meijers-Heijboer, E.J., Frank Kooy, R., Yntema, H.G., et al. (2015). Two male adults with pathogenic AUTS2 variants, including a two-base pair deletion, further delineate the AUTS2 syndrome. Eur. J. Hum. Genet. *23*, 803–807.

Beunders, G., van de Kamp, J., Vasudevan, P., Morton, J., Smets, K., Kleefstra, T., de Munnik, S.A., Schuurs-Hoeijmakers, J., Ceulemans, B., Zollino, M., et al. (2016). A detailed clinical analysis of 13 patients with AUTS2 syndrome further delineates the phenotypic spectrum and underscores the behavioural phenotype. J. Med. Genet. *53*, 523–532.

Blümcke, I., Suter, B., Behle, K., Kuhn, R., Schramm, J., Elger, C.E., and Wiestler, O.D. (2000). Loss of hilar mossy cells in Ammon's horn sclerosis. Epilepsia *41 Suppl 6*, S174–S180.

Boldrini, M., Fulmore, C.A., Tartt, A.N., Simeon, L.R., Pavlova, I., Poposka, V., Rosoklija, G.B., Stankov, A., Arango, V., Dwork, A.J., et al. (2018). Human Hippocampal Neurogenesis Persists throughout Aging. Cell Stem Cell *22*, 589–599.e5.

Bonora, E., Beyer, K.S., Lamb, J.A., Parr, J.R., Klauck, S.M., Benner, A., Paolucci, M., Abbott, A., Ragoussis, I., Poustka, A., et al. (2003). Analysis of reelin as a candidate gene for autism. Mol. Psychiatry *8*, 885–892.

Bouchard-Cannon, P., Mendoza-Viveros, L., Yuen, A., Kærn, M., and Cheng, H.Y.M. (2013). The Circadian Molecular Clock Regulates Adult Hippocampal Neurogenesis by Controlling the Timing of Cell-Cycle Entry and Exit. Cell Rep. *5*, 961–973.

Broadbent, N.J., Gaskin, S., Squire, L.R., and Clark, R.E. (2010). Object recognition

memory and the rodent hippocampus. Learn. Mem. *17*, 5–11.

Brogna, S., Sato, T.A., and Rosbash, M. (2002). Ribosome components are associated with sites of transcription. Mol. Cell *10*, 93–104.

Bru, C., Courcelle, E., Carrère, S., Beausse, Y., Dalmar, S., and Kahn, D. (2005). The ProDom database of protein domain families: More emphasis on 3D. Nucleic Acids Res. *33*.

Brunne, B., Franco, S., Bouché, E., Herz, J., Howell, B.W., Pahle, J., Müller, U., May, P., Frotscher, M., and Bock, H.H. (2013). Role of the postnatal radial glial scaffold for the development of the dentate gyrus as revealed by reelin signaling mutant mice. Glia *61*, 1347–1363.

Canitano, R., and Pallagrosi, M. (2017). Autism spectrum disorders and schizophrenia spectrum disorders: Excitation/inhibition imbalance and developmental trajectories. Front. Psychiatry *8*.

Capra, J.A., Erwin, G.D., McKinsey, G., Rubenstein, J.L.R., and Pollard, K.S. (2013). Many human accelerated regions are developmental enhancers. Philos. Trans. R. Soc. B Biol. Sci. *368*, 20130025–20130025.

Cassiday, L.A. (2002). Having it both ways: transcription factors that bind DNA and RNA. Nucleic Acids Res. *30*, 4118–4126.

Cembrowski, M.S., Wang, L., Sugino, K., Shields, B.C., and Spruston, N. (2016). Hipposeq: A comprehensive RNA-seq database of gene expression in hippocampal principal neurons. Elife *5*.

Cescon, M., Chen, P., Castagnaro, S., Gregorio, I., and Bonaldo, P. (2016). Lack of collagen VI promotes neurodegeneration by impairing autophagy and inducing apoptosis during aging. Aging (Albany. NY). *8*, 1083–1101.

Chancey, J.H., Poulsen, D.J., Wadiche, J.I., and Overstreet-Wadiche, L. (2014). Hilar Mossy Cells Provide the First Glutamatergic Synapses to Adult-Born Dentate Granule Cells. J. Neurosci. *34*, 2349–2354.

Chang, B.S., Duzcan, F., Kim, S., Cinbis, M., Aggarwal, A., Apse, K.A., Ozdel, O., Atmaca, M., Zencir, S., Bagci, H., et al. (2007). The role of RELN in lissencephaly and neuropsychiatric disease. Am. J. Med. Genet. Part B Neuropsychiatr. Genet. *144*, 58–63.

Chisholm, K., Lin, A., Abu-Akel, A., and Wood, S.J. (2015). The association between autism and schizophrenia spectrum disorders: A review of eight alternate models of co-occurrence. Neurosci. Biobehav. Rev. *55*, 173–183.

Cho, C.-H. (2012). Molecular mechanism of circadian rhythmicity of seizures in temporal lobe epilepsy. Front. Cell. Neurosci. *6*.

Chojnicka, I., Gajos, K., Strawa, K., Broda, G., Fudalej, S., Fudalej, M., Stawiński, P., Pawlak, A., Krajewski, P., Wojnar, M., et al. (2013). Possible Association between Suicide Committed under Influence of Ethanol and a Variant in the AUTS2 Gene. PLoS One *8*,

e57199.

Cooper, R.A., Richter, F.R., Bays, P.M., Plaisted-Grant, K.C., Baron-Cohen, S., and Simons, J.S. (2017). Reduced Hippocampal Functional Connectivity During Episodic Memory Retrieval in Autism. Cereb. Cortex *27*, 888–902.

Cornew, L., Roberts, T.P.L., Blaskey, L., and Edgar, J.C. (2012). Resting-state oscillatory activity in autism spectrum disorders. J. Autism Dev. Disord. *42*, 1884–1894.

Curie, T., Mongrain, V., Dorsaz, S., Mang, G.M., Emmenegger, Y., and Franken, P. (2013). Homeostatic and Circadian Contribution to EEG and Molecular State Variables of Sleep Regulation. Sleep *36*, 311–323.

Dang, W., Zhang, Q., Zhu, Y.S., and Lu, X.Y. (2014). The Evidence for the Contribution of the Autism Susceptibility Candidate 2 (AUTS2) Gene in Heroin Dependence Susceptibility. J. Mol. Neurosci. *54*, 811–819.

Dardenne, E., PolayEspinoza, M., Fattet, L., Germann, S., Lambert, M.P., Neil, H., Zonta, E., Mortada, H., Gratadou, L., Deygas, M., et al. (2014). RNA Helicases DDX5 and DDX17 Dynamically Orchestrate Transcription, miRNA, and Splicing Programs in Cell Differentiation. Cell Rep. *7*, 1900–1913.

Das, S.R., Mechanic-Hamilton, D., Korczykowski, M., Pluta, J., Glynn, S., Avants, B.B., Detre, J.A., and Yushkevich, P.A. (2009). Structure specific analysis of the hippocampus in temporal lobe epilepsy. Hippocampus *19*, 517–525.

De, S., Varsally, W., Falciani, F., and Brogna, S. (2011). Ribosomal proteins' association with transcription sites peaks at tRNA genes in Schizosaccharomyces pombe. RNA *17*, 1713–1726.

Dequéant, M.L., Glynn, E., Gaudenz, K., Wahl, M., Chen, J., Mushegian, A., and Pourquié, O. (2006). A complex oscillating network of signaling genes underlies the mouse segmentation clock. Science (80-.). *314*, 1595–1598.

Desjardins, S., Doyen, C., Contejean, Y., Kaye, K., and Paubel, P. (2009). Traitement dun enfant autiste par la naltrexone. Encephale *35*, 168–172.

Díaz-Negrillo, A. (2013). Influence of sleep and sleep deprivation on ictal and interictal epileptiform activity. Epilepsy Res. Treat. *2013*, 492524.

Doan, R.N., Bae, B. Il, Cubelos, B., Chang, C., Hossain, A.A., Al-Saad, S., Mukaddes, N.M., Oner, O., Al-Saffar, M., Balkhy, S., et al. (2016). Mutations in Human Accelerated Regions Disrupt Cognition and Social Behavior. Cell *167*, 341–354.e12.

Dobin, A., Davis, C.A., Schlesinger, F., Drenkow, J., Zaleski, C., Jha, S., Batut, P., Chaisson, M., and Gingeras, T.R. (2013). STAR: Ultrafast universal RNA-seq aligner. In Bioinformatics, pp. 15–21.

Dodds, T.J. (2017). Prescribed Benzodiazepines and Suicide Risk. Prim. Care Companion CNS Disord. *19*.

Donald, S., Humby, T., Fyfe, I., Segonds-Pichon, A., Walker, S.A., Andrews, S.R., Coadwell, W.J., Emson, P., Wilkinson, L.S., and Welch, H.C.E. (2008). P-Rex2 regulates Purkinje cell dendrite morphology and motor coordination. Proc. Natl. Acad. Sci. U. S. A. *105*, 4483–4488.

Drakew, A., Deller, T., Heimrich, B., Gebhardt, C., Del Turco, D., Tielsch, A., Förster, E., Herz, J., and Frotscher, M. (2002). Dentate granule cells in reeler mutants and VLDLR and ApoER2 knockout mice. Exp. Neurol. *176*, 12–24.

Elsen, G.E., Hodge, R.D., Bedogni, F., Daza, R.A.M., Nelson, B.R., Shiba, N., Reiner, S.L., and Hevner, R.F. (2013). The protomap is propagated to cortical plate neurons through an Eomes-dependent intermediate map. In Proceedings of the National Academy of Sciences, pp. 4081–4086.

Englund, C. (2005). Pax6, Tbr2, and Tbr1 Are Expressed Sequentially by Radial Glia, Intermediate Progenitor Cells, and Postmitotic Neurons in Developing Neocortex. J. Neurosci. *25*, 247–251.

Eriksson, P.S., Perfilieva, E., Björk-Eriksson, T., Alborn, A.-M., Nordborg, C., Peterson, D.A., and Gage, F.H. (1998). Neurogenesis in the adult human hippocampus. Nat. Med. *4*, 1313–1317.

Farrugia, A.J., and Calvo, F. (2016). The Borg family of Cdc42 effector proteins Cdc42EP1-5. In Biochemical Society Transactions, pp. 1709–1716.

Fatemi, S.H. (2002). The role of Reelin in pathology of autism. Mol. Psychiatry *7*, 919–920.

Fatemi, S.H., Reutiman, T.J., Folsom, T.D., and Thuras, P.D. (2009). GABAAreceptor downregulation in brains of subjects with autism. J. Autism Dev. Disord. *39*, 223–230.

Fietz, S.A., Lachmann, R., Brandl, H., Kircher, M., Samusik, N., Schroder, R., Lakshmanaperumal, N., Henry, I., Vogt, J., Riehn, A., et al. (2012). Transcriptomes of germinal zones of human and mouse fetal neocortex suggest a role of extracellular matrix in progenitor self-renewal. Proc. Natl. Acad. Sci. *109*, 11836–11841.

Finger, J.H., Smith, C.M., Hayamizu, T.F., McCright, I.J., Xu, J., Law, M., Shaw, D.R., Baldarelli, R.M., Beal, J.S., Blodgett, O., et al. (2017). The mouse Gene Expression Database (GXD): 2017 update. Nucleic Acids Res. *45*, D730–D736.

Foley, P., Bunyan, D., Stratton, J., Dillon, M., and Lynch, S.A. (2009). Further case of rubinstein-taybi syndrome due to a deletion in EP300. Am. J. Med. Genet. Part A *149*, 997–1000.

Folsom, T.D., and Fatemi, S.H. (2013). The involvement of Reelin in neurodevelopmental disorders. Neuropharmacology *68*, 122–135.

Fox, A.H., Lam, Y.W., Leung, A.K.L., Lyon, C.E., Andersen, J., Mann, M., and Lamond, A.I. (2002). Paraspeckles: A novel nuclear domain. Curr. Biol. *12*, 13–25.

Fuller-Pace, F. V. (2013). The DEAD box proteins DDX5 (p68) and DDX17 (p72): Multi-

tasking transcriptional regulators. Biochim. Biophys. Acta - Gene Regul. Mech. *1829*, 756–763.

Gabis, L., Pomeroy, J., and Andriola, M.R. (2005). Autism and epilepsy: Cause, consequence, comorbidity, or coincidence? Epilepsy Behav. *7*, 652–656.

Gandal, M.J., Haney, J.R., Parikshak, N.N., Leppa, V., Ramaswami, G., Hartl, C., Schork, A.J., Appadurai, V., Buil, A., Werge, T.M., et al. (2018). Shared molecular neuropathology across major psychiatric disorders parallels polygenic overlap. Science (80-.). *359*, 693–697.

Gao, Z., Lee, P., Stafford, J.M., Schimmelmann, M. Von, Schaefer, A., and Reinberg, D. (2014). An AUTS2-Polycomb complex activates gene expression in the CNS. Nature *516*, 349–354.

Ge, X., Shi, Y., Li, J., Zhang, Z., Lin, X., Zhan, J., Ge, H., Xu, J., Yu, Q., Leng, Y., et al. (2015). Development of the human fetal hippocampal formation during early second trimester. Neuroimage *119*, 33–43.

Geoffray, M.-M., Nicolas, A., Speranza, M., and Georgieff, N. (2017). Are circadian rhythms new pathways to understand Autism Spectrum Disorder? J. Physiol.

Glickman, G. (2010). Circadian rhythms and sleep in children with autism. Neurosci. Biobehav. Rev. *34*, 755–768.

Gorski, J. a, Talley, T., Qiu, M., Puelles, L., Rubenstein, J.L.R., and Jones, K.R. (2002). Cortical excitatory neurons and glia, but not GABAergic neurons, are produced in the Emx1-expressing lineage. J. Neurosci. *22*, 6309–6314.

Green, R.E., Krause, J., Briggs, A.W., Maricic, T., Stenzel, U., Kircher, M., Patterson, N., Li, H., Zhai, W., Fritz, M.H.Y., et al. (2010). A draft sequence of the neandertal genome. Science (80-.). *328*, 710–722.

Grunstein, M.M., and Grunstein, J.S. (1982). Maturational effect of enkephalin on respiratory control in newborn rabbits. J Appl Physiol *53*, 1063–1070.

Ha, S., Tripathi, P.P., Mihalas, A.B., Hevner, R.F., and Beier, D.R. (2017). C-Terminal Region Truncation of RELN Disrupts an Interaction with VLDLR, Causing Abnormal Development of the Cerebral Cortex and Hippocampus. J. Neurosci. *37*, 960–971.

Harmony, T. (2013). The functional significance of delta oscillations in cognitive processing. Front. Integr. Neurosci. *7*.

Harvey, A.G., Mullin, B.C., and Hinshaw, S.P. (2006). Sleep and circadian rhythms in children and adolescents with bipolar disorder. Dev. Psychopathol. *18*, 1147–1168.

Hauri, S., Comoglio, F., Seimiya, M., Gerstung, M., Glatter, T., Hansen, K., Aebersold, R., Paro, R., Gstaiger, M., and Beisel, C. (2016). A High-Density Map for Navigating the Human Polycomb Complexome. Cell Rep. *17*, 583–595.

Hauser, K.F., Houdi, A.A., Turbek, C.S., Elde, R.P., and Maxson, W. (2000). Opioids intrinsically inhibit the genesis of mouse cerebellar granule neuron precursors in vitro: Differential impact of μ and δ receptor activation on proliferation and neurite elongation. Eur. J. Neurosci. *12*, 1281–1293.

Heckers, S., and Konradi, C. (2002). Hippocampal neurons in schizophrenia. J. Neural Transm. *109*, 891–905.

Hennig, S., Kong, G., Mannen, T., Sadowska, A., Kobelke, S., Blythe, A., Knott, G.J., Iyer, S.S., Ho, D., Newcombe, E.A., et al. (2015). Prion-like domains in RNA binding proteins are essential for building subnuclear paraspeckles. J. Cell Biol. *210*, 529–539.

Hevner, R.F., Hodge, R.D., Daza, R.A.M., and Englund, C. (2006). Transcription factors in glutamatergic neurogenesis: Conserved programs in neocortex, cerebellum, and adult hippocampus. Neurosci. Res. *55*, 223–233.

Hodge, R.D., and Hevner, R.F. (2011). Expression and actions of transcription factors in adult hippocampal neurogenesis. Dev. Neurobiol. *71*, 680–689.

Hodge, R.D., Kowalczyk, T.D., Wolf, S.A., Encinas, J.M., Rippey, C., Enikolopov, G., Kempermann, G., and Hevner, R.F. (2008). Intermediate Progenitors in Adult Hippocampal Neurogenesis: Tbr2 Expression and Coordinate Regulation of Neuronal Output. J. Neurosci. *28*, 3707–3717.

Hodge, R.D., Garcia, A.J., Elsen, G.E., Nelson, B.R., Mussar, K.E., Reiner, S.L., Ramirez, J.-M., and Hevner, R.F. (2013). Tbr2 Expression in Cajal-Retzius Cells and Intermediate Neuronal Progenitors Is Required for Morphogenesis of the Dentate Gyrus. J. Neurosci. *33*, 4165–4180.

Hori, K., and Hoshino, M. (2017). Neuronal migration and AUTS2 syndrome. Brain Sci. *7*.

Hori, K., Nagai, T., Shan, W., Sakamoto, A., Taya, S., Hashimoto, R., Hayashi, T., Abe, M., Yamazaki, M., Nakao, K., et al. (2014). Cytoskeletal Regulation by AUTS2 in Neuronal Migration and Neuritogenesis. Cell Rep. *9*, 2166–2179.

Hori, K., Nagai, T., Shan, W., Sakamoto, A., Abe, M., Yamazaki, M., Sakimura, K., Yamada, K., and Hoshino, M. (2015). Heterozygous disruption of autism susceptibility candidate 2 causes impaired emotional control and cognitive memory. PLoS One *10*, e0145979.

Hornig, M., Bresnahan, M.A., Che, X., Schultz, A.F., Ukaigwe, J.E., Eddy, M.L., Hirtz, D., Gunnes, N., Lie, K.K., Magnus, P., et al. (2018). Prenatal fever and autism risk. Mol. Psychiatry *23*, 759–766.

Hudson, W.H., and Ortlund, E.A. (2014). The structure, function and evolution of proteins that bind DNA and RNA. Nat. Rev. Mol. Cell Biol. *15*, 749–760.

Hulbert, S.W., and Jiang, Y.H. (2016). Monogenic mouse models of autism spectrum disorders: Common mechanisms and missing links. Neuroscience *321*, 3–23.

Imayoshi, I., and Kageyama, R. (2011). The role of notch signaling in adult neurogenesis.

Mol. Neurobiol. *44*, 7–12.

Iwasaki, T., Chin, W.W., and Ko, L. (2001). Identification and Characterization of RRM-containing Coactivator Activator (CoAA) as TRBP-interacting Protein, and Its Splice Variant as a Coactivator Modulator (CoAM). J. Biol. Chem. *276*, 33375–33383.

Jinde, S., Zsiros, V., Jiang, Z., Nakao, K., Pickel, J., Kohno, K., Belforte, J.E., and Nakazawa, K. (2012). Hilar Mossy Cell Degeneration Causes Transient Dentate Granule Cell Hyperexcitability and Impaired Pattern Separation. Neuron *76*, 1189–1200.

Jinde, S., Zsiros, V., and Nakazawa, K. (2013). Hilar mossy cell circuitry controlling dentate granule cell excitability. Front. Neural Circuits *7*.

Kalscheuer, V.M., FitzPatrick, D., Tommerup, N., Bugge, M., Niebuhr, E., Neumann, L.M., Tzschach, A., Shoichet, S.A., Menzel, C., Erdogan, F., et al. (2007). Mutations in autism susceptibility candidate 2 (AUTS2) in patients with mental retardation. Hum. Genet. *121*, 501–509.

Kaplan, G., and McCracken, J.T. (2012). Psychopharmacology of autism spectrum disorders. Pediatr. Clin. North Am. *59*, 175–187.

Kapoor, M., Wang, J.C., Wetherill, L., Le, N., Bertelsen, S., Hinrichs, A.L., Budde, J., Agrawal, A., Bucholz, K., Dick, D., et al. (2013). A meta-analysis of two genome-wide association studies to identify novel loci for maximum number of alcoholic drinks. Hum. Genet. *132*, 1141–1151.

Karimi, P., Kamali, E., Mousavi, S.M., and Karahmadi, M. (2017). Environmental factors influencing the risk of autism. J. Res. Med. Sci. *22*, 27.

Kfir, N., Lev-Maor, G., Glaich, O., Alajem, A., Datta, A., Sze, S.K., Meshorer, E., and Ast, G. (2015). SF3B1 Association with Chromatin Determines Splicing Outcomes. Cell Rep. *11*, 618–629.

Khanzada, N., Butler, M., and Manzardo, A. (2017). GeneAnalytics Pathway Analysis and Genetic Overlap among Autism Spectrum Disorder, Bipolar Disorder and Schizophrenia. Int. J. Mol. Sci. *18*, 527.

Knott, G.J., Bond, C.S., and Fox, A.H. (2016). The DBHS proteins SFPQ, NONO and PSPC1: A multipurpose molecular scaffold. Nucleic Acids Res. *44*, 3989–4004.

Kosugi, S., Hasebe, M., Tomita, M., and Yanagawa, H. (2009). Systematic identification of cell cycle-dependent yeast nucleocytoplasmic shuttling proteins by prediction of composite motifs. Proc. Natl. Acad. Sci. *106*, 10171–10176.

Kowalska, E., Ripperger, J.A., Hoegger, D.C., Bruegger, P., Buch, T., Birchler, T., Mueller, A., Albrecht, U., Contaldo, C., and Brown, S.A. (2013). NONO couples the circadian clock to the cell cycle. Proc. Natl. Acad. Sci. *110*, 1592–1599.

de la Barra, F., Skoknic, V., Alliende, A., Raimann, E., Cortés, F., and Lacassie, Y. (1986). Gemelas con autismo y retardo mental asociado a translocación cromosómica balanceada

(7;20). Rev. Chil. Pediatr. *57*, 549–554.

Langmead, B., Trapnell, C., Pop, M., and Salzberg, S.L. (2009). Ultrafast and memory-efficient alignment of short DNA sequences to the human genome. Genome Biol. *10*, R25.

Lau, C. (2015). Development of suck and swallow mechanisms in infants. Ann. Nutr. Metab. *66*, 7–14.

Law, V., Knox, C., Djoumbou, Y., Jewison, T., Guo, A.C., Liu, Y., MacIejewski, A., Arndt, D., Wilson, M., Neveu, V., et al. (2014). DrugBank 4.0: Shedding new light on drug metabolism. Nucleic Acids Res. *42*.

Leemhuis, J., and Bock, H.H. (2011). Reelin modulates cytoskeletal organization by regulating Rho GTPases. Commun. Integr. Biol. *4*, 254–257.

Li, G., Berger, O., Han, S.M., Paredes, M., Wu, N.C., and Pleasure, S.J. (2008). Hilar mossy cells share developmental influences with dentate granule neurons. Dev. Neurosci. *30*, 255–261.

Li, G., Kataoka, H., Coughlin, S.R., and Pleasure, S.J. (2009a). Identification of a transient subpial neurogenic zone in the developing dentate gyrus and its regulation by Cxcl12 and reelin signaling. Development *136*, 327–335.

Li, H., Handsaker, B., Wysoker, A., Fennell, T., Ruan, J., Homer, N., Marth, G., Abecasis, G., and Durbin, R. (2009b). The Sequence Alignment/Map format and SAMtools. Bioinformatics *25*, 2078–2079.

Liberzon, A., Subramanian, A., Pinchback, R., Thorvaldsdóttir, H., Tamayo, P., and Mesirov, J.P. (2011). Molecular signatures database (MSigDB) 3.0. Bioinformatics *27*, 1739–1740.

Liberzon, A., Birger, C., Thorvaldsdóttir, H., Ghandi, M., Mesirov, J.P., and Tamayo, P. (2015). The Molecular Signatures Database Hallmark Gene Set Collection. Cell Syst. *1*, 417–425.

López, M., García-Oguiza, A., Armstrong, J., García-Cobaleda, I., García-Miñaur, S., Santos-Simarro, F., Seidel, V., and Domínguez-Garrido, E. (2018). Rubinstein-Taybi 2 associated to novel EP300 mutations: Deepening the clinical and genetic spectrum. BMC Med. Genet. *19*.

Lysetskiy, M., Földy, C., and Soltesz, I. (2005). Long- and short-term plasticity at mossy fiber synapses on mossy cells in the rat dentate gyrus. Hippocampus *15*, 691–696.

Malaeb, S.N., Davis, J.M., Pinz, I.M., Newman, J.L., Dammann, O., and Rios, M. (2014). Effect of sustained postnatal systemic inflammation on hippocampal volume and function in mice. Pediatr. Res. *76*, 363–369.

Mazurek, M.O., Lu, F., Macklin, E.A., and Handen, B.L. (2018). Factors associated with DSM-5 severity level ratings for autism spectrum disorder. Autism 136236131875531.

McRae, J.F., Clayton, S., Fitzgerald, T.W., Kaplanis, J., Prigmore, E., Rajan, D., Sifrim, A., Aitken, S., Akawi, N., Alvi, M., et al. (2017). Prevalence and architecture of de novo mutations in developmental disorders. Nature *542*, 433–438.

Mefford, H.C., Muhle, H., Ostertag, P., von Spiczak, S., Buysse, K., Baker, C., Franke, A., Malafosse, A., Genton, P., Thomas, P., et al. (2010). Genome-wide copy number variation in epilepsy: novel susceptibility loci in idiopathic generalized and focal epilepsies. PLoS Genet. *6*.

Meng, S., Su, Z., Liu, Z., Wang, N., and Wang, Z. (2015). Rac1 contributes to cerebral ischemia reperfusion-induced injury in mice by regulation of Notch2. Neuroscience *306*, 100–114.

Menke, L.A., Gardeitchik, T., Hammond, P., Heimdal, K.R., Houge, G., Hufnagel, S.B., Ji, J., Johansson, S., Kant, S.G., Kinning, E., et al. (2018). Further delineation of an entity caused by CREBBP and EP300 mutations but not resembling Rubinstein-Taybi syndrome. Am. J. Med. Genet. Part A.

Merico, D., Isserlin, R., Stueker, O., Emili, A., and Bader, G.D. (2010). Enrichment map: A network-based method for gene-set enrichment visualization and interpretation. PLoS One *5*.

Miles, J.H. (2011). Autism spectrum disorders-A genetics review. Genet. Med. *13*, 278–294.

Ming, X., Patel, R., Kang, V., Chokroverty, S., and Julu, P.O. (2016). Respiratory and autonomic dysfunction in children with autism spectrum disorders. Brain Dev. *38*, 225–232.

Mircsof, D., Langouët, M., Rio, M., Moutton, S., Siquier-Pernet, K., Bole-Feysot, C., Cagnard, N., Nitschke, P., Gaspar, L., Žnidarių, M., et al. (2015). Mutations in NONO lead to syndromic intellectual disability and inhibitory synaptic defects. Nat. Neurosci. *18*, 1731–1736.

Muhle, R.A., Reed, H.E., Stratigos, K.A., and Veenstra-VanderWeele, J. (2018). The Emerging Clinical Neuroscience of Autism Spectrum Disorder. JAMA Psychiatry *75*, 514.

Myung, W., Kim, J., Lim, S.-W., Shim, S., Won, H.-H., Kim, S., Kim, S., Lee, M.-S., Chang, H.S., Kim, J.-W., et al. (2015). A genome-wide association study of antidepressant response in Koreans. Transl. Psychiatry *5*, e672.

O'Brown, Z.K., Van Nostrand, E.L., Higgins, J.P., and Kim, S.K. (2015). The Inflammatory Transcription Factors NFκB, STAT1 and STAT3 Drive Age-Associated Transcriptional Changes in the Human Kidney. In PLoS Genetics, p.

Oeseburg, B., Dijkstra, G.J., Groothoff, J.W., Reijneveld, S.A., and Jansen, D.E.M.C. (2011). Prevalence of chronic health conditions in children with intellectual disability: A systematic literature review. Intellect. Dev. Disabil. *49*, 59–85.

Oksenberg, N., Stevison, L., Wall, J.D., and Ahituv, N. (2013). Function and Regulation of

AUTS2, a Gene Implicated in Autism and Human Evolution. PLoS Genet. *9*, e1003221.

Oksenberg, N., Haliburton, G.D.E., Eckalbar, W.L., Oren, I., Nishizaki, S., Murphy, K., Pollard, K.S., Birnbaum, R.Y., and Ahituv, N. (2014). Genome-wide distribution of Auts2 binding localizes with active neurodevelopmental genes. Transl. Psychiatry *4*, e431.

Okur, V., Cho, M.T., Henderson, L., Retterer, K., Schneider, M., Sattler, S., Niyazov, D., Azage, M., Smith, S., Picker, J., et al. (2016). De novo mutations in CSNK2A1 are associated with neurodevelopmental abnormalities and dysmorphic features. Hum. Genet. *135*, 699–705.

Oliveira, A.M.M., Estévez, M.A., Hawk, J.D., Grimes, S., Brindle, P.K., and Abel, T. (2011). Subregion-specific p300 conditional knock-out mice exhibit long-term memory impairments. Learn. Mem. *18*, 161–169.

Pancetti, F., Bosser, R., Krehan, A., Pyerin, W., Itarte, E., and Bachs, O. (1999). Heterogeneous nuclear ribonucleoprotein A2 interacts with protein kinase CK2. Biochem. Biophys. Res. Commun. *260*, 17–22.

Pang, T., Atefy, R., and Sheen, V. (2008). Malformations of Cortical Development. Neurologist *14*, 181–191.

Parikh, M.S., Kolevzon, A., and Hollander, E. (2008). Psychopharmacology of Aggression in Children and Adolescents with Autism: A Critical Review of Efficacy and Tolerability. J. Child Adolesc. Psychopharmacol. *18*, 157–178.

Pennucci, R., Tavano, S., Tonoli, D., Gualdoni, S., and de Curtis, I. (2011). Rac1 and Rac3 GTPases regulate the development of hilar mossy cells by affecting the migration of their precursors to the hilus. PLoS One *6*.

Pernía-Andrade, A.J., and Jonas, P. (2014). Theta-Gamma-Modulated Synaptic Currents in Hippocampal Granule Cells InVivo Define a Mechanism for Network Oscillations. Neuron *81*, 140–152.

Pilkington, G.R., and Parker, R. (2008). Pat1 Contains Distinct Functional Domains That Promote P-Body Assembly and Activation of Decapping. Mol. Cell. Biol. *28*, 1298–1312.

Pollard, K.S., Salama, S.R., King, B., Kern, A.D., Dreszer, T., Katzman, S., Siepel, A., Pedersen, J.S., Bejerano, G., Baertsch, R., et al. (2006). Forces shaping the fastest evolving regions in the human genome. PLoS Genet. *2*, 1599–1611.

Prabhakar, S., Noonan, J.P., Pääbo, S., and Rubin, E.M. (2006). Accelerated evolution of conserved noncoding sequences in humans. Science (80-.). *314*, 786.

Prakash, S., Robbins, P.W., and Wyler, D.J. (1995). Cloning and analysis of murine cDNA that encodes a fibrogenic lymphokine, fibrosin. Proc. Natl. Acad. Sci. *92*, 2154–2158.

Rakitina, D. V., Taliansky, M., Brown, J.W.S., and Kalinina, N.O. (2011). Two RNA-binding sites in plant fibrillarin provide interactions with various RNA substrates. Nucleic Acids Res. *39*, 8869–8880.

Raymond, G. V., Bauman, M.L., and Kemper, T.L. (1995). Hippocampus in autism: a Golgi analysis. Acta Neuropathol. *91*, 117–119.

Reinstein, E., Tzur, S., Cohen, R., Bormans, C., and Behar, D.M. (2016). Intellectual disability and non-compaction cardiomyopathy with a de novo NONO mutation identified by exome sequencing. Eur. J. Hum. Genet. *24*, 1635–1638.

Rifaioglu, A.S., Doğan, T., Saraç, Ö.S., Ersahin, T., Saidi, R., Atalay, M.V., Martin, M.J., and Cetin-Atalay, R. (2018). Large-scale automated function prediction of protein sequences and an experimental case study validation on PTEN transcript variants. Proteins Struct. Funct. Bioinforma. *86*, 135–151.

Roelfsema, J.H., White, S.J., Ariyürek, Y., Bartholdi, D., Niedrist, D., Papadia, F., Bacino, C.A., den Dunnen, J.T., van Ommen, G.-J.B., Breuning, M.H., et al. (2005). Genetic Heterogeneity in Rubinstein-Taybi Syndrome: Mutations in Both the CBP and EP300 Genes Cause Disease. Am. J. Hum. Genet. *76*, 572–580.

Rosen, T.E., Mazefsky, C.A., Vasa, R.A., and Lerner, M.D. (2018). Co-occurring psychiatric conditions in autism spectrum disorder. Int. Rev. Psychiatry 1–22.

Saitoh, O. (2001). Development of the hippocampal formation from2 to 42 years: MRI evidence of smaller area dentata in autism. Brain *124*, 1317–1324.

Scharfman, H.E. (2017). Advances in understanding hilar mossy cells of the dentate gyrus. Cell Tissue Res. 1–10.

Scharfman, H.E., and Myers, C.E. (2013). Hilar mossy cells of the dentate gyrus: a historical perspective. Front. Neural Circuits *6*, 106.

Schorry, E.K., Keddache, M., Lanphear, N., Rubinstein, J.H., Srodulski, S., Fletcher, D., Blough-Pfau, R.I., and Grabowski, G.A. (2008). Genotype-phenotype correlations in Rubinstein-Taybi syndrome. Am. J. Med. Genet. Part A *146*, 2512–2519.

Schumann, G., Coin, L.J., Lourdusamy, A., Charoen, P., Berger, K.H., Stacey, D., Desrivieres, S., Aliev, F.A., Khan, A.A., Amin, N., et al. (2011). Genome-wide association and genetic functional studies identify autism susceptibility candidate 2 gene (AUTS2) in the regulation of alcohol consumption. Proc. Natl. Acad. Sci. *108*, 7119–7124.

Schwartz, R., Ting, C.S., and King, J. (2001). Whole proteome pI values correlate with subcellular localizations of proteins for organisms within the three domains of life. Genome Res. *11*, 703–709.

Scott, D.A., Hernandez-Garcia, A., Azamian, M.S., Jordan, V.K., Kim, B.J., Starkovich, M., Zhang, J., Wong, L.J., Darilek, S.A., Breman, A.M., et al. (2017). Congenital heart defects and left ventricular non-compaction in males with loss-of-function variants in NONO. J. Med. Genet. *54*, 47–53.

Sengun, E., Yararbas, K., Kasakyan, S., and Alanay, Y. (2016). AUTS2 Syndrome in a 68-year-old female: Natural history and further delineation of the phenotype. Am. J. Med.

Genet. Part A *170*, 3231–3236.

Seress, L., Ábrahám, H., Czéh, B., Fuchs, E., and Léránth, C. (2008). Calretinin expression in hilar mossy cells of the hippocampal dentate gyrus of nonhuman primates and humans. Hippocampus *18*, 425–434.

Sorrells, S.F., Paredes, M.F., Cebrian-Silla, A., Sandoval, K., Qi, D., Kelley, K.W., James, D., Mayer, S., Chang, J., Auguste, K.I., et al. (2018). Human hippocampal neurogenesis drops sharply in children to undetectable levels in adults. Nature *555*, 377–381.

Staley, K.J., and Dudek, F.E. (2006). Interictal Spikes and Epileptogenesis. Epilepsy Curr. *6*, 199–202.

Stein, M.B., McCarthy, M.J., Chen, C.Y., Jain, S., Gelernter, J., He, F., Heeringa, S.G., Kessler, R.C., Nock, M.K., Ripke, S., et al. (2018). Genome-wide analysis of insomnia disorder. Mol. Psychiatry 1–13.

Subhash, S., and Kanduri, C. (2016). GeneSCF: A real-time based functional enrichment tool with support for multiple organisms. BMC Bioinformatics *17*, 365.

Subramanian, A., Tamayo, P., Mootha, V.K., Mukherjee, S., Ebert, B.L., Gillette, M.A., Paulovich, A., Pomeroy, S.L., Golub, T.R., Lander, E.S., et al. (2005). Gene set enrichment analysis: A knowledge-based approach for interpreting genome-wide expression profiles. Proc. Natl. Acad. Sci. *102*, 15545–15550.

Sultana, R., Yu, C.E., Yu, J., Munson, J., Chen, D., Hua, W., Estes, A., Cortes, F., De La Barra, F., Yu, D., et al. (2002). Identification of a novel gene on chromosome 7q11.2 interrupted by a translocation breakpoint in a pair of autistic twins. Genomics *80*, 129–134.

Sundararajan, T., Manzardo, A.M., and Butler, M.G. (2018). Functional analysis of schizophrenia genes using GeneAnalytics program and integrated databases. Gene *641*, 25–34.

Suzuki, I.K., Gacquer, D., Heurck, R. Van, Kumar, D., Wojno, M., Bilheu, A., Herpoel, A., Cheron, J., Polleux, F., Detours, V., et al. (2017). Hominin-specific NOTCH2 paralogs expand human cortical neurogenesis through regulation of Delta/Notch interactions. bioRxiv 221358.

Szklarczyk, D., Franceschini, A., Wyder, S., Forslund, K., Heller, D., Huerta-Cepas, J., Simonovic, M., Roth, A., Santos, A., Tsafou, K.P., et al. (2015). STRING v10: Protein-protein interaction networks, integrated over the tree of life. Nucleic Acids Res. *43*, D447–D452.

Tan, W., Sherman, D., Turesson, J., Shao, X.M., Janczewski, W.A., and Feldman, J.L. (2012). Reelin demarcates a subset of pre-Bötzinger complex neurons in adult rat. J. Comp. Neurol. *520*, 606–619.

Trapnell, C., Hendrickson, D.G., Sauvageau, M., Goff, L., Rinn, J.L., and Pachter, L. (2013). Differential analysis of gene regulation at transcript resolution with RNA-seq. Nat. Biotechnol. *31*, 46–53.

Tronche, F., Kellendonk, C., Kretz, O., Gass, P., Anlag, K., Orban, P.C., Bock, R., Klein, R., and Schütz, G. (1999). Disruption of the glucocorticoid receptor gene in the nervous system results in reduced anxiety. Nat. Genet. *23*, 99–103.

Turgeon, B., and Meloche, S. (2009). Interpreting Neonatal Lethal Phenotypes in Mouse Mutants: Insights Into Gene Function and Human Diseases. Physiol. Rev. *89*, 1–26.

Turner, T.N., Hormozdiari, F., Duyzend, M.H., McClymont, S.A., Hook, P.W., Iossifov, I., Raja, A., Baker, C., Hoekzema, K., Stessman, H.A., et al. (2016). Genome Sequencing of Autism-Affected Families Reveals Disruption of Putative Noncoding Regulatory DNA. Am. J. Hum. Genet. *98*, 58–74.

Visel, A. (2004). GenePaint.org: an atlas of gene expression patterns in the mouse embryo. Nucleic Acids Res. *32*, 552D–556.

Wang, H., Yuan, Y., Zhang, Z., Yan, H., Feng, Y., and Li, W. (2014). Dysbindin-1C is required for the survival of hilar mossy cells and the maturation of adult newborn neurons in dentate gyrus. J. Biol. Chem. *289*, 29060–29072.

Wang, J., Weaver, I.C.G., Gauthier-Fisher, A., Wang, H., He, L., Yeomans, J., Wondisford, F., Kaplan, D.R., and Miller, F.D. (2010). CBP histone acetyltransferase activity regulates embryonic neural differentiation in the normal and Rubinstein-Taybi syndrome brain. Dev. Cell *18*, 114–125.

Wang, S., Sun, H., Ma, J., Zang, C., Wang, C., Wang, J., Tang, Q., Meyer, C.A., Zhang, Y., and Liu, X.S. (2013). Target analysis by integration of transcriptome and ChIP-seq data with BETA. Nat. Protoc. *8*, 2502–2515.

Wang, Y., Li, Y., Yue, M., Wang, J., Kumar, S., Wechsler-Reya, R.J., Zhang, Z., Ogawa, Y., Kellis, M., Duester, G., et al. (2018). N6-methyladenosine RNA modification regulates embryonic neural stem cell self-renewal through histone modifications. Nat. Neurosci. *21*, 195–206.

Waters, J.E., Astle, M. V., Ooms, L.M., Balamatsias, D., Gurung, R., and Mitchell, C.A. (2008). P-Rex1 - a multidomain protein that regulates neurite differentiation. J. Cell Sci. *121*, 2892–2903.

William, D.A., Saitta, B., Gibson, J.D., Traas, J., Markov, V., Gonzalez, D.M., Sewell, W., Anderson, D.M., Pratt, S.C., Rappaport, E.F., et al. (2007). Identification of oscillatory genes in somitogenesis from functional genomic analysis of a human mesenchymal stem cell model. Dev. Biol. *305*, 172–186.

Wulff, K., Dijk, D.J., Middleton, B., Foster, R.G., and Joyce, E.M. (2012). Sleep and circadian rhythm disruption in schizophrenia. Br. J. Psychiatry *200*, 308–316.

Yamada, T., Kerever, A., Yoshimura, Y., Suzuki, Y., Nonaka, R., Higashi, K., Toida, T., Mercier, F., and Arikawa-Hirasawa, E. (2017). Heparan sulfate alterations in extracellular matrix structures and fibroblast growth factor-2 signaling impairment in the aged neurogenic niche. J. Neurochem. *142*, 534–544.

Yamaguchi, Y. (2001). Heparan sulfate proteoglycans in the nervous system: Their diverse roles in neurogenesis, axon guidance, and synaptogenesis. Semin. Cell Dev. Biol. *12*, 99–106.

Yan, Y., Zhao, W., Huang, Y., Tong, H., Xia, Y., Jiang, Q., and Qin, J. (2017). Loss of Polycomb Group Protein Pcgf1 Severely Compromises Proper Differentiation of Embryonic Stem Cells. Sci. Rep. *7*.

Yang, P., Zhang, J., Shi, H., Zhang, J., Xu, X., Xiao, X., and Liu, Y. (2014). Developmental profile of neurogenesis in prenatal human hippocampus: An immunohistochemical study. Int. J. Dev. Neurosci. *38*, 1–9.

Yassa, M.A., and Stark, C.E.L. (2011). Pattern separation in the hippocampus. Trends Neurosci. *34*, 515–525.

Yoon, J., Seo, Y., Kim, J., and Lee, I. (2011). Hippocampus is required for paired associate memory with neither delay nor trial uniqueness. Learn. Mem. *19*, 1–8.

Yoon, K.J., Ringeling, F.R., Vissers, C., Jacob, F., Pokrass, M., Jimenez-Cyrus, D., Su, Y., Kim, N.S., Zhu, Y., Zheng, L., et al. (2017). Temporal Control of Mammalian Cortical Neurogenesis by m6A Methylation. Cell *171*, 877–889.e17.

Yue, Y., Liu, J., and He, C. (2015). RNA N6-methyladenosine methylation in post-transcriptional gene expression regulation. Genes Dev. *29*, 1343–1355.

Zappone, C.A. (2004). Translamellar Disinhibition in the Rat Hippocampal Dentate Gyrus after Seizure-Induced Degeneration of Vulnerable Hilar Neurons. J. Neurosci. *24*, 853–864.

Zerbo, O., Qian, Y., Yoshida, C., Grether, J.K., Van de Water, J., and Croen, L.A. (2015). Maternal Infection During Pregnancy and Autism Spectrum Disorders. J. Autism Dev. Disord. *45*, 4015–4025.

Zhang, B., Xu, Y.-H., Wei, S.-G., Zhang, H.-B., Fu, D.-K., Feng, Z.-F., Guan, F.-L., Zhu, Y.-S., and Li, S.-B. (2014). Association Study Identifying a New Susceptibility Gene (AUTS2) for Schizophrenia. Int. J. Mol. Sci. *15*, 19406–19416.

Zhang, Y., Liu, T., Meyer, C.A., Eeckhoute, J., Johnson, D.S., Bernstein, B.E., Nussbaum, C., Myers, R.M., Brown, M., Li, W., et al. (2008). Model-based analysis of ChIP-Seq (MACS). Genome Biol. *9*.

Zhao, J., Ohsumi, T.K., Kung, J.T., Ogawa, Y., Grau, D.J., Sarma, K., Song, J.J., Kingston, R.E., Borowsky, M., and Lee, J.T. (2010). Genome-wide Identification of Polycomb-Associated RNAs by RIP-seq. Mol. Cell *40*, 939–953.

Zimmermann, N., Ferrer Acosta, A.M.B., Kohlhase, J., and Bartsch, O. (2007). Confirmation of EP300 gene mutations as a rare cause of Rubinstein-Taybi syndrome. Eur. J. Hum. Genet. *15*, 837–842.

Data Attribution

The conceptualization of this thesis project was completed by Anthony S, Castanza (ASC), and Robert F. Hevner (RFH). Experimental design was completed by ASC and RFH. The acquisition and establishment of genetically modified mice was completed by ASC, RFH and Ray A. M. Daza (RAMD). The AUTS2 mouse colony was maintained and confirmed by genotyping by ASC and RAMD. The TBR1 mouse colony was maintained and confirmed by genotyping by Eitan S. Kaplan (ESK). Immunohistochemistry on TBR1 deficient mice was performed by ESK. The TBR2 mouse colony was maintained and confirmed by genotyping by Anca B. Mihalas (ABM). Tissue processing, histology, in-situ hybridizations, immunohistochemistry, and image acquisition were conducted by ASC. Tissue collections, immunoprecipitations, RNA-immunoprecipitations, Western blotting and RNA preparations were conducted by ASC. Library preparations and RNA-sequencing were performed by Chris D. Frazar (CDF) at the Northwest Genomics Core. Protein mass-spec detection was performed by Young Ah Goo (YAG). Sequencing and mass-spec data analysis was performed by ASC. Plethysmographic recordings and analysis were performed by Sanja Ramirez (SR). EEG electrode implantations and recording analysis was performed by Franck Kalume (FK). Video-EEG monitoring was performed by Michelle Bard (MB) and Rufi Dalvi (RD). ASC generated the figures used throughout this dissertation. The organization and writing of this dissertation was completed by ASC, with guidance from RFH, JMR, C. Dirk Keene (CDK) and James M. Olson (JMO).